

High-Temperature Methane Oxidation in Catalytic Micro-Channels

by

Michael Wartmann

October 2005

Institut für Chemische Verfahrenstechnik

Universität Stuttgart

Böblinger Str. 72, D-70199 Stuttgart

Advisor:

Prof. Dr. Götz Veser

Department of Chemical and Petroleum Engineering

University of Pittsburgh

1232 Benedum Hall

Pittsburgh, PA 15261 (USA)

Dipl.-Ing. Vanessa Gepert

Institut für Chemische Verfahrenstechnik

Universität Stuttgart

Böblinger Str. 72, D-70199 Stuttgart

Abstract

High-Temperature Methane Oxidation in Catalytic Micro-Channels

Michael Wartmann

High-temperature catalytic reactions have been intensively studied for many decades due to their large industrial potential, such as in pyrolysis, total oxidation and partial oxidation of hydrocarbons. These reaction systems are characterized by extreme reaction temperatures where homogeneous reactions can occur in parallel to catalytic reactions. The appearance of homogeneous reactions in catalytic processes is usually an undesired feature because it complicates the understanding of catalytic reaction mechanisms, leads to selectivity losses, and often to hazardous potentially explosive conditions. Since solid phases in high-temperature catalysis tend to adsorb radicals, which are typically formed in homogeneous reactions, the presence of a solid catalyst can eventually lead to quenching of homogeneous gas-phase reactions.

In catalytic reaction systems with characteristic dimensions in the sub-millimeter range, large surface-to-volume ratios lead to intensified influence of catalytic reactions on the overall reaction behavior. These so-called micro-reactors offer short transport paths and large catalytic surfaces in which homogeneous reactions can be effectively suppressed. Hence, by avoiding homogeneous reactions, explosive behavior and formation of undesired side products such as nitric oxides can possibly be inhibited.

In the present study, the oxidation of methane in micro-reactors was numerically investigated. Catalytic combustion of methane on platinum constitutes an important reaction system both for scientific and industrial applications. Reactive flow simulations in a single tubular micro-channel were carried out using a two-dimensional boundary layer model that incorporates both detailed surface and homogeneous elementary-step chemistry.

The influence of various parameters such as temperature, pressure and reactant composition was tested to investigate homogeneous-heterogeneous interactions and main reaction pathways. Obtained results demonstrate distinct influence of catalytic reactions on homogeneous ignition in catalytic micro-reactors. For reactor diameters of $d < 200 \mu\text{m}$ complete suppression of homogeneous reactions could be observed up to $T = 2000 \text{ K}$ for ambient pressure conditions. In addition, suppression of Prompt- NO_x formation in catalytic micro-channel reactors was detected resulting from quenching of radical producing gas-phase reactions. In further studies, simulations with a three-dimensional Navier-Stokes model for detailed reactor geometries as well as experimental studies will be carried out to confirm observations from ignition studies in the present work.

Acknowledgments

First of all, I would like to thank my advisor at the University of Pittsburgh, Prof. Götz Veser, for giving me the opportunity to conduct research in his group and also for his constant support and guidance throughout the development of my diploma thesis.

I am especially grateful for this opportunity because I was given the chance to increase my knowledge with a challenging and interesting research topic in a very pleasant and inspiring working environment in his group.

Furthermore, I would like to thank my lab-mates Katie, Tengfei, and Tom who made my work experience in the group a lot more enjoyable. I also want to thank my friends from Pittsburgh in particular Abigale, Jeff, Katie, Willi, and Zhi-Ping for their support and the great time we have had together.

Finally, I would like to thank Prof. Hasse, Prof. Nieken and, in particular, Prof. Eigenberger for their support, for facilitating this project, and accepting this work as a diploma thesis.

I appreciate the help and support from Vanessa as my advisor in Stuttgart.

Financial support by the “Solvay Stiftung” is gratefully acknowledged.

Many thanks and kisses to my parents, my sister, and my friends from Germany for their constant support.

Contents

1 Deutsche Zusammenfassung	1
2 Introduction	5
3 Fundamentals	7
3.1 Process Intensification in High-Temperature Catalysis	7
3.2 High-Temperature Catalysis and Catalytic Micro-Reactors	8
3.3 Previous Work on Catalytic Micro-Reactors	9
3.4 Oxidation of Methane	11
3.4.1 Homogeneous Oxidation	11
3.4.2 Heterogeneous Oxidation	14
3.5 NO _x formation	16
3.5.1 Thermal NO formation	17
3.5.2 Prompt NO Formation	17
3.5.3 NO formation through Diazenyl	17
4 Numerical Simulation	19
4.1 Model Overview	19
4.2 Boundary-Layer Model	19
4.2.1 Assumptions	19
4.2.2 Physical Parameters	21
4.3 CHEMKIN Software Package	22
4.3.1 Program Structure	22
4.3.2 Numerical Parameters	24
5 Results	25
5.1 Oxidation of Methane	25
5.1.1 Ignition behavior	26
5.1.2 Size Effects in Micro-Channel Reactors	28
5.1.3 Low-Temperature Transition Point	33
5.1.4 High-Temperature Transition Point	35
5.1.5 Homogeneous-Heterogeneous Interactions at High Temperatures	43
5.1.6 Pressure Variation	47
5.1.7 Variation of Inlet Composition	50
5.1.8 Adiabatic Wall	52
5.1.9 Comparison of Surface Mechanisms	53
5.2 NO _x Formation	55

6 Summary and Outlook	61
6.1 Summary	61
6.2 Outlook	62
A Model Description	67
A Surface Mechanisms	69
B Model Validation	72
B.1 Continuum Assumption	72
B.2 Laminar Flow	73
B.3 Convection-Dominant Behavior in the Main Flow Direction	73
B.4 Pressure Drop	73

List of Tables

2	Table of parameters from fitting of the function $d = a * \exp(-\frac{T_{tr}}{T_0})$ to calculated T_{tr} versus d	48
3	Table of parameters from re-fitting of the function $d = a * \exp(-\frac{T_{tr}}{T_0})$ to calculated T_{tr} versus d with averaged parameter T_0	48
4	Transition temperatures for a $250 \mu\text{m}$ channel at different pressure conditions. . . .	49
5	Surface reaction mechanism for methane oxidation by Deutschmann et al.[25]. . . .	70
6	Surface reaction mechanism for methane oxidation by Aghalayam et al.[27]. . . .	71
7	Surface reaction mechanism NO reduction by Chatterjee et al.[4].	72
8	Pressure drop calculation for $p = 1$ bar, $T = 1500$ K and $v = 9$ m/s.	74

List of Figures

1	Schematic of research approach to investigate and develop catalytic micro-reactors for high temperature fuel gas combustion.	8
2	Reaction pathway analysis of carbon species flux (GRI-Mech 3.0 [10]) with an isothermal CSTR, residence time = 30 ms, T = 1400 K, p = 1 bar, stoichiometric ratio of CH ₄ in air $\Phi = 1.0$, all fluxes are normalized with respect to CH ₄ →CH ₃ , fluxes smaller than 1.0 % are not shown.	13
3	Reaction pathway analysis with an isothermal CSTR for the surface mechanism by Aghalayam et al. [27], residence time = 30 ms, T = 1400 K, p = 1 bar, stoichiometric ratio of CH ₄ in air $\Phi = 1.0$, catalytic surface to volume ratio = 8 mm ⁻¹ , all fluxes are normalized with respect to CH ₄ →CH ₃ , fluxes smaller than 1.0 % are not shown.	15
4	Schematic of a micro-reactor channel including main assumptions of the boundary-layer model.	20
5	Structure of software package CHEMKIN 4.0 for reactive flow simulations of methane oxidation with the CRESLAF module.	23
6	Methane concentration profile of a 2.5 mm catalytic reactor at T = 1650 K, p = 1 bar and stoichiometric ratio of CH ₄ in air $\Phi = 1.0$. r = 0.0 mm marks the center line of the reactor.	26
7	Ignition distance at the center line versus temperature for channel with d = 2.5 mm, p = 1 bar and stoichiometric ratio of CH ₄ in air $\Phi = 1.0$ for the three different cases with coupled mechanism compared to inert wall and pure catalytic case.	27
8	Ignition distance at center line versus temperature for channel diameters between d = 75 μm and d = 4.0 mm , p = 1 bar and stoichiometric ratio of CH ₄ in air $\Phi = 1.0$	29
9	CH ₄ (left) and H radical (right) concentration for three different diameters d = 2.5 mm (top), d = 1.0 mm (middle) and d = 500 μm (bottom),T = 1650 K, p = 1 bar, and stoichiometric ratio of CH ₄ in air $\Phi = 1.0$	31
10	Maximum hydrogen radical concentration as a function of temperature and diameter.	32
11	Ignition distances at the center line versus temperature and diameter for channel diameters between d = 50 μm and d = 2.5 mm, p = 1 bar and stoichiometric ratio of CH ₄ in air $\Phi = 1.0$. The left plot shows a comparison of ignition distances for the fully coupled mechanism with pure catalytic simulations, whereas the right graph compares the heterogeneous-homogeneous mechanism to inert wall behavior.	33
12	Schematic of transition temperature calculation between ignition distances of the pure catalytic and the coupled case.	34

13	Transition temperatures versus diameter for transition from heterogeneously to homogeneously dominated behavior for $p = 1$ bar and stoichiometric ratio of CH_4 in air $\Phi = 1.0$. Left graph shows linear curves, right graph shows logarithmic diameter axis.	35
14	Ignition distance at center line versus temperature for channel diameters between $d = 2$ mm and $d = 10$ mm, $p = 1$ bar and stoichiometric ratio of CH_4 in air $\Phi = 1.0$ for high temperature conditions.	36
15	CH_4 concentration for four different diameters $d = 10.0$ mm (upper left), $d = 4.0$ mm (upper right), $d = 1.0$ mm (lower left), and $d = 250 \mu\text{m}$ (lower right) at $T = 1700$ K, $p = 1$ bar, and stoichiometric ratio of CH_4 in air $\Phi = 1.0$ for a non-catalytic inert wall.	38
16	Schematic of transition temperature calculation by determination of deviation between ignition distances of the inert wall and the coupled case.	39
17	Transition temperatures versus diameter for the high-temperature transition (diamonds) from het./hom. influenced regime to homogeneously dominated behavior in comparison to low-temperature transition (circles) for $p = 1$ bar and stoichiometric ratio of CH_4 in air $\Phi = 1.0$. Left graph shows linear diameter axis, right graph shows logarithmic diameter axis.	40
18	$\ln r$ as a function of $1/T$ for transition to wall independent behavior. The function gradient represents the apparent overall activation energy E/\mathfrak{R} , whereas the y-coordinate functions to determine the ratio of reaction to transport rate.	42
19	Concentration profiles and initiating, chain-branching and propagating reaction rates at the center line versus axial coordinate compared to surface reaction rates at $T = 1700$ K, $p = 1$ bar and stoichiometric ratio of CH_4 in air $\Phi = 1.0$. The upper left graph shows reactions rates from inlet to the homogenous ignition point. The upper right graph shows initial reaction behavior with logarithmic reaction rates. Lower graphs depict concentration profiles of molecular (left) and radical species (right).	44
20	Rates of initiating homogeneous reactions at channel inlet center versus temperature compared to methane adsorption/reaction step, $d = 2.0$ mm, $p = 1$ bar and stoichiometric ratio of CH_4 in air $\Phi = 1.0$	45
21	Reaction pathway analysis with an isothermal surface CSTR for $T = 2000$ K, residence time = 30 ms, $p = 1$ bar, $A_v = 160.0 \text{ cm}^{-1}$ and a stoichiometric ratio of CH_4 in air $\Phi = 1.0$, all fluxes are normalized with respect to $\text{CH}_4 \rightarrow \text{CH}_3$, fluxes smaller than 0.3 % are not shown.	46
22	Transition temperatures versus diameter for transition from heterogeneously to homogeneously dominated behavior for $p = 0.5\text{-}5$ bar and stoichiometric ratio of CH_4 in air $\Phi = 1.0$	47

23	Fit of transition temperatures versus diameter and pressure for transition from heterogeneously to homogeneously dominated behavior for a stoichiometric ratio of CH ₄ in air $\Phi = 1.0$	49
24	Transition temperatures versus diameter for transition from heterogeneously to homogeneously dominated behavior for $p = 1.0$ bar and stoichiometric ratio of CH ₄ in air and pure oxygen $\Phi = 1.0$	50
25	Transition temperatures versus diameter for transition from heterogeneously to homogeneously dominated behavior for $p = 1.0$ bar and $\Phi = 0.2\text{-}1.0$ of CH ₄ in air .	51
26	Transition temperatures versus diameter for transition from heterogeneously to homogeneously dominated behavior in channels with adiabatic compared to isothermal wall for $p = 1.0$ bar and $\Phi = 0.2$ of CH ₄ in air.	53
27	Comparison of transition temperatures versus diameter for transition from heterogeneously to homogeneously dominated behavior of different mechanisms by Deutschmann et. al. [25] and Aghalayam et. al. [27] at $p = 1.0$ bar and stoichiometric ratio of CH ₄ in air $\Phi = 1.0$	54
28	NO concentration versus axial distance for channel diameter of $d = 2.5$ mm (left), $d = 750 \mu\text{m}$ (middle) and $d = 250 \mu\text{m}$ (right) at $p = 1.0$ bar for a stoichiometric ratio of methane in air $\Phi = 1.0$	56
29	Maximum NO concentration in ppm vs. channel diameter and temperature. The dark area depicts NO concentration less than 1 ppm.	57
30	NO concentration versus axial distance for channel diameter of $d = 750 \mu\text{m}$ and different equivalent ratios at $p = 1.0$ bar and $T = 1650$ K.	58
31	NO formation pathway analysis with an isothermal CSTR at $T = 1700$ K, residence time = 30 ms, $p = 1$ bar, stoichiometric ratio of CH ₄ in air $\Phi = 1.0$, all fluxes are normalized with respect to overall N ₂ conversion rate, fluxes smaller than 1.0 % are not shown.	59
32	Homogeneous NO forming reaction rates versus axial distance at $T = 2500$ K, $p = 1$ bar and stoichiometric ratio of CH ₄ in air $\Phi = 1.0$ in a $250 \mu\text{m}$ channel.	60

Nomenclature

Latin Symbols

A	[m ²]	area
a	[mm]	fitting parameter
A_v	[-]	surface-to-volume ratio
C	[-]	constant
c_i	[mol/m ³]	concentration
c_p	[J/kgK]	specific heat at constant pressure
\hat{D}	[-]	mean numerical deviation
D_{ij}	[m ² /s]	binary diffusion coefficient of species i and j
D_{min}	[-]	minimum numerical deviation to determine transition temperature
D_{num}	[-]	numerical deviation
d	[mm]	diameter
d_0	[mm]	fitting parameter
E	[kJ/mol]	activation energy
h_i	[J/kg]	specific enthalpy of species i
k	[Nm/K]	Boltzmann constant $k = 1.3807 \cdot 10^{-23}$ Nm/K
k_∞	[1/s]	frequency factor
Kn	[-]	Knudsen number
l	[mm]	reactor length
\dot{m}	[kg/s]	mass flux
MW_i	[-]	molecular weight of species i
N_g	[-]	number of gas-phase species
p	[bar]	pressure
p_0	[bar]	fitting parameter
p_1	[bar]	fitting parameter
Δp	[bar]	pressure drop
Pe	[-]	Peclet number
R	[-]	ratio of reaction to transport rate
R	[-]	correlation coefficient
r	[mm]	radius
r^*	[mol/cm ³ s]	apparent volumetric reaction rate for surface reactions
$r_{reaction}$	[mol/cm ³ s]	reaction rate
\mathfrak{R}	[J/molK]	universal gas constant
Re	[-]	Reynolds number
S	[-]	sticking coefficient

s	[mol/cm ³]	surface site density
T	[K]	temperature
t_{abs}	[\cdot]	absolute tolerance
t_{ign}	[s]	ignition delay
t_{rel}	[\cdot]	relative tolerance
T_{tr}	[K]	transition temperature
T_0	[K]	fitting parameter
V	[m ³]	volume
w_i	[\cdot]	mass fraction of species i
x	[m]	length
x_i	[\cdot]	mole fraction of species i
X_{ign}	[m]	ignition distance
z	[mm]	axial distance

Greek Symbols

β	[\cdot]	exponent for temperature dependence of rate coefficient term
η	[Pa·s]	viscosity
λ	[W/mK]	conductivity
λ_i	[m]	mean free path of species i
ξ	[\cdot]	normalized stream function
ρ	[kg/m ³]	density
σ	[Å]	molecular radius
v	[m/s]	velocity
\tilde{v}	[m/s]	average velocity
v_i^D	[m/s]	diffusive velocity of species i
Φ	[\cdot]	equivalence ratio
Ψ	[\cdot]	stream function

Subscripts

cat	catalytic
i,j	species i, j
min	minimum
max	maximum

1 Deutsche Zusammenfassung

Methanoxidation in katalytischen Mikroreaktoren

Heterogen katalysierte Gasphasenreaktionen, wie z.B. Pyrolyse-, partielle Oxidations- und Verbrennungsreaktionen von Kohlenwasserstoffen, sind aufgrund ihres industriellen Potentials seit Jahrzehnten Gegenstand intensiver Forschung. Bei der Hochtemperaturkatalyse können homogene Reaktionen parallel zu katalytischen Reaktionen in Temperaturbereichen auftreten, in denen die Aktivierungsenergie des homogenen Reaktionswegs überwunden wird. Das Auftreten homogener Reaktionen ist in katalytischen Systemen in der Regel unerwünscht, da Selektivitäten dadurch verringert werden und homogene Reaktionen zu potentiell explosiblen Zuständen führen können. Homogene Oxidationsreaktionen sowie Explosionsgrenzen von Oxidationssystemen können jedoch effektiv durch die Präsenz katalytischer Oberflächen beeinflusst werden. Reaktoren, in denen große katalytische Oberflächen durch Miniaturisierung des Reaktionskanals im Bereich von Mikrometern realisiert werden, haben daher die Eigenschaft, bei Anwendung in Prozessen mit heterogen katalysierten Oxidationsreaktionen das Reaktionsverhalten vorteilhaft zu beeinflussen.

Solche Reaktoren besitzen auf dem Gebiet der chemischen Reaktionstechnik ein großes Potential sowohl für wissenschaftliche Untersuchungen als auch für technische Anwendungen. Die geringen Abmessungen führen dabei nicht nur zu besonders kompakten Reaktoren, die ideal für dezentrale und mobile Anwendungen geeignet sind, sondern daraus resultieren auch geringe Reaktorvolumina und somit erhöhte Reaktorsicherheit. Die kurzen Transportwege in Mikrokanälen und die damit einhergehenden ungewöhnlich hohen Wärme- und Stoffübertragungskoeffizienten im Vergleich zu konventionellen Reaktoren führen schließlich zu besonders effizienten und gut kontrollierbaren Reaktoren.

Ein wesentliche Eigenschaft dieser Mikroreaktoren ist die ungewöhnlich große katalytisch aktive Oberfläche im Vergleich zum vorhandenen Gasvolumen. Dies ist besonders für die Hochtemperaturkatalyse von großem wissenschaftlichem wie auch technischem Interesse, da die Anwesenheit katalytischer Wände zur Unterdrückung homogener Gasphasenreaktionen führen kann. Zum Einen ist dies auf die relative Beschleunigung katalytischer Reaktionen durch die große spezifische Katalysatoroberfläche im Vergleich zum Gasvolumen zurückzuführen, zum Anderen aber auch auf das sogenannte "Quenching" von Radikalen. d.h. das Abfangen hochreaktiver radikalischer Reaktionsträger aus der Gasphase durch Wandreaktionen. Dieses Verhalten ist nicht nur aus sicherheitstechnischen Aspekten von Bedeutung, sondern kann auch das Umsatzverhalten bei oxidativen, stark exothermen Reaktionen wesentlich beeinflussen und - unter rein wissenschaftlichen Gesichtspunkten - eine klare Unterscheidung zwischen homogenen und katalytischen Beiträgen an der Gesamtreaktion ermöglichen.

Dieser Aspekt katalytischer Mikroreaktoren wurde erstmals durch die Untersuchung der Wasserstoffoxidation in Luft, eines hoch explosiven Systems, durch Veser et al. [11, 12, 34] in katalytischen Mikroreaktoren belegt und erklärt. Die Ergebnisse der experimentellen und numerischen Untersuchungen zeigten, dass Radikal-Wand-Reaktionen zu einer vollständigen Unterdrückung homogener Reaktionen und korrekt dimensionierte katalytische Mikroreaktoren somit zu intrinsischer Reaktorsicherheit führen können. Gleichzeitig konnte allerdings auch gezeigt werden, dass diese intrinsische Reaktorsicherheit stark sowohl von der Natur des katalytischen Wandmaterials als auch vom Gesamtdruck im Mikroreaktor abhängt.

Im Rahmen der vorliegenden Arbeit wurde dieser Ansatz auf die katalytische Umsetzung von Methan mit Luft unter Hochtemperaturbedingungen erweitert. Dabei wurde der Einfluss verschiedener Parameter wie Durchmesser des Reaktionskanals, Reaktionstemperatur, Reaktordruck sowie unterschiedlicher katalytischer Oberflächenmechanismen auf die katalytische Verbrennung von Methan zu CO_2 und H_2O in detaillierten Simulationsrechnungen untersucht. Das untersuchte Reaktionssystem ist nicht nur von fundamentaler Bedeutung für die petrochemische Industrie und die Energieversorgung, sondern auch nach wie vor Gegenstand intensiver wissenschaftlicher Forschung. Die Komplexität des untersuchten Reaktionssystems ist hierbei gegenüber der Wasserstoffoxidation aufgrund verschiedener möglicher Reaktionswege deutlich erhöht.

Außer den erwähnten Aspekten der Reaktorsicherheit (Unterdrückung potentiell explosiver Homogenreaktionen in Methan/Luft-Gemischen) und der Aufklärung der bestimmenden Reaktionsmechanismen (katalytische versus homogene Reaktionen) wurde in der vorliegenden Arbeit die Bildung von Stickoxiden unter Hochtemperaturbedingungen untersucht. Da sich Stickoxide ausschließlich in homogenen Gasphasenreaktionen bilden, wurde hier insbesondere die Möglichkeit überprüft, durch geeignete Auslegung katalytischer Mikrokanäle die Bildung dieser unerwünschten und umweltschädlichen Nebenprodukte vollständig zu unterdrücken. Neben der Vermeidung von sogenanntem thermischem NO_x , d.h. Stickoxiden, die sich aufgrund der hohen Reaktionstemperaturen durch direkte Oxidation des Luftstickstoffs bilden, ist insbesondere die Unterdrückung von Prompt- NO_x in Mikroreaktionskanälen von Interesse, d.h. von Stickoxiden, die durch Radikalreaktionen aufgrund der Methanoxidation gebildet werden.

Als Simulationswerkzeug wurde das kommerzielle Softwarepaket CHEMKIN [31] verwendet, das eine Modellierung der Reaktionen und der Stoff-, Wärme- und Impulsaustauschvorgänge in der Gasphase und an der katalytischen Wand ermöglicht. In der verwendeten Software ist ein zweidimensionales Grenzschichtmodell implementiert, das die detaillierte Beschreibung der reaktiven Strömung im Reaktionskanal erlaubt. Im verwendeten Modell wird die Beschreibung der Strömung mit detaillierten Elementarkinetiken für die Reaktionen in der Gasphase und auf der Katalysatoroberfläche gekoppelt, was eine genaue Beschreibung der Wechselwirkung zwischen Reaktion und Strömung und insbesondere auch zwischen katalytischen Wand- und homogenen Gasphasenreaktionen ermöglicht. Die zur Simulation des gewählten Stoffsystems notwendigen thermodynamischen Daten und Transporteigenschaften wurden aus frei zugänglichen Daten-

banken (NASA, NIST) entnommen. Für die Beschreibung der homogenen Reaktionen wurde die homogene Elementarkinetik GRI-Mechanismus 3.0 [10] und für die katalytischen Reaktionen verschiedene Platin-Oberflächenmechanismen [13, 25, 27] verwendet und getestet.

Durch die in dieser Arbeit durchgeführten Untersuchungen konnte ein wesentlicher Einfluss der katalytischen Reaktionen auf das Gesamtreaktionsverhalten in Mikroreaktoren aufgezeigt werden. Die Unterdrückung homogener Reaktionen aufgrund der großen spezifischen Katalysatoroberflächen und der kurzen Transportwege konnte in Mikroreaktoren bis zu sehr hohen Temperaturen beobachtet werden. Die Konzentration von Radikalen in Mikroreaktionskanälen wird durch Radikaladsorptionsvorgänge mit der katalytischen Oberfläche signifikant verringert. Tatsächlich konnte gezeigt werden, dass Mikroreaktoren mit Kanaldurchmessern von $d < 200 \mu\text{m}$ das Potential besitzen, homogene Reaktionen bis zu Temperaturen von $T = 2000 \text{ K}$ vollständig zu unterdrücken. Daher kann für den technisch relevanten Temperaturbereich, der durch Material- und Katalysatorbeständigkeit der Reaktoren auf Maximaltemperaturen von $T \approx 1600 \text{ K}$ begrenzt ist, eine vollständige Vermeidung homogener Reaktionen und potentiell eine inhärente Sicherheit bei der Oxidation von Methan in Mikroreaktoren erreicht werden.

Des Weiteren konnte gezeigt werden, dass Transportlimitierungen innerhalb des katalytischen Kanals bei Reaktordurchmessern im Millimeterbereich auftreten. Tatsächlich werden für genügend hohe Temperaturen die Reaktionsraten der homogenen Reaktionen im Vergleich zu den Transportvorgängen zwischen Reaktorkern und Wand groß genug, so dass die homogene Zündung im Kern des Reaktors nicht mehr von katalytischen Reaktionen an der Wand beeinflusst wird. Die starke Beschleunigung homogener Reaktionen bei hohen Temperaturen ist hierbei begründet durch den sehr schnellen Zerfall von Methan in Radikale. Dessen Zerfallsprodukte werden jedoch in kleinen Mikrokanälen schnell absorbiert und dadurch explosives Verhalten und hohe Radikalkonzentrationen dadurch vermieden.

Um die Unterdrückung von homogenen Reaktionen für verschiedene Reaktionsbedingungen zu untersuchen, wurden Druck und Ausgangszusammensetzung am Eintritt des Reaktors variiert. Die Simulationsergebnisse zeigten hierbei, dass die Unterdrückung von homogenen Reaktionen bei veränderten Drücken und Eduktzusammensetzungen ebenfalls möglich ist. Insbesondere die Variation des Druckes hatte einen wesentlichen Effekt auf das Reaktionsverhalten, das mit größeren Drücken zunehmend durch homogene Reaktionen beeinflusst wird. Unterschiedliche Eduktzusammensetzungen hatten dagegen lediglich einen geringen Einfluss auf die Unterdrückung homogener Reaktionen.

In weiteren Simulationen wurden im Rahmen dieser Arbeit die Auswirkungen der Unterdrückung homogener Reaktionen auf die Stickoxidbildung bei der Methanoxidation untersucht. Durch die Dominanz katalytischer Reaktionen für Reaktionskanäle mit Durchmessern im Bereich von Mikrometern wurden Radikalkonzentrationen vermindert, die für die Initiierung des Prompt- NO_x Mechanismus eine wesentliche Größe darstellen. Daher konnte eine signifikante Verminderung

von Stickoxiden in Mikrokanälen bis hin zu hohen Temperaturen beobachtet werden.

Zusammenfassend kann festgestellt werden, dass Mikroreaktoren das Potential besitzen, homogene Reaktionen bei genügend kleinen Durchmessern effizient zu unterdrücken. Dies ermöglicht insbesondere einen sicheren Reaktorbetrieb auch unter extremen Bedingungen, wie z.B. hohen Temperaturen, ermöglicht. Zudem ist es in solchen Reaktoren möglich, die Bildung von Stickoxiden zu vermeiden, so dass Mikroreaktoren eine umweltfreundliche und sichere Variante für die Verbrennung von Kohlenwasserstoffen in dezentralen und mobilen Anwendungen darstellen.

Die Unterdrückung von homogenen Reaktionen kann prinzipiell ebenfalls bei Oxidationssystemen mit langkettigeren Kohlenwasserstoffen beobachtet werden. Die Untersuchungen könnten in zukünftigen Arbeiten auf komplexere Oxidationssysteme erweitert werden. Zudem ist die Unterdrückung von homogenen Reaktionen interessant in Systemen mit partiellen Oxidationsreaktionen, in denen dadurch die Selektivität von Zwischenprodukten erhöht werden könnte.

Um die Ergebnisse aus den Simulationen mit dem Grenzschichtmodell zu verifizieren, werden in zukünftigen Untersuchungen sowohl experimentelle Untersuchungen als auch numerische Methoden mit dem detaillierten dreidimensionalen Navier-Stokes Modell zum Einsatz kommen. Hierbei könnte in numerischen Untersuchungen insbesondere das Strömungs- und Mischungsverhalten in realen Reaktorgeometrien untersucht werden, um einen experimentellen Versuchsaufbau eines einfachen Mikroreaktors auf möglichst effizientes Mischungsverhalten der in den Reaktionskanal eintretenden Edukte hin zu optimieren.

Diese Simulationen könnten zusammen mit experimentellen Untersuchungen eines einfachen Mikroreaktionskanals dazu dienen, das beobachtete Unterdrückungsverhalten von Homogenreaktionen aus den Simulationen mit dem Grenzschichtmodell zu bestätigen. Einen weiteren, wichtigen Aspekt der zukünftigen Arbeiten würde zudem die gezielte Untersuchung von Oberflächenkinetiken bei der Wasserstoff- und Methanoxidation, ohne den störenden Einfluss homogener Reaktionen unter extremen Temperaturbedingungen darstellen.

2 Introduction

High-temperature catalytic reactions have been intensively studied for many decades due to their great industrial potential, such as in pyrolysis, total oxidation i.e. combustion and partial oxidation of hydrocarbons. In high-temperature catalytic systems, homogeneous reactions can occur in parallel to catalytic reactions, since temperatures are high enough to overcome activation energies of the homogeneous reaction pathway. The appearance of homogeneous reactions is usually an undesired feature because it complicates the understanding of catalytic reaction mechanisms, leads to selectivity losses and often to hazardous potentially explosive conditions. In fact, homogeneous oxidation reactions and thus explosion limits of oxidation systems are strongly affected by interaction with surfaces, in particular, if surfaces act as a catalyst. As a consequence, homogeneous oxidation mechanisms can strongly be affected by reactors with intensified influence of a present solid catalyst. In recent years, improvements of theoretical and experimental methods facilitated down-scaling of reactive systems to sub-millimeter dimensions and allowed to design and develop new miniaturized catalytic reactors with large catalytic surfaces compared to small reactor volumes.

Such small scale systems with characteristic dimensions in the micrometer range, show large potential both for scientific and industrial applications. Small dimensions not only lead to compact reactors, which are especially suitable for decentralized and mobile applications, but also to little reactor volumes and consequently to enhanced reactor safety [39]. Additionally, short transport ways result in fast mass and heat transfer compared to conventional reactors and improve both reaction efficiency and temperature control.

Most importantly, catalytic reactive systems with characteristic dimensions in the sub-millimeter scale can incorporate large surface-to-volume ratios. This is of scientific and industrial interest especially in the field of high-temperature catalysis, since catalytic walls in so called micro-reactors can be expected to suppress undesirable gas phase reactions. On the one hand, suppression of homogeneous reactions can be traced to a relative acceleration of catalytic reactions due to large catalyst surfaces compared to the gas volume, and ,on the other hand, to the quenching of radicals, i.e. absorption and conversion into products or recombination into reactants.

Quenching behavior due to catalyst surfaces is not only an important aspect concerning safety issues, but can also provide a scientific method to clearly distinguish between heterogeneous and homogeneous contributions in experimental investigation of catalytic oxidation systems.

This effect was first shown in previous studies by Veser et al. [11, 12, 35]. Hydrogen oxidation in air, a highly explosive system, was applied as a test reaction to show quenching effects in catalytic micro-channels. Results of experimental [11] and numerical [34] investigations validated that radical-wall reactions can lead to complete suppression and, therefore, to intrinsically safe reactors. Furthermore, these results revealed that inherent safety is strongly dependent on catalytic wall materials as well as on total pressure.

In the present work, the approach was extended to catalytic oxidation of methane in air under high temperature conditions. The influence of various parameters such as pressure, fuel content, and surface mechanisms on catalytic combustion of methane to water and carbon dioxide was investigated in detailed numerical simulations. C1 oxidation systems are of significant importance to the petrochemical industry and to power supply companies as well as still an important field of research. Compared to the hydrogen/air oxidation system, methane oxidation shows higher complexity and new aspects such as selectivity of reactions that must be taken into consideration. Beside the aspects of reactor safety, this work deals with formation of nitric oxides under high temperature conditions. Since nitric oxides exclusively form in homogeneous reactions, the possibility of NO_x suppression due to suitable channel dimensions was investigated.

In this study, simulations of reactive laminar flow in micro-channels were carried out based on a two-dimensional boundary-layer model including detailed descriptions of homogeneous and heterogeneous reaction pathways by elementary-step kinetics of surface and gas phase reactions. Explosion inhibition and NO_x quenching effects due to decreasing reaction channels dimensions could be observed and constitute a reliable basis for further experimental investigations.

3 Fundamentals

3.1 Process Intensification in High-Temperature Catalysis

During the last decades, process intensification has been a major objective in chemical engineering research. Increasing knowledge in the role of interactions between transport, thermodynamics and reaction in chemical processes enable industry to apply integrated and intensified process applications. Increased energy efficiency, product selectivity, waste reduction, safety improvement and miniaturization for flexible and mobile applications have been incentives for researchers to get a more thorough understanding of chemical processes. In recent years, scientists in the field of chemical engineering achieved to investigate molecular and microscopic behavior of chemical processes which facilitates understanding the complex macroscopic behavior of regarded systems. As previously mentioned, process intensification or integration can lead to simplified and highly efficient processes. In the field of thermal separation of liquid fluids, reactive distillation, i.e. a process with distillation and reaction in one unit, facilitates to combine separate unit operation steps, since thermal separation can be enhanced by reaction and vice versa in one apparatus. Moreover, due to higher selectivity and purity of the desired products, subsequent separation steps can be omitted. To design such processes, interaction between reaction, heat or diffusive transport, and thermodynamics has to be well understood and standardized design methods for process scale-up have to be developed [21].

High-temperature catalytic partial and total oxidation processes also show a large potential for intensification. Modern micro-fabrication techniques allow customized reactor design that can facilitate micro-scale reactor dimensioning. This enables research on small and highly efficient reaction systems. Understanding the complex interplay of surface and homogeneous reactions together with mass and heat transport represents the core issue in developing those reactors for various applications. Such reactors are in particular beneficial as they can increase the selectivity of catalytic reactions and suppress homogeneous reactions for the regarded oxidation systems. Homogeneous ignition is generally caused by the fast proceeding and high exothermicity of oxidation reactions as soon as certain temperatures are exceeded. In the following, thermal acceleration of kinetics and radical formation can lead to explosive runaway of a reactor and further to catalyst deactivation and reactor destruction or even pose a safety hazard.

As a consequence, both hot spots in catalytic reactors and fast radical formation must be avoided. By down-sizing reaction channels, heat and radical transport to the catalyst wall of a channel can be drastically improved. As previously shown in [34] for the hydrogen/air system, safe reactor operation over a wide range of conditions can be achieved by down-sizing the reaction channel to sub-millimeter dimensions for oxidation of hydrogen in air.

Such reactors with microscale channels, in this work referred to as micro-channel- or micro-reactors, offer a wide range of scientific as well as industrial applications. On the one hand,

reactions of gaseous fuels on various catalyst surfaces can be studied for extreme conditions, since homogeneous reactions can potentially be suppressed and do not influence the overall reaction behavior. On the other hand, micro-reactors could be utilized as mobile and decentralized devices due to their inherent safety and compactness [39], as for example in “on-site” energy production for decentralized natural gas sources such as coal mines, oil wells, and in particular biomass gas applications.

3.2 High-Temperature Catalysis and Catalytic Micro-Reactors

In general, catalysts are classically used to lower activation barriers for a certain reaction pathway so that a reaction can proceed more efficiently and faster than the uncatalysed reaction. In the study of heterogeneous catalysis, homogeneous pathways are often neglected, since low temperatures inhibit homogeneous reactions. For high temperature conditions, both heterogeneous and homogeneous reactions can contribute significantly and appear as competitive reaction pathways. To investigate the overall behavior of competitive homogeneous and heterogeneous paths, a thorough understanding of the respective oxidation systems has to be developed both for catalytic and homogeneous reactions. Therefore, experimental as well as theoretical methods have to be applied as described in Figure 1.

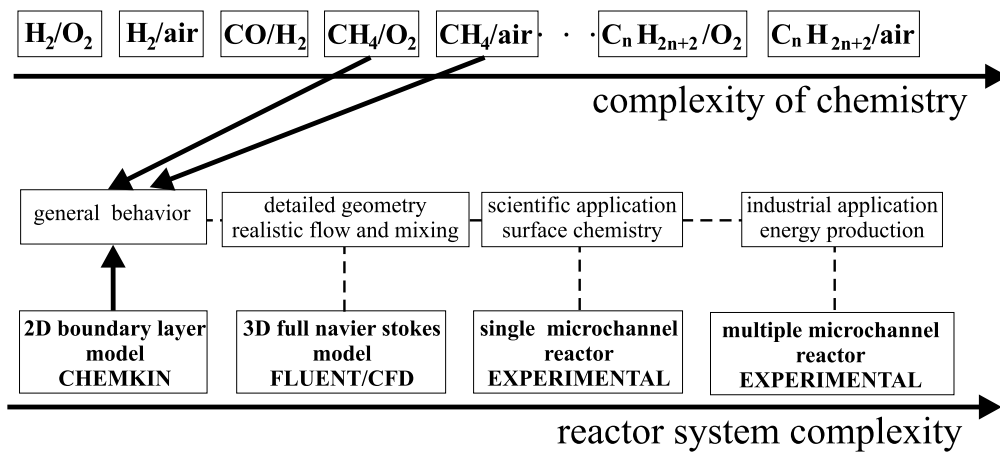


Figure 1: Schematic of research approach to investigate and develop catalytic micro-reactors for high temperature fuel gas combustion.

Dealing with high-temperature fuel oxidation, the complexity of the reaction behavior increases significantly from hydrogen over methane to systems with higher hydrocarbons as depicted in Figure 1. In general, oxidation reaction systems can be described by elementary-step reaction mechanisms. In these mechanisms, reaction sets of larger hydrocarbons incorporate elementary reactions of smaller hydrocarbons and the hydrogen oxidation subset [32]. The number of reactions thus increases significantly from hydrogen with 30 reactions and small hydrocarbons such

as methane to higher hydrocarbons with a few hundred steps. Likewise, the amount of possible reaction pathways increases and selectivities of certain reaction pathways play an important role. Furthermore, if air instead of pure oxygen is applied as an oxidant, nitrogen chemistry contributions are not negligible and thus have to be taken into consideration.

To obtain a thorough understanding, a crucial point in the field of fuel oxidation are detailed simulations, in particular, if both catalytic and homogeneous pathways are active in reactive flow systems. Since reactions are extremely fast, many occurring radical species or intermediate products only exist for a brief moment in time and thus cannot be detected by experimental methods. Detailed simulations with carefully developed and theoretically profound mechanisms reveal dominating reaction pathways and allow identification of key reactions and species for the ignition behavior of fuel oxidation in catalytic micro-channels. From the simplest possible boundary-layer model to investigate general reaction behavior, more detailed approaches with a full three-dimensional Navier-Stokes model have to be applied in order to account for real mixing and geometry effects of a specific reactor design.

Overall, a thorough understanding of ignition behavior in heterogeneous-homogeneous oxidation systems can only be achieved with experimental investigation in simple reactor setups in combination with numerical simulations with different model types. In further steps, complex and coupled multiple micro-channel reactors could be developed and applied for decentralized energy production.

3.3 Previous Work on Catalytic Micro-Reactors

In the past, numerous research groups have developed and investigated micro-chemical systems. Gas-phase reactions nowadays belong to the most frequently investigated processes in micro-structured reactors. Investigation of such processes is supposed to be advantageous if chemical reactions have high reaction rates with large heat release and involve multiple phases. This includes in particular oxidation reactions that are catalysed by a solid catalyst. Consequently, different reactor concepts have been developed in the past years to investigate high-temperature catalytic oxidation processes. Micro-fabrication techniques originated in the field of microelectronics have been used to manufacture microstructures on silicon wafers [39]. Different reactor setups such as multi-plate stack micro reactors in cross [20] and counter [37] flow configurations, single- [6] and multi-channel [33] chip reactors, miniaturized fixed- and packed-bed [36] reactors, and thin wire reactors [12] have been developed by various research groups.

Catalyst deposition is a particular challenging part in developing catalytic micro-channel reactors. In many micro-reactor setups, thin film coating and wash-coats as catalyst carriers have been used to deposit solid catalysts on the walls inside the micro-channel. Catalyst particle deposition has been carried out by wet chemical post-treatment, for example by impregnation via precursor solutions. In some applications, grain and powder beds have been employed as a solid catalyst

in micro-channels. This method revealed to be not very favorable, as high pressure drops result, the laminar flow pattern is changed in a way more difficult to describe by simulation, and it is difficult to generate these materials in a reliable manner. In order to solve the intricate problem of catalyst deposition in micro-channels, different techniques have been applied tailored to the specific problem with thin-film methods like chemical vapor deposition (CVD), aerosol techniques, sol-gel methods to be the most successful ones [39].

Although microscale catalyst deposition and fabrication of catalytic micro-channel reactors has been a challenging part in this field of research, many academic groups show first promising results and applications of micro-reactors for different oxidation systems. Partial oxidation, where the target or value product is supposed to be only partially oxidized, is the most frequently investigated class of reactions. Usually, partial oxidation reactions are highly exothermic and release large amounts of energy. In addition, total oxidation reactions act as side or consecutive reactions and further increase release of thermal energy which subsequently leads to lower target product selectivities as it enhances total oxidation. Since micro-reactor applications allow tailoring of residence times and offer enhanced heat transfer properties, high selectivities of target products could be achieved for different partial oxidation systems. It has been shown that micro-reactors allow safe processing of otherwise hazardous oxidations such as the partial oxidation of ethylene to ethylene oxide. In fact, the reaction enthalpy of the total oxidation of ethylene to carbon dioxide is more than ten times larger than that of partial oxidation, which induces locally very hot temperatures with corresponding negative consequences on the reaction course. Micro-reactors exhibited beneficial properties for the ethylene oxide reaction in particular concerning heat management which allowed safe operation in the explosive regime [14] and facilitates high ethylene oxide selectivities.

Another important aspect which leads to advanced features of micro-reactors is the high ratio of catalytic surface to the gas volume that allows safe reactor operation of potentially explosive total oxidation reactions due to radical quenching effects. Veser et al. performed micro-reactor simulations [34] and experiments [11] in a thin wire micro-reactor and proved complete suppression of explosive behavior due to radical quenching in the hydrogen/oxygen system.

Within the last years, various other groups have successfully applied different micro-reactors for chemical processing applications such as phosgene synthesis [36], hydrocarbon [33] and alcohol [6] dehydrogenation, and synthesis of different target products such as isoprene [37] and methane [16] by partial oxidation reactions. Overall, micro-reactors are increasingly studied by researchers and promise a variety of different applications. As they are compact and exhibit an intensification of heat and mass transfer as well as catalyst availability in the reaction zone, micro reactor processes feature better control of hazardous reactions and thus enhanced safety and target product selectivities.

3.4 Oxidation of Methane

In general, reactions occurring in high-temperature methane oxidation systems can be represented at different levels of complexity. Modeling typical high-temperature combustion processes requires a detailed understanding of the complex radical chemistry that is occurring in these systems particularly if catalytic surface reactions as well as homogeneous reaction contribute to the overall combustion process [17]. In recent years, researchers developed methods to investigate the intricate elementary chemical reaction processes which are occurring during homogeneous or catalytic ignition [32]. With regard to numerical modeling of fuel combustion, scientists developed advanced methods to solve highly non-linear equation systems that can be applied due to increasing computational power. A prerequisite for these models are, as previously mentioned, detailed mechanisms with elementary-step kinetics. In order to determine parameters of elementary-step kinetics for various temperatures, pressures and methane/oxygen ratios, experimental methods for estimation and measurement of elementary reaction rates even for rapid reactions with unstable almost undetectable species were developed [38]. Provided that a mechanism is carefully developed and validated, this modeling approach offers precise predictions for a wide range of conditions which could not be accomplished with a global reaction system or reduced mechanisms [32].

3.4.1 Homogeneous Oxidation

With regard to homogeneous combustion, methane is probably one of the most frequently studied hydrocarbon fuels, partly because it is the simplest hydrocarbon and partly because it is the main component in natural gas. As a consequence, detailed and reliable homogeneous methane oxidation mechanisms have been successfully developed in the past decades. Although the dominating mechanism for homogeneous methane oxidation shows numerous reaction pathways [32], ignition behavior of methane can be precisely determined dependent on the temperature and pressure regime. In contrast to heterogeneous mechanisms, homogeneous methane oxidation is comparatively well understood, since surface chemistry is far more complex and thus development of consistent and profound surface mechanisms has been carried out fairly recently. Modern hydrocarbon combustion mechanisms include nitrogen-cycle chemistry leading to nitric oxide formation and abatement [38]. There are a number of methane/air reaction mechanisms that have been developed [1, 17, 19], the most popular one being GRI-Mech [10] which was employed as homogeneous mechanism in this work.

The GRI-Mech is a compilation of 325 elementary chemical reactions and associated rate coefficient expressions and thermochemical parameters for the 53 species involved in them. The conditions for which the GRI-Mech was optimized are roughly 1000 to 2500 K, 0.01 to 10 bar, and equivalence ratio from 0.1 to 5 for premixed systems. It consists of all important steps to describe natural gas ignition including NO formation and reduction but it does not account for soot formation.

Homogeneous methane oxidation mechanisms such as the GRI-Mech are extremely complex and show various oxidation routes and thus typical reaction behavior of homogeneous methane combustion is explained and key reactions are identified and categorized in the present section. In general, homogeneous methane oxidation proceeds through different steps of radical formation and destruction in elementary reactions and can be classified in three different main reaction steps:

1. Initiation step:

Collision and reaction between reactants or decomposition reactions that form first radical species.

2. Chain-propagating or chain-branching step:

Collision and reaction between a radical and reactant species that form the same amount of radical species (chain-propagating) or increase the number of radicals (chain-branching).

3. Chain-terminating step:

Collision and reaction between radical species that deplete radicals and form stable products or recombine to initial reactants or intermediate products.

Homogeneous methane oxidation begins with radical production caused by initiation reaction steps. Once first radicals are formed, the chain-branching reactions proceed and create a radical pool. With time progressing, a critical amount of radicals is exceeded and thus a kinetic explosion can occur and creates larger numbers of intermediate and radical species. Finally, the oxidation concludes with domination of chain-terminating steps that form stable combustion products such as water and carbon dioxide. Explosive behavior, in general, is strongly dependent on the pressure, temperature regime and composition of reactants. Dependent on mass and heat transfer in the reactive zone, kinetic explosion can occur prior to thermal explosion and vice versa. Overall, explosive behavior can be characterized by high temperature rise and strong increase of radical concentration, whereas occurrence of thermal and kinetic explosion more or less proceed in parallel and often can not be separated. Nevertheless, radical formation and kinetic explosion constitute the main initiation processes for ignition in micro-structured systems with fast heat and diffusive mass transfer.

To exemplify the homogeneous combustion process of methane in air, a carbon reaction flux analysis of the GRI-Mech 3.0 [10] was performed and illustrated in Figure 2. High temperature and ambient pressure conditions were chosen as well as a stoichiometric ratio of methane in air. Since the overall reaction rate of molecular methane to the methyl radical is the fastest step ($r = 7.4 \cdot 10^{-7} \text{ mol/cm}^3\text{s}$), all following reactions were normalized with respect to this step.

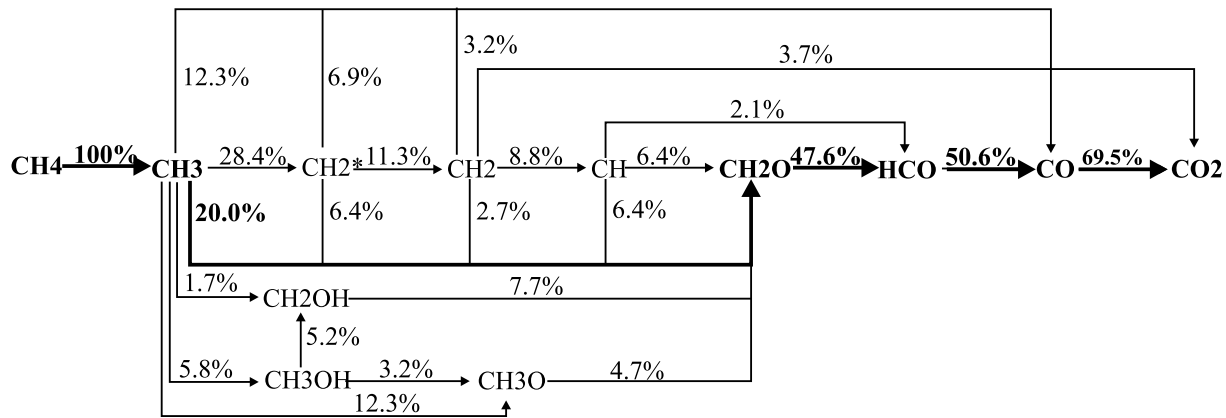


Figure 2: Reaction pathway analysis of carbon species flux (GRI-Mech 3.0 [10]) with an isothermal CSTR, residence time = 30 ms, T = 1400 K, p = 1 bar, stoichiometric ratio of CH_4 in air $\Phi = 1.0$, all fluxes are normalized with respect to $\text{CH}_4 \rightarrow \text{CH}_3$, fluxes smaller than 1.0 % are not shown.

Initiation of the oxidation process occurs through the following reaction



or at high temperatures, by



Subsequently, methane is consumed by abstraction reactions with the O/H radical pool:



The methyl radical (CH_3) formed in these reactions is the key species in methane oxidation as it is comparatively unreactive and stable and may build up in fairly high concentrations [32]. In the next reaction steps, methyl radicals are mostly converted into the molecular species formaldehyde (CH_2O) through the reactions:



Reaction VII occurs mainly at higher temperatures and depletes O/OH/H radicals from the O/H radical pool, as it is a chain-terminating step. Here, the following chain-branching reaction plays an important role, since it replenishes the O/H radical pool:



In further steps, reactions between formaldehyde and O/H radicals lead to the formyl radical (HCO), which subsequently dissociates thermally or reacts with oxygen to form carbon monoxide. In a last step, carbon monoxide forms carbon dioxide by reacting with molecular oxygen or oxygen radicals. The performed carbon flux analysis shows good agreement with corresponding literature, see Reinke et al. [24] and [32].

3.4.2 Heterogeneous Oxidation

A detailed, theoretically profound surface mechanism is a crucial part of any numerical investigation in catalytic methane combustion processes. Similarly to homogeneous combustion, development of surface mechanisms for catalytic combustion has been an important field of research for many years. As previously mentioned, homogeneous mechanisms are, in contrast to surface mechanisms, fairly better understood. In contrast to homogeneous chemistry, surface reactions exhibit a much more complex behavior. In fact, surface chemistry models have to account for adsorption and desorption, reaction and propagation behavior on the surface. In many cases, reaction behavior is strongly dependent on surface site characteristics that can for example be modeled as edge sites, threefold sites or even a simple catalyst molecule. Furthermore, surface coverage of different species can significantly influence the chemistry of catalytic reactions. In the study of catalytic partial oxidation of methane, Veser et al. proposed a close correlation between oxygen and carbon species coverages and hydrogen selectivity. In fact, detailed adsorption interactions and surface propagation behavior for a certain catalyst is extremely difficult to model in a generic and theoretically profound way. Additionally, homogeneous-heterogeneous interactions of reactions complicate experimental investigations and therefore parameters without homogeneous influence are difficult to obtain [32].

Nevertheless, research groups have improved theoretical as well as experimental methods to gain a more thorough understanding of the complex reaction processes on catalyst surfaces. Earlier modeling of methane oxidation on platinum used one-step or simplified chemistry models [29, 40] to describe surface reactions. Due to change in the rate-limiting step with temperature or composition in most catalytic oxidation systems [26], detailed surface reactions mechanisms for methane oxidation are essential to capture the underlying physics and develop predictive models for catalytic oxidation processes. Several surface reactions mechanisms have been proposed in literature [3, 5, 13, 25, 27]. Most of these mechanisms use many kinetic parameters obtained from independent surface science experiments. The remaining kinetic parameters have been tuned to fit

to general experimental results such as conversion or selectivity data, mostly for partial oxidation of methane under fuel rich conditions.

The surface mechanism mostly used in the present work by Aghalayam et al. [27] shows several advantages over other existing mechanisms. This mechanism was developed as a comprehensive set of elementary reaction paths on the surface. The authors ensured thermodynamic consistency in energetics of this mechanism and accounted for adsorbate-adsorbate interactions in the activation energies of all surface reactions. Various surface paths have been employed for methane decomposition by using experimental data sets of different reliable literature sources augmented by further experiments. To identify important reaction pathways, sensitivity as well as reaction pathway analysis have been performed. The used mechanism was extensively validated through comparison of predictions against redundant experiments over a wide range of operating conditions. It promises a potential of extrapolation towards high temperature conditions where no experimental data is available, since it was developed with a complete and elementary-step set of reactions similar to homogeneous mechanisms.

As done in the previous section for the homogeneous GRI mechanism, a carbon reaction flux analysis for the surface mechanism by Aghalayam et al. [27] was performed and depicted in figure 3. High temperature and low pressure conditions were likewise chosen as well as a stoichiometric ratio of methane in air. The methane adsorption step was used as a reference flux. All following reaction steps were normalized with respect to this reaction rate.

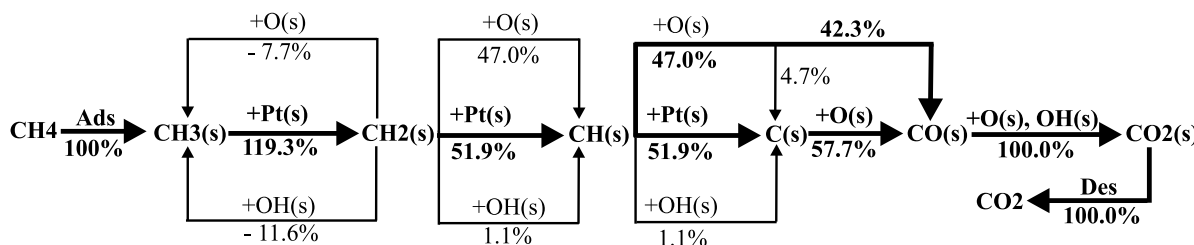
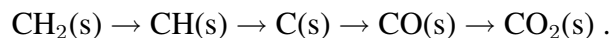


Figure 3: Reaction pathway analysis with an isothermal CSTR for the surface mechanism by Aghalayam et al. [27], residence time = 30 ms, T = 1400 K, p = 1 bar, stoichiometric ratio of CH_4 in air $\Phi = 1.0$, catalytic surface to volume ratio = 8 mm^{-1} , all fluxes are normalized with respect to $\text{CH}_4 \rightarrow \text{CH}_3$, fluxes smaller than 1.0 % are not shown.

The performed pathway analysis reveals the main oxidation path as well as the main interacting O/H surface species for chosen conditions. The selected surface-to-volume ratio as well as residence time corresponds to a tubular reaction channel with a diameter of $d = 500 \mu\text{m}$. Surface species are denoted by an appended (s). Obviously, the pyrolytic pathway dominates the surface reaction behavior for the first decomposition steps from $\text{CH}_4(\text{s})$ to $\text{CH}_2(\text{s})$. In the following, oxygen-assisted pathways gain more importance for the sequence



As shown in figure 3, the oxidation of CH(s) exhibits two different pathways via indirect oxidation with C(s) as intermediate species or by direct oxidation to CO(s). In fact, oxygen and pyrolytic pathways, as well as oxidation via OH(s) varies for different reactant compositions. Furthermore, OH formation occurs through both direct oxidation of adsorbed hydrogen on the surface and oxidation of hydrocarbon species [27]. In fact, the used mechanism incorporates coupling behavior of O/H and C/O chemistry and thus images a realistic picture of the real surface reaction steps, whereas other mechanisms uncouple these chemistry sets. Consequently, the Aghalayam mechanism realistically predicts oxidation behavior for different reactant compositions and surface coverages, where other mechanisms only consider the pyrolytic surface path.

3.5 NO_x formation

Emissions of nitrogen oxides from combustion systems constitute important environmental concerns. Since formation of nitric oxides (NO_x) in hydrocarbon/air systems is almost exclusively caused by oxidation of molecular nitrogen, NO_x may be controlled by modification of the combustion process. Nitrogen chemistry in combustion processes has been an important field of research and thus NO_x formation mechanisms have been studied intensely.

Five separate homogeneous mechanisms that can lead to the formation of nitric oxides in significant quantities have been identified. These include:

- Thermal NO formation
- Prompt NO formation
- NO formation through nitrous oxide (N₂O)
- NO formation through diazenyl (NNH)
- Fuel NO formation

The first four mechanisms are initiated by fixation of the molecular nitrogen contained in combustion air, whereas fuel NO formation occurs through oxidation of fuel-bound nitrogen. Since investigations in this work assume pure methane to be the only fuel reactant species, fuel NO formation will not be further described in this section. Moreover, relevant pressure and temperature ranges clearly favor NO formation through thermal and prompt NO routes. Nevertheless, NO production through diazenyl significantly contributes and its role in NO formation can therefore not be neglected. Overall, thermal, prompt and diazenyl pathways appear to be the main NO mechanism for high temperature and ambient pressure conditions. In this study, typical NO formation pathways, as described in this section, are incorporated in the GRI-Mech for methane combustion in air. To account for possible surface reduction of NO on platinum, NO surface reactions were extracted from a mechanism for oxidation of higher hydrocarbons with air by Chatterjee et al. [4]

(appendix A). In the following sections, the three relevant homogeneous mechanisms thermal, prompt, and diazenyl NO are described in more detail.

3.5.1 Thermal NO formation

Of the four mechanisms that involve fixation of N₂ from the combustion in air, the thermal NO or Zeldovich NO mechanism [41] is the most significant [32]. This pathway is the dominating source at high temperatures and relatively long residence times. It consists of the reactions:



The first step, IX, is rate limiting and has very high activation energies. In addition to availability of oxygen, the thermal mechanism thus requires high temperatures to be efficient. It occurs primarily in the post-flame zone, which is typically characterized by relatively high temperatures and fairly long residence times.

3.5.2 Prompt NO Formation

A second NO formation route in natural gas combustion is given by the prompt NO mechanism [2]. This formation pathway can be the dominating source of NO under conditions characterized by lower temperatures, fuel-rich conditions, and short residence times. Prompt NO formation is initiated by attack of CH_i radicals on N₂ forming hydrogen cyanide (HCN). Hydrogen cyanide is subsequently converted to N atoms through the sequence of steps:



The nitrogen atoms are then oxidized to NO by reaction with OH (XI). At lower temperatures the oxidation mechanism for HCN is more complicated, involving formation and consumption of a number of pollutant species including oxycyanides for example HOCHN, amines (NH_i), and nitrous oxide.

3.5.3 NO formation through Diazenyl

The diazenyl mechanism for formation of NO was discovered fairly recently [18]. The initiating step is the addition of a hydrogen atom to N₂:



Reaction XII is rapidly equilibrated at high temperatures. The diazenyl radical has a short lifetime and is almost completely recycled to N₂. However, a small fraction of NNH may react with oxygen atoms in the very fast reactions



Both imidogen (NH) and nitrous oxide may subsequently be oxidized to NO. This reaction mechanism is mostly active for fuel-rich systems in the presence of sufficient oxygen.

4 Numerical Simulation

4.1 Model Overview

Models of reactive flow in catalytic micro-channel reactors under high temperature conditions must incorporate convective and diffusive mass transport, energy transfer and as well image the interactions between homogeneous and surface reactions. Depending on the flow conditions, certain approximations and simplifications may be appropriate in representing the heat and mass transfer.

The most comprehensive models are based on solving complete Navier-Stokes equations, considering both axial and radial mass, momentum and energy transport. However, such models are computationally expensive, difficult to develop, and difficult to employ. Plug-flow models, on the other hand, are relatively simple to write and easily solved on a personal computer. Since no diffusive terms remain, the plug-flow equations form a differential-algebraic-equation (DAE) initial-value problem for the axial variation of the mean species composition. An intermediate alternative is to base models on the boundary-layer equations, wherein axial (flow-wise) diffusive transport is neglected, but detailed transport to and from the channel walls is retained. These models represent a very significant reduction in computational expense compared to a Navier-Stokes formulation, but an increase in computational expense relative to the plug-flow model and are applicable for laminar flow problems that are convection dominant into the main flow direction. Results of previous studies revealed that boundary-layer and Navier-Stokes models are in excellent agreement over a wide range of flow conditions [22] applied to typical oxidation problems. The plug-flow model, however, overpredicts conversion rates especially in case the catalytic reactions are mass transport limited [22]. In addition, since plug-flow models do not consider diffusion to and from the catalyst wall, they are not suitable for investigation of quenching effects in reactive tubular flow problems.

In general, the boundary-layer model offers a detailed image of transport and reaction interactions in reactive channel flow with a reasonable computational expense. Due to these features the boundary-layer model is well suited for studies of homogeneous and catalytic reaction interplay with a large number of different parameter combinations as done in this work.

4.2 Boundary-Layer Model

4.2.1 Assumptions

In general, boundary-layer models have been successfully applied to laminar, convection dominant flow problems for many different applications such as condensation and vaporization or heat transfer problems in flow over plain surfaces.

In this work, the boundary layer model (Figure 4) was employed as a two-dimensional approach

to image reactive channel flow facilitated by the given symmetry to the center line in a tubular reactor. In a boundary-layer approximation, effects of radial diffusion and dispersion of species, mass and energy are taken into account. To achieve high throughput and avoid back-mixing in a typical micro-channel oxidation systems, flow is usually set to high velocities. Short contact-times and therefore fast conversion rates in these intensified systems ensure complete conversion of the fed reactants in short micro-structured reactors. As a consequence, flow in micro-channel reactors are generally highly convection dominant ($\text{Pe} \gg 1$, see appendix B.3) in flow direction. Hence, diffusive heat and mass transport can be neglected in axial direction.

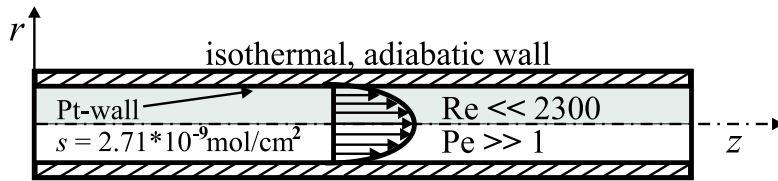


Figure 4: Schematic of a micro-reactor channel including main assumptions of the boundary-layer model.

Moreover, small dimensions of micro-channel flow lead to small Reynolds numbers and thus to laminar flow characteristics for a wide range of parameters. For detailed calculations of Reynolds numbers see appendix B.2.

In concept, ignition is typically a time dependent problem and therefore must be described with transient models. In reactive flow problems, temporal delay of ignition can be transformed into a spatial delay and thus a stationary flow problem can be solved to image a transient ignition problem. In fact, the applied model describes the system state at the exact moment of ignition and breaks down with time progressing because it does not account for axial heat transfer by the wall. In real reaction channels, heat transfer along the wall subsequently leads to upstream traveling of the ignition front in the channel. In the present work, wall boundary conditions were either set to isothermal or adiabatic wall behavior.

In our simulations, flow enters the channel in a fully developed parabolic velocity profile with uniform reactant composition. In real micro-channels, reactants are fed into the catalytic zone through separate inlet channels to avoid homogeneous reactions in the non-catalytic reactor inlet section. As a consequence, mixing in real micro-channels is one of the major issues, since in laminar flow problems mixing can only occur by diffusive transport. Hence, the applied model approximates ignition for ideal mixing conditions. Nevertheless, the applied boundary layer model is perfectly suitable to conduct general ignition studies in reactive micro-channel flow, but results have to be confirmed in future studies with full Navier-Stokes models for a detailed reactor geometry.

A multicomponent Stephan-Maxwell approach is employed to model diffusive transport in radial direction due to its higher accuracy compared to a mixture-averaged model.

Under applied high temperature and moderate pressure conditions, it can be assumed that the gaseous flow shows ideal gas behavior with good proximity and thus real effects of thermodynamic properties can be neglected. In addition, the ideal gas law is applied as equation of state (EOS).

Since surface reactions represent wall boundary conditions and these form a set of algebraic constraints, the equation system exhibits a differential index of one [9] and requires consistent initial values for the surface site fractions.

To simplify the numerical procedure, the boundary layer equations are recast using the von Mises transformation [7], in which the cross-stream coordinate is replaced by the stream function as an independent variable. The overall resulting equation system has to be solved simultaneously and is shown in appendix A and the CHEMKIN manual [31].

4.2.2 Physical Parameters

In the previous section, the used boundary-layer model was described and typical features of the model were explained. In order to apply the boundary-model on the specific methane combustion problem, physical parameters and parameter ranges have to be defined.

As a first parameter, the temperature was varied between $T = 750$ K and $T = 2500$ K. The lower limit was set to 750 K, as homogeneous as well as surface reactions are not in an ignited state and proceed very slowly. Limitations in convergence and validity of the surface mechanisms delimit the maximum temperature to 2500 K, whereas convergence could not be achieved at temperatures higher than $T \approx 2200$ K for micro-dimensions below $100 \mu\text{m}$.

In addition, typical channel diameters ranged from $50 \mu\text{m}$ to 10 mm, where the lower limit was determined by increasing pressure drop and practical limitations of micro-fabrication of reaction channels for experimental setups. The upper limit was given due to model limitations, as large diameters greater than 10 mm show Reynolds numbers near the critical value for turbulent channel flow of $Re_{crit} = 2300$.

Pressures values were chosen to investigate the relevant pressure range in future experiments. Furthermore, simulations have been carried out for different reactant compositions ranging from fuel-lean to stoichiometric concentrations of methane in air and oxygen.

The reactor length was adjusted to ensure complete conversion of reactants into products inside the modeled channel.

The wall is assumed to be a monolayer of polycrystalline platinum with a site density of $s = 2.71 * 10^{-9} \text{ mol/cm}^2$ [27].

Elementary-step kinetics are applied for homogeneous as well as surface chemistry which leads to 28 homogeneous and 11 surface species in 325 homogeneous and 53 surface reactions.

Initial surface coverages for 11 surface species at the inlet were calculated by a simple plug-flow model to provide consistent initial surface site fractions for the boundary-layer simulations.

4.3 CHEMKIN Software Package

The CHEMKIN software¹ was designed to facilitate the modeling of chemically reacting flow problems, especially those involving multicomponent molecular transport and elementary-step kinetics. It provides various software tools and different models that are mainly designed to solve reactive flow problems of gaseous mixtures such as high-temperature oxidation and chemical vapor deposition, see CHEMKIN Theory Manual [31].

The CHEMKIN 4.0 software package includes the following model approaches that were employed to investigate methane combustion in micro-channels:

- **Equilibrium:**

Software tool to calculate equilibrium state parameters and composition.

- **CSTR and batch reactors:**

The CHEMKIN 4.0 Software package includes various CSTR and batch reactor models for transient and steady state simulations.

- **Channel flow reactors:**

Channel flow models of different complexities from plug flow assumptions to two-dimensional boundary-layer models with two spatial coordinates.

In the present work, the described software modules of the CHEMKIN 4.0 software package were applied. To estimate equilibrium concentrations of reactive flow problems the Equilibrium module was used. The CSTR software tool [15, 28] provided data to analyze surface as well as gas phase methane oxidation mechanisms. The 2D boundary-layer model which was used for laminar channel flow calculations in reactive micro-channels is implemented in CHEMKIN's Chemically Reacting Shear-Layer Flow (CRESLAF) module [23].

4.3.1 Program Structure

Figure 5 shows a schematic of the CHEMKIN software application CRESLAF. CHEMKIN has a modular structure with accessible interfaces between the main program units. The CRESLAF module represents the core unit which incorporates the boundary-layer equations as well as the common PDE solver DASSL and the ODE solver TWOPNT. Thermodynamic and transport data of occurring species have to be specified in NASA standard compliant input files. Thermodynamic data are given as polynomial fits to temperature for species enthalpy, entropy, and heat capacity. From these parameters, species thermodynamic properties, thermal transport properties, and reaction equilibrium constants are calculated by the CHEMKIN pre-processor. Convective

¹ CHEMKIN was developed at Sandia National Laboratories and an open source project for many years. Since 1996 CHEMKIN has been distributed and supported commercially by Reaction Design, Inc. (San Diego, CA).

and diffusive transport properties such as thermal conductivity, viscosity and binary diffusion coefficients for gaseous radical and molecular species are determined by the Dixon-Lewis theory [8] from detailed molecular parameters such as Lennard-Jones potentials, collision diameters, and dipole moments. Likewise, the CHEMKIN pre-processor a priori calculates polynomial fits for the temperature-dependent parts of the kinetic theory expressions for the transport properties to maximize computational efficiency. In general, the pre-processor is structured to do a large portion of the transport and thermodynamic data calculations outside the core unit CRESLAF.

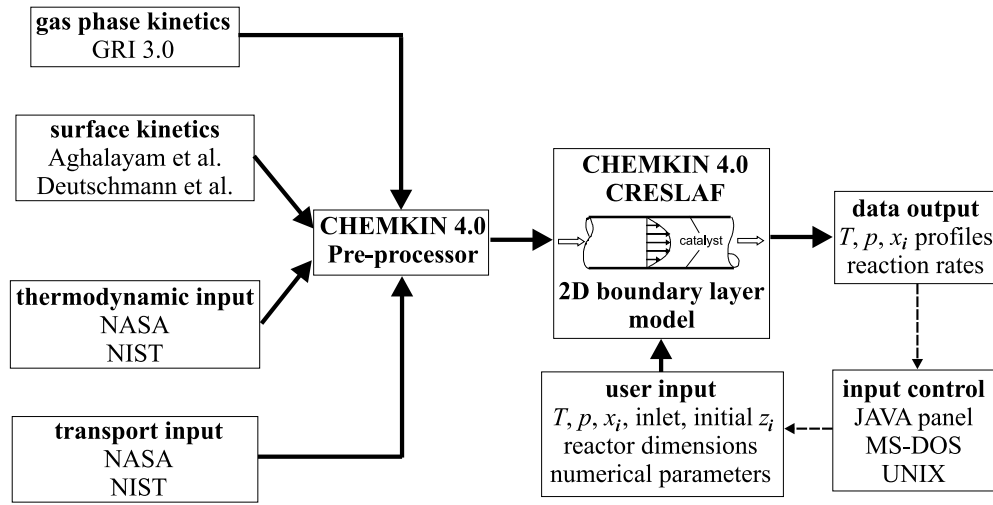


Figure 5: Structure of software package CHEMKIN 4.0 for reactive flow simulations of methane oxidation with the CRESLAF module.

In addition, gas phase chemistry and surface chemistry files are required input for the CRESLAF module. Kinetic input files are likewise pre-processed and stored in linking files so that easy accessibility is customized for the main solver.

User related input information like numerical parameters, state variables, inlet conditions, reactor dimensions and initial surface site fractions are provided in a standardized input file.

In a standard simulation run TWOPNT solves an ODE system to determine consistent initial surface site fractions with initial user provided guesses as a starting point. In case consistent values for the reactor inlet are found, the PDE solver DASSL subsequently solves the equation system with given relative and absolute tolerances in an adaptive process in axial direction using the method of lines. Species, temperature, pressure and reaction rate profiles are perpetually stored into output files.

The CHEMKIN software package can be fully controlled by a UNIX or MS-DOS terminal and additionally provides a JAVA panel to specify input and process output data.

In this work, CRESLAF was embedded in an algorithm consisting of C-programs and shell-UNIX and batch-MS-DOS scripts to conduct automated simulations due to the large number of parameter combinations.

4.3.2 Numerical Parameters

As mentioned in the previous section, the CRESLAF module incorporates the advanced PDE solver DASSL together with TWOPNT, a common ODE solver, to determine consistent initial values of surface site fractions. In order to optimize convergence and accuracy of reactive channel flow simulations, different numerical parameters are adjustable for the specific problem. The axial grid point distance is determined by an adaptive algorithm which adjusts the step size to meet previously defined absolute and relative tolerances which were chosen as $t_{abs} = 10^{-6}$ and $t_{rel} = 10^{-3}$. Lower tolerances were chosen for the calculation of small radical or molecular species. In radial direction, transport and reaction are approximated by a fixed grid with adjustable non-uniform gridpoint distribution as an additional feature. The radial grid point distribution was set to 40 gridpoints with a higher grid density at the catalytic wall. The influence of numerical parameters on simulation results was tested and accuracy was set sufficiently high to exclude effects of numerical parameters on obtained solution profiles.

Simulations were conducted on a 2.6 gHz Pentium personal computer, whereas typical integration times varied between 1 and 10 minutes for a single run dependent on accuracy, physical and numerical parameter and the used mechanisms.

5 Results

In previous studies, simulations [34] as well as experiments [11] revealed quenching effects and complete suppression of homogeneous reactions for the hydrogen oxidation system. As exemplified in chapter 3, the methane oxidation system shows a similar potential for quenching of homogeneous explosions and suppression of environmentally harmful NO_x species by down-sizing channel diameters.

In the present chapter, simulation results of methane oxidation in air and oxygen are illustrated. Section 5.1.1 deals with homogeneous-heterogeneous interactions and consequences on ignition behavior. Size-effects on ignition due to reduction of diameters are exemplified in section 5.1.2. In the following sections, transition of ignition behavior is explained from lower to intermediate temperatures with dominant heterogeneous surface reactions (section 5.1.3) and for intermediate to higher temperatures with strong influence of the homogeneous mechanism (section 5.1.5). Explanations for the distinctive influence of homogeneous reactions at temperatures above $T \approx 1800$ K are given in section 5.1.4. In addition, effects of pressure (section 5.1.6), reactants composition (sections 5.1.7), and different thermal wall conditions (section 5.1.8) are illustrated. Section 5.1.9 shows a comparison of quenching effects for two different surface reaction kinetics.

Size effects on NO formation of the methane/air oxidation are discussed in section 5.2.

5.1 Oxidation of Methane

In principle, methane oxidation can be performed through either the homogeneous oxidation pathway or by catalytic combustion. At sufficiently high temperatures, formation of a radical pool can cause homogeneous ignition of fuel/oxygen mixtures even though surface reactions are likewise active. Under these conditions, homogeneous and catalytic pathways can become competitive. To investigate interaction of homogeneous and catalytic reactions in tubular flow configurations, simulations have been conducted with both homogeneous and catalytic elementary-step kinetics under high temperature conditions.

Experimental methods to investigate either homogeneous or heterogeneous contributions to the overall conversion are limited in real micro-reactor configurations with fast oxidation reactions. Numerical simulation with detailed elementary-step kinetics opens up new possibilities for investigation of high temperature oxidation processes, since catalytic and homogeneous contributions can clearly be identified in simulation results.

Detailed laminar channel-flow simulations have been conducted for various conditions together with CSTR pathway analysis. Ignition behavior due to homogeneous or catalytic reactions could be investigated and the detailed reaction path could be revealed. To clarify homogeneous and catalytic contributions to the overall oxidation process, both simulations with an inert wall and pure catalytic simulations without the homogeneous mechanism have been carried out and compared

to simulations with a fully coupled homogeneous and heterogeneous reactive system. This, in particular, is a major advantage of numerical simulation, since transition from catalytically to homogeneously dominated behavior can be qualitatively and quantitatively observed by determining contributions of either pathway.

5.1.1 Ignition behavior

As explained in chapter 3, homogeneous ignition can be categorized into the main steps initiation, chain-propagation and -branching, and chain-termination. Initiation, chain-propagation and -branching subsequently lead to a strong increase of radical concentration and possibly to kinetic explosion. In oxidation systems, ignition is delayed due to the time that is required to form a certain critical amount of radicals, the so-called radical pool. Ignition delay leads to an ignition point further downstream the channel, where the fuel is combusted very rapidly (figure 6).

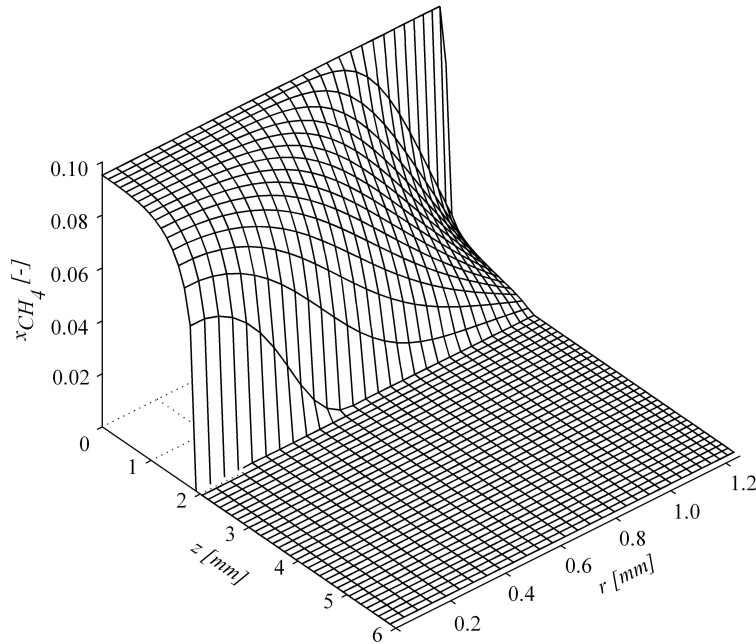


Figure 6: Methane concentration profile of a 2.5 mm catalytic reactor at $T = 1650$ K, $p = 1$ bar and stoichiometric ratio of CH_4 in air $\Phi = 1.0$. $r = 0.0$ mm marks the center line of the reactor.

In laminar channel flow with a constant flow velocity v a temporal ignition delay t_{ign} can be transposed into a spatial ignition distance X_{ign}

$$X_{ign} = v * t_{ign}. \quad (1)$$

In this work, ignition distance X_{ign} is defined as the distance between the channel inlet to the point

within the reactor where 50% of methane is converted at the center line of the channel. Thereby, ignition delay of homogeneous reactions can be determined with good proximity, since homogeneous reactions lead to a fast depletion of methane after ignition. In case catalytic reactions dominate the reaction behavior, the delay in methane conversion is mainly caused by transport of methane and products from the channel center to the wall and vice versa, as catalytic reactions are ignited without delay at the channel entrance for investigated temperature conditions. As soon as temperatures become high enough to overcome activation energies of radical formation reactions, homogeneous influences accelerate methane conversion at the center line and lead to a strong shortening of ignition distances. Therefore, the chosen definition of ignition distance can be used as an indicator for homogeneous effects in a catalytic micro-channel.

Figure 7 shows ignition distance as a function of temperature for three different cases in a 2.5 mm channel. To identify contributions of the homogeneous reactions versus surface reactions, simulations with homogeneous reactions only and catalytic reactions only are used as reference cases and compared to the coupled case in figure 7.

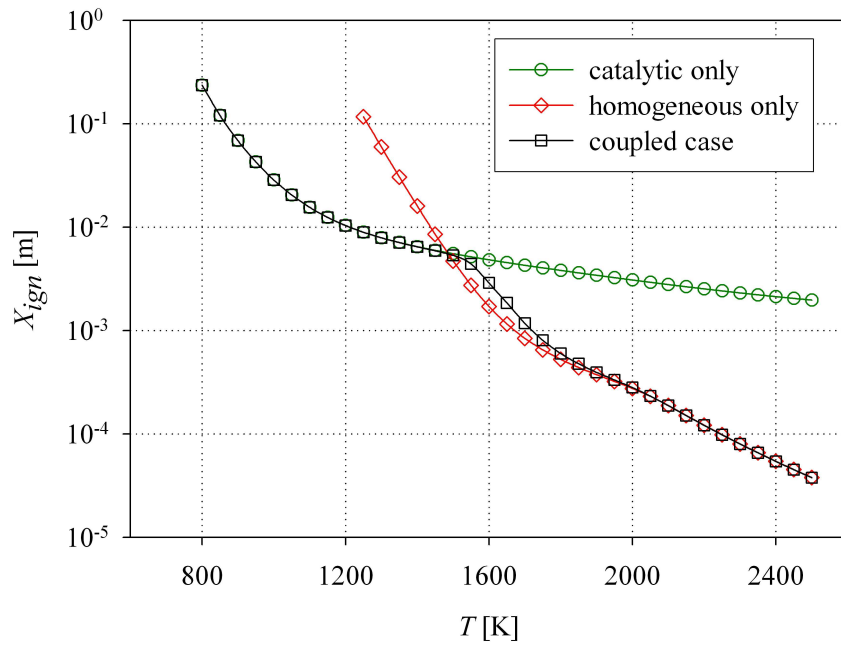


Figure 7: Ignition distance at the center line versus temperature for channel with $d = 2.5$ mm, $p = 1$ bar and stoichiometric ratio of CH_4 in air $\Phi = 1.0$ for the three different cases with coupled mechanism compared to inert wall and pure catalytic case.

Circles represent the pure catalytic case, diamonds the inert wall case, and squares the fully coupled case with combined heterogeneous and homogeneous reaction behavior. Since ignition distance values decrease by orders of magnitude from centimeter to micrometer range with increasing temperature due to exponential temperature dependence of chemical reactions, ignition distance is plotted in a logarithmic scale.

In general, ignition distance for the coupled case can be divided into three sections. For lower temperatures smaller than 1450 K, ignition distances of the coupled case are identical with the pure catalytic case. Due to their smaller activation energies, heterogeneous reactions dominate over homogeneous reactions for these temperature conditions.

The regime between 1450 and 2000 K marks a transition area where both mechanisms contribute significantly to the overall reaction behavior. Homogeneous reactions strongly decrease ignition distance for temperatures higher than 1450 K, since radical initiation step reactions are fast enough to form a radical pool and lead to homogeneous ignition. However, this transition area is likewise influenced by surface reactions. Radicals are adsorbed and converted into products or recombined into reactants on the catalyst surface next to the wall. In fact, surface radical adsorption reactions delay homogeneous ignition to larger distances for the coupled case compared to the inert wall case.

For high temperatures, homogeneous reactions dominate ignition behavior, since curves of the coupled case and the inert wall case merge at about 2000 K. Transport of radicals to the wall is relatively slow compared to the very fast homogeneous reactions so that radical quenching effects by the wall can no more influence homogeneous reactions at the channel center line. A detailed description of this behavior is given in section 5.1.4.

Overall, the ignition curve for the coupled case shows a low-temperature regime with catalytic domination, and a high-temperature regime with strong homogeneous influence up to complete domination of ignition, and a transition regime where both pathways considerably contribute.

5.1.2 Size Effects in Micro-Channel Reactors

Reduction of channel size can lead to large surface-to-volume ratios and therefore to a strong increase of the available catalyst surface in tubular reactive flow channels in combination with intensified transport conditions. To exemplify characteristic behavior of ignition with increasing surface-to volume ratios, diameters of reactor channels were varied between 50 μm and 10 mm. Figure 8 shows ignition distance versus temperature for six different diameters between 75 μm and 4 mm. For millimeter diameters, ignition curves show qualitatively the same behavior as described in figure 7, i.e. they show two distinctive branches for higher and lower temperature.

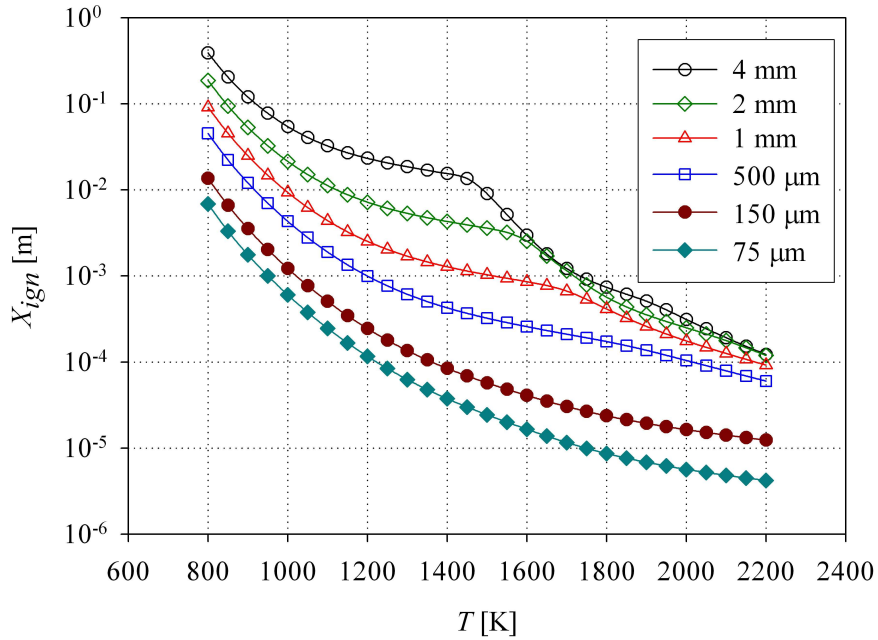


Figure 8: Ignition distance at center line versus temperature for channel diameters between $d = 75 \mu\text{m}$ and $d = 4.0 \text{ mm}$, $p = 1 \text{ bar}$ and stoichiometric ratio of CH_4 in air $\Phi = 1.0$.

In the catalytically dominated regime, strong size effects can be noticed, since ignition distances become significantly shorter for decreasing diameters, whereas homogeneously dominated high temperature branches differ slightly. In addition, a shift of the transition point from low to high temperature branches can be observed: It becomes less pronounced, moves to higher temperatures with decreasing diameters, and apparently disappears for $150 \mu\text{m}$ and $75 \mu\text{m}$ channels.

Two major effects lead to the apparently strong shortening of ignition distances in conjunction with a shift of the transition point from catalytically to homogeneously dominated regimes with decreasing diameters. As a fact, the surface-to-volume ratio plays an important role and scales with $1/d$:

$$A_v = \frac{A_{cylinder}}{V_{cylinder}} = \frac{\pi dl}{\frac{\pi}{4}d^2l} = \frac{4}{d}. \quad (2)$$

This leads to progressively larger numbers of available surface sites as well as to shorter transport paths for radical species and reactants between the channel center and the catalytic wall in smaller reactors. Therefore, both conversion of reactants can be significantly accelerated and radical quenching behavior can be enhanced by down-scaling of the reactor channel. It can be expected that concentration of radicals are considerably reduced by quenching effects through reduction of channel size which is investigated and depicted in the following paragraphs.

To observe qualitative change in reaction behavior for decreasing diameters, concentration profiles

of methane and hydrogen radicals are pictured in figure 9 for three different diameters 2.5 mm (upper), 1.0 mm (middle), and 500 μm (lower). The left plots show CH_4 concentrations whereas the right plots illustrate the H radical concentration.

For a 2.5 mm reactor, catalytic reactions at the wall immediately start at the channel inlet and lead to a strong decrease of methane concentration next to the wall. Due to the depletion of methane at the wall, a concentration gradient develops that causes diffusive transport of methane from the region between channel center and wall so that further methane from the channel core is converted into products by catalytic wall reactions. However, the center of the reaction channel remains relatively unaffected by catalytic reactions and thus a radical pool is formed by homogeneous reactions. As soon as a critical amount of radicals is formed at approximately $z = 2.0 \text{ mm}$, homogeneous reactions proceed rapidly and deplete remaining methane.

The concentration of H radicals appears as an expressive indicator of homogeneous reactions. In the upper right plot, a sharp peak of H radicals to fairly high concentrations can be observed in particular at the channel center. Obviously, as expected from ignition distance curves in figure 8, a 2.5 mm channel exhibits a fast acceleration of methane conversion due to homogeneous reactions for $T = 1650 \text{ K}$. Concentration plots for a 1.0 mm channel show an evident alteration of concentration profiles. Steep methane or hydrogen radical concentration gradients at the center line cannot be observed and H radical concentrations are reduced by two orders of magnitude. Hence, the influence of catalytic wall reactions leads to reduction of radical concentration for the investigated millimeter scale channel.

However, H radicals at the reactor center indicate homogeneous influence which is further abated for a channel diameter of 500 μm . In fact, H radicals are almost completely suppressed and show numerically insignificant values. The methane concentration profile further indicates a clear domination of catalytic reactions, since methane is consumed within a distinctively shorter distance across the entire channel radius.

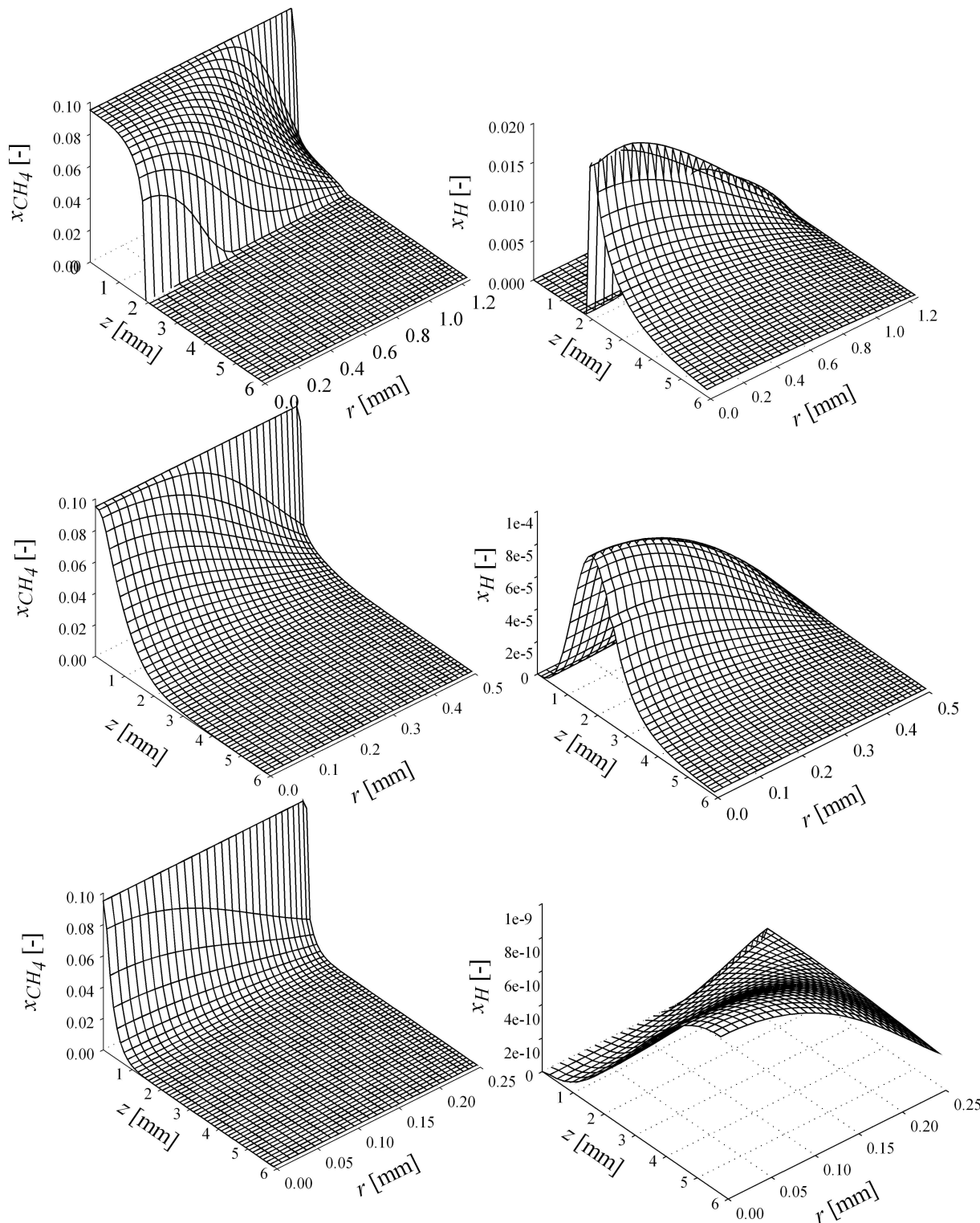


Figure 9: CH_4 (left) and H radical (right) concentration for three different diameters $d = 2.5 \text{ mm}$ (top), $d = 1.0 \text{ mm}$ (middle) and $d = 500 \mu\text{m}$ (bottom), $T = 1650 \text{ K}$, $p = 1 \text{ bar}$, and stoichiometric ratio of CH_4 in air $\Phi = 1.0$.

Hydrogen radical concentration indicates homogeneously influenced ignition and in particular exhibits explosive behavior, in case hydrogen radicals build up substantially. To further investigate the connection between radical concentration and homogeneous reactions, the maximum hydrogen radical concentration is imaged as a function of diameter and temperature in figure 10. Hydrogen concentration shows a plateau of fairly high H radical concentrations for large diameters and high temperatures which indicates ignition of homogeneous reactions. For decreasing diameter and temperature, the maximum H radical concentration shows a steep drop to distinctively lower values. This indicates, that in channels with micrometer dimensions formation of radical species and thus homogeneous reactions can be effectively suppressed. The influence of homogeneous reactions diminishes with decreasing diameters so that significant build-up of radicals and thus transition to homogeneous ignition subsequently requires higher temperatures. For channel diameters of $d \leq 100 \mu\text{m}$, no significant H radical concentration is formed for the complete relevant temperature range.

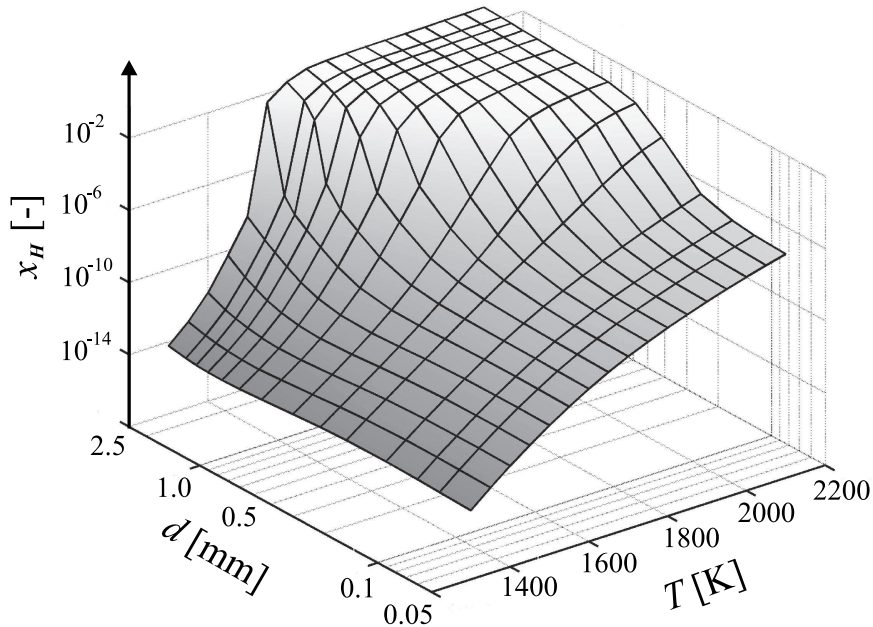


Figure 10: Maximum hydrogen radical concentration as a function of temperature and diameter.

To further explain and quantify observed quenching of homogeneous ignition due to size reduction of reactor channels, ignition distance values of the coupled case for diameters between $50 \mu\text{m}$ and 2.5 mm are compared with corresponding results of inert wall and pure catalytic simulations. The following figure 11 depicts ignition distance as a function of temperature and diameter for the coupled compared to pure catalytic (left) and inert wall behavior (right). Ignition distance of the coupled case shows, as previously explained in figure 8 a low temperature area where

catalytic reactions dominate and a high temperature area with strong homogeneous influence. Domination of catalytic behavior at lower temperatures is clearly confirmed in the left graph of figure 11, since the pure catalytic area exactly agrees with the ignition distance area of the coupled case for low temperatures. For larger diameters and higher temperatures, ignition distances of the two cases differ significantly and thus homogeneous influence on the ignition behavior is clearly visible. The transition point, where homogeneous reactions show first effects on ignition distances for increasing temperature, is defined as transition temperature T_{tr} . Following the plot to smaller diameters, T_{tr} shifts to higher temperatures and disappears at $d \approx 150 \mu\text{m}$ for investigated maximum temperatures of $T = 2200 \text{ K}$. In addition, a strong shortening of ignition distances is observable in the same region due to an increase of the specific surface and shorter transport ways with decreasing diameters.

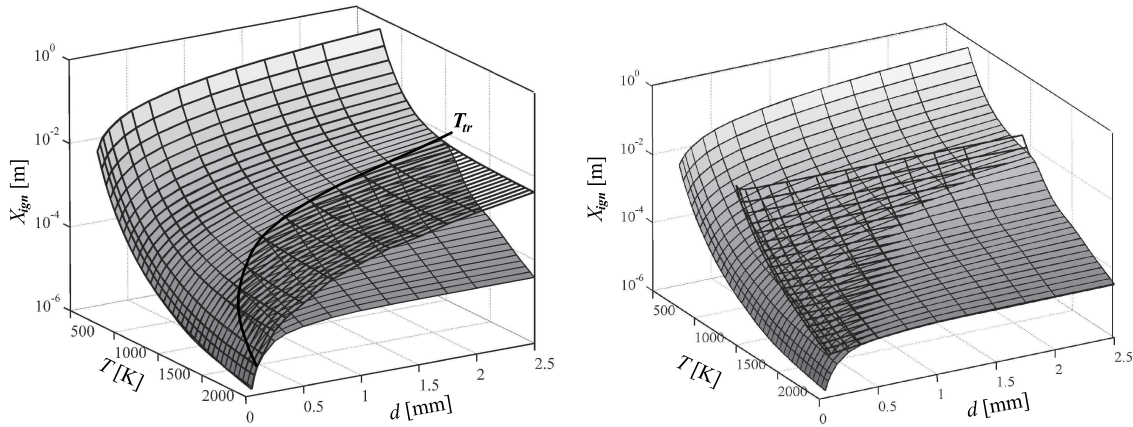


Figure 11: Ignition distances at the center line versus temperature and diameter for channel diameters between $d = 50 \mu\text{m}$ and $d = 2.5 \text{ mm}$, $p = 1 \text{ bar}$ and stoichiometric ratio of CH_4 in air $\Phi = 1.0$. The left plot shows a comparison of ignition distances for the fully coupled mechanism with pure catalytic simulations, whereas the right graph compares the heterogeneous-homogeneous mechanism to inert wall behavior.

In the comparison of inert wall versus coupled case in figure 11, the same behavior is reflected, i.e. strong size effects and therefore an enhanced impact of the catalytic mechanism for small diameters can be noted. Obviously, ignition distance values of the inert wall case exhibit little dependence on channel size.

5.1.3 Low-Temperature Transition Point

As exemplified in the previous section, the transition point or temperature, where homogeneous reactions begin to have a substantial influence on the ignition behavior, shifts towards higher temperatures with decreasing diameters and apparently disappears for diameters smaller than $150 \mu\text{m}$. In order to quantitatively determine transition temperatures for different diameters, values of

ignition distances of the coupled and the pure catalytic case are compared by calculating relative deviations as pictured in figure 12. Following equation is employed to calculate relative deviation D between ignition distance of the coupled case X_{ign} and the pure catalytic case $X_{ign,cat}$:

$$D = \frac{X_{ign,cat} - X_{ign}}{X_{ign,cat}} \quad (3)$$

in which the relative deviation D is given in percent. Calculation of deviation for $T = 800 - 2250$ K has been performed for diameters between $50 \mu\text{m}$ and 4 mm. Since ignition distances are determined by simulations for discrete temperature steps of $\Delta T = 50$ K, cubic spline interpolation was applied to interpolate intermediate ignition distance values in between two simulation points using MATLAB². Calculations of relative deviation for low temperature branches exhibit an average value of $\hat{D} \approx 0.3\%$ and a maximum deviation of about $D_{num} \approx 0.5\%$ due to numerical inaccuracies.

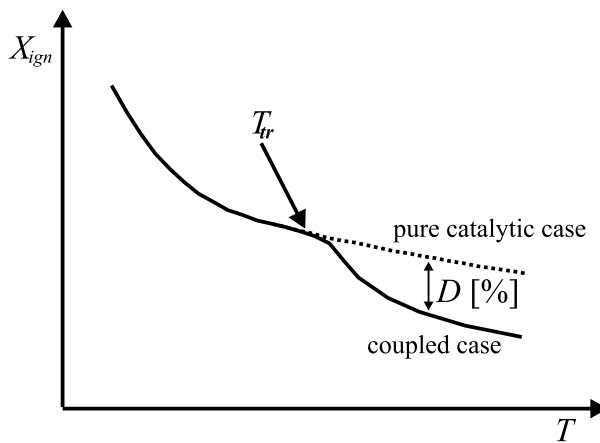


Figure 12: Schematic of transition temperature calculation between ignition distances of the pure catalytic and the coupled case.

To set a criterion for homogeneous influence on ignition, a minimum deviation was chosen as $D_{min} = 1.0\%$ to determine transition temperature. This corresponds to twice the maximum value $D_{num} = 0.5\%$ to safely exclude influences by numerical inaccuracies. In the following, calculated transition temperatures can be used to quantitatively clarify influence of diameter on ignition behavior and compare transition temperatures for different conditions such as pressure, inlet composition or even surface mechanisms.

In Figure 13 transition temperatures T_{tr} are displayed as a function of diameter on a linear scale (left) and a logarithmic scale (right). The left graph shows a steep increase of T_{tr} with smaller diameters from approximately 1400 K for a 4.0 mm diameter to 2200 K for a $50 \mu\text{m}$ channel. Obviously, both graphs demonstrate exponential dependence of diameter and transition temperature.

² Numerical software tool, Math Works Inc., Natick, Massachusetts, USA.

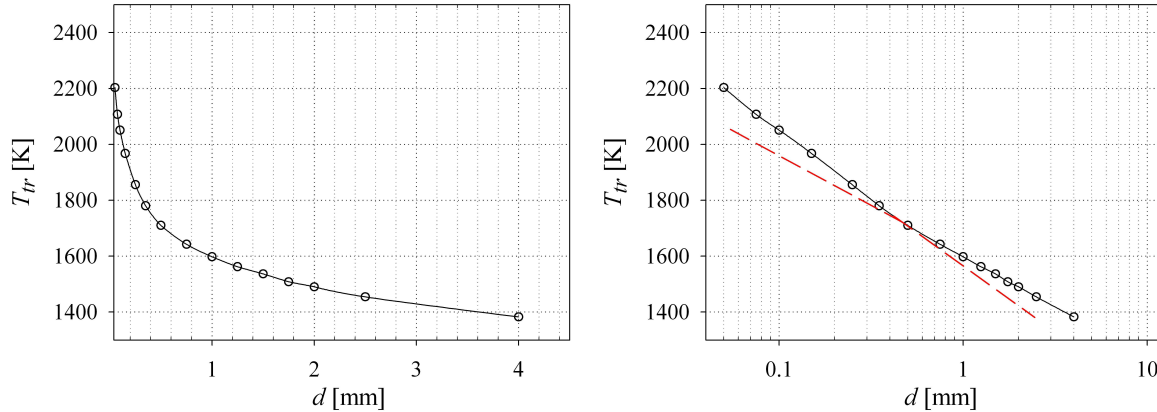


Figure 13: Transition temperatures versus diameter for transition from heterogeneously to homogeneously dominated behavior for $p = 1$ bar and stoichiometric ratio of CH_4 in air $\Phi = 1.0$. Left graph shows linear curves, right graph shows logarithmic diameter axis.

A more detailed analysis of the logarithmic curve shows that it actually consists of two straight lines with a transition point at about $d = 300 \mu\text{m}$, where the line for larger diameters has a smaller gradient than the line for small diameters. This transition at diameters of $d = 300 - 400 \mu\text{m}$ is caused by the effect of increasing number of surface sites in conjunction with significant shortening of transport ways that could already be observed in the previous section (figures 8, 9, and 11). For decreasing diameters the gradient of T_{tr} becomes steeper across the transition point and reveals that catalytic reactions increasingly gain influence for smaller reactor dimensions. In fact, for reactor channels of about $d = 100 \mu\text{m}$ homogeneous reactions can be suppressed up to temperatures above 2000 K. Consequently, as an experimental setup can be operated up to a maximum temperature of about 1600 K due to thermal expansion mismatch of reactor material and catalyst as well as possible melting of platinum thin films or agglomeration of catalyst particles, homogeneous reactions are suppressible for the entire technically relevant temperature range. However, complete quenching of homogeneous reactions cannot be observed, since this would imply a change to infinitely large gradients. In fact, homogeneous influence can be seen even for very small diameters of $d \approx 50-100 \mu\text{m}$ although transition temperatures become considerably high.

5.1.4 High-Temperature Transition Point

As explained in section 5.1.1, ignition behavior for catalytic channels in general consists of three main regimes for varying temperature: A low temperature regime where catalytic reactions are predominant, a high temperature regime with prevailing homogeneous reactions, and a temperature range in between in which both reaction pathways are active and compete. The first transition was discussed above in the previous section 5.1.3.

The second transition point can in particular be observed for large diameters as depicted in figure 14. The graph displays ignition distance curves for the coupled case in the intermediate temperature regime where heterogeneous and homogeneous reaction pathways act competitively.

Size effects can be observed, since for decreasing diameters, ignition distances become significantly shorter. For increasing temperatures, curves for different diameters progressively merge into one curve. The first ignition curve with a diameter of $d = 8$ mm becomes identical with the 10 mm curve at approximately 1750 K, while the curves for smaller diameters merge in the order of decreasing diameters at 1850 K ($d = 6$ mm), 1950 K ($d = 4$ mm), and 2200 K ($d = 2$ mm). In fact, since ignition distances are defined and calculated as 50 % conversion of methane at the center line, ignition behavior in the reactor core apparently becomes independent of catalytic wall reactions.

This wall independence appears to be caused by transport limitations. Surface reactions can apparently no more influence the reaction behavior at the center line for reaction channels in the millimeter range if a certain temperature is exceeded. For channel diameters of $d < 2$ mm down to microscale channels as previously shown in figure 8, ignition distance becomes significantly shorter over the entire investigated temperature range between 750 K and 2200 K. Consequently, channels with relatively small diameters $d < 2$ mm show influence by surface reactions for temperatures in which mechanisms are still valid ($T < 2500$ K).

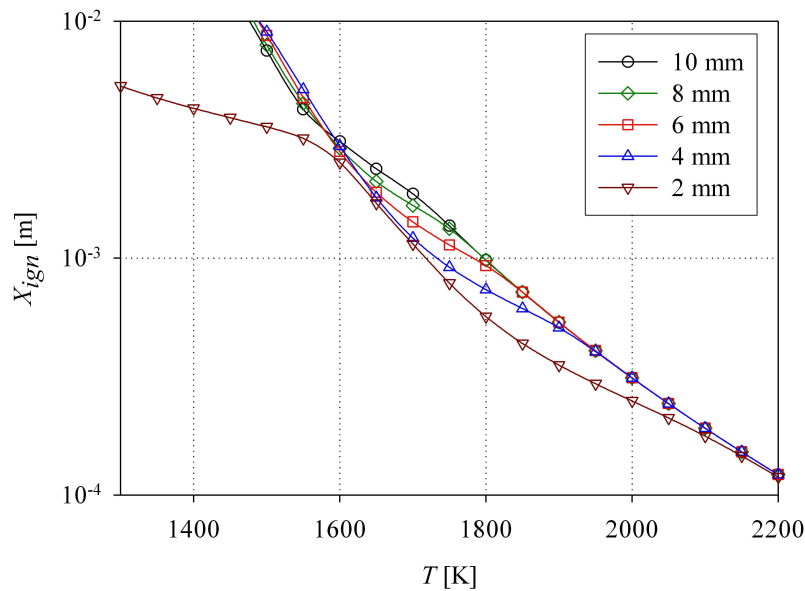


Figure 14: Ignition distance at center line versus temperature for channel diameters between $d = 2$ mm and $d = 10$ mm, $p = 1$ bar and stoichiometric ratio of CH_4 in air $\Phi = 1.0$ for high temperature conditions.

To further clarify the observed effect, concentration profiles of methane in an inert wall channel are depicted for constant temperature $T = 2000$ K and different diameters in figure 15. Inert wall conditions were chosen to exclusively investigate transport effects of homogeneous concentration profiles without surface reactions.

In fact, the shape of methane concentration profiles changes significantly with decreasing diameters. Generally, all channels show relatively rapid methane consumption at the ignition front. Ignition in the 10 mm channel occurs comparatively early next to the wall, whereas ignition at the center line happens further downstream. Actually, the ignition front reflects the parabolic velocity profile that is imposed on the reactive flow in the channel. The smaller the channel diameter, the more ignition takes place at the same distance from the reactor entrance for the center line as well as near the wall. This effect can be explained by small channel sizes that affect the transport of species in radial direction. Homogeneous reactions immediately start at the entrance of the reactor so that radicals are formed by initiation and multiplied by chain-branching reactions cross the entire entrance area of the reactor channel. Since velocities at the center line ($v = 9$ m/s) are significantly higher than at the wall ($v = 0$ m/s) due to the no-slip assumption of laminar flow, molecules and radicals move relatively faster in the core than at the wall. This subsequently causes the formation of a concentration gradient between wall and center line of the channel, as an arbitrary cross section before ignition shows relatively higher concentrations of methane at the center line compared to the wall. Radicals are therefore transported from the wall to the center line while methane diffuses to the wall. In smaller channels, transport ways are significantly shorter and thus the explained concentration equilibration process is fairly faster than in large channels. Wall reactions additionally enhance transport processes in catalytic channels, since methane is constantly depleted near the wall and concentration gradients are even more pronounced. In conclusion, transport between reaction center and wall plays a significant role and can be the limiting factor dependent on the transport dimensions and reaction temperature in catalytic channels.

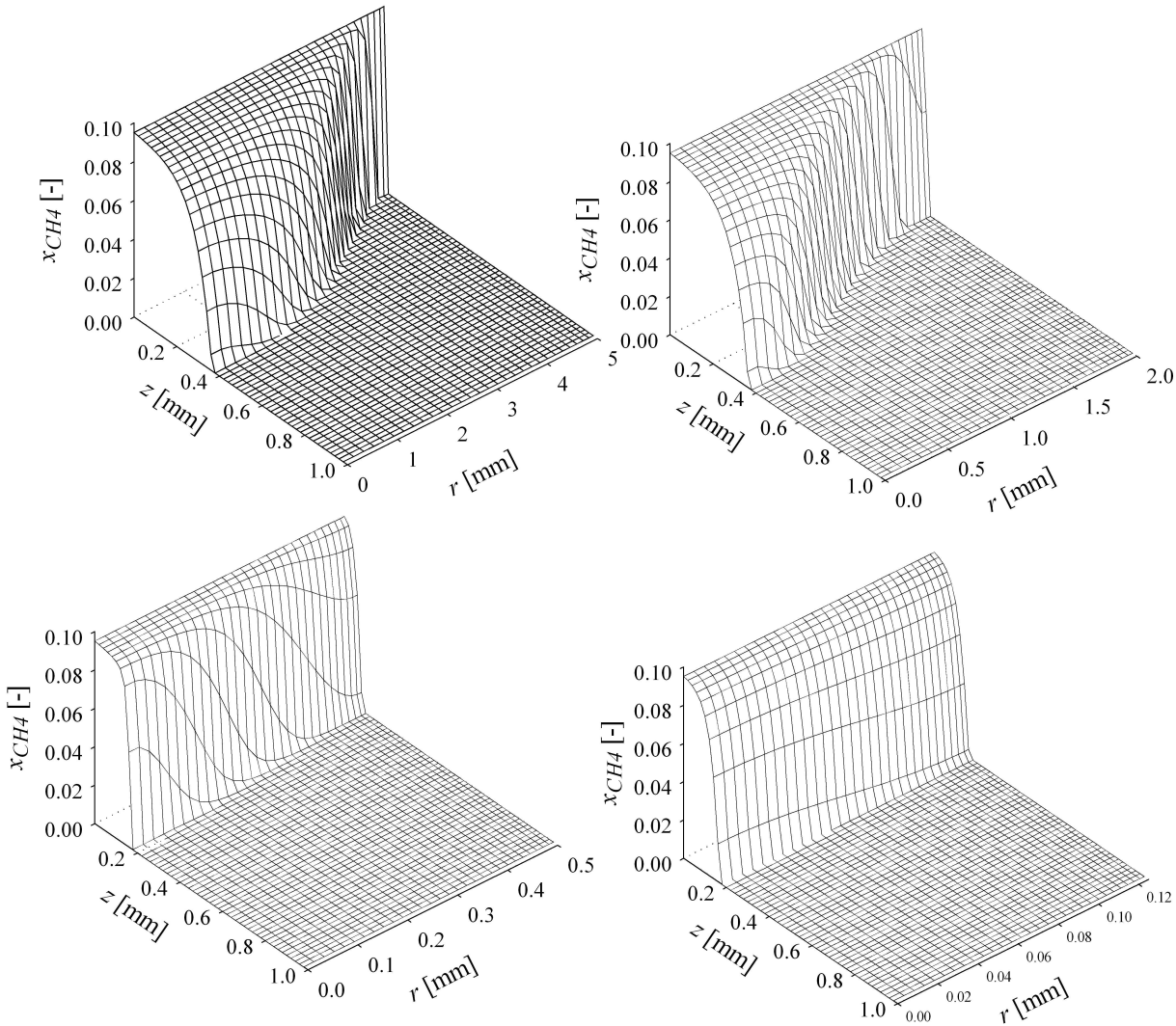


Figure 15: CH_4 concentration for four different diameters $d = 10.0 \text{ mm}$ (upper left), $d = 4.0 \text{ mm}$ (upper right), $d = 1.0 \text{ mm}$ (lower left), and $d = 250 \mu\text{m}$ (lower right) at $T = 1700 \text{ K}$, $p = 1 \text{ bar}$, and stoichiometric ratio of CH_4 in air $\Phi = 1.0$ for a non-catalytic inert wall.

To quantify and prove the transition to wall independent behavior, a similar approach as in section 5.1.3 was applied. Since wall independence implies that catalytic wall reactions have no influence on ignition behavior at the channel center, ignition curves of the inert wall and coupled case are supposed to merge for sufficiently high temperatures. Hence, deviation of ignition distances have been calculated and, similarly to the method in section 5.1.3, a deviation of $D = 1.0 \%$ was chosen to determine the transition temperature of wall independence (figure 16).

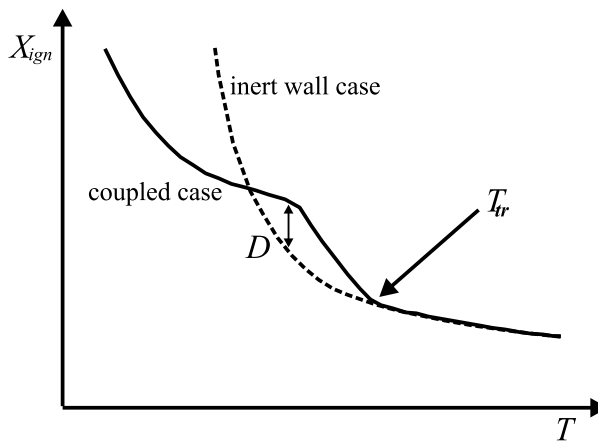


Figure 16: Schematic of transition temperature calculation by determination of deviation between ignition distances of the inert wall and the coupled case.

Temperatures for the transition to wall independence are likewise plotted as a function of linear scale (left) and logarithmic scale (right) diameter together with transition temperatures for the low-temperature transition point from figure 17. Transition temperatures for wall independence show a very strong increase with reduced diameters. A transition temperature of $T_{tr} \approx 2400$ K marks the last point, where homogenous ignition occurs without influence of catalytic reactions below 2500 K for a 1 mm channel. For smaller diameters, transport becomes fast enough to affect homogeneous reactions at the centerline even for very high temperatures, as already shown in the right graph of figure 11. A critical diameter occurs at about $d = 500 \mu\text{m}$, where for smaller diameters ignition distances of the coupled case are well below the inert case.

As depicted in figure 17, different regimes for ignition behavior can be determined. In the area below the low transition temperature graph, ignition is completely controlled by surface reactions so that homogeneous influences can be neglected. For temperatures between the two transition curves, both mechanisms contribute significantly and show competitive behavior. The area above the high-temperature transition line represents a regime where surface reactions exhibit no influence on ignition distances.

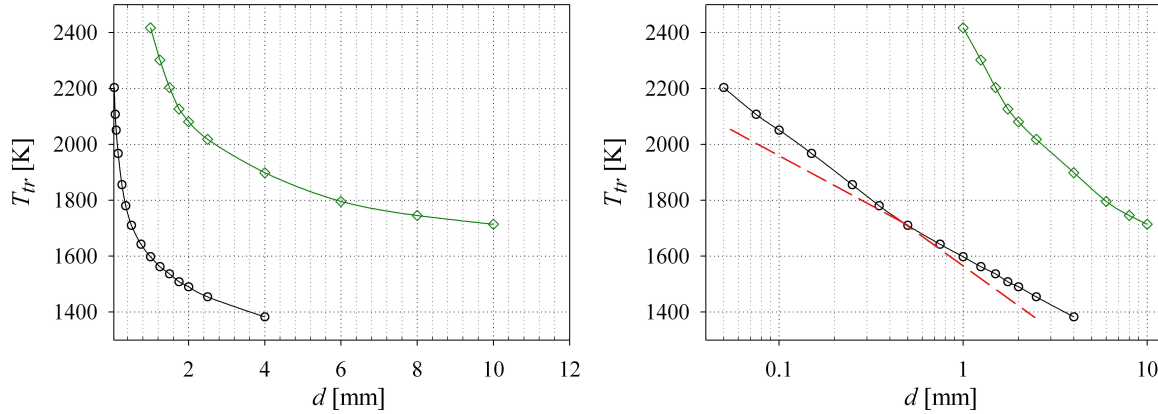


Figure 17: Transition temperatures versus diameter for the high-temperature transition (diamonds) from het./hom. influenced regime to homogeneously dominated behavior in comparison to low-temperature transition (circles) for $p = 1$ bar and stoichiometric ratio of CH_4 in air $\Phi = 1.0$. Left graph shows linear diameter axis, right graph shows logarithmic diameter axis.

Obviously, interaction of transport and reaction lead to surface or wall independent behavior at high temperatures. In detail, homogeneous reactions at the center line apparently become fast compared to diffusive transport so that radical quenching by catalytic reactions can no longer influence the ignition delay at the channel center. This implies that at sufficiently high temperatures the ratio R of the homogeneous reaction rate $r_{reaction}$ to diffusive transport rate $r_{transport}$ of radicals or reactant species exceeds a certain value and consequently leads to transport limitations. A general expression for the reaction rate is given by

$$r_{reaction} = k_\infty \exp\left(-\frac{E}{RT}\right) c_i, \quad (4)$$

whereas the diffusive transport is

$$r_{transport} = D_{i,j} \frac{\partial c_i}{\partial x} \quad (5)$$

for a Fickian approach which is appropriate for diffusion of species with small concentrations compared to the main bulk species. The reaction rate is given in first order of c_i , and it is assumed that c_i denotes the concentration of a radical species such as H, OH or O which is relatively small compared to reactant concentrations as for example the concentration of methane. Hence, the reaction rate is dependent on the radical concentration in first order and concentration of methane and oxygen are assumed to be constant with good proximity prior to homogeneous ignition.

The transport path is characterized by the distance from the center line to the wall of a reactor. Radical species concentrations are assumed to have a maximum concentration c_{max} on the center line and a negligible concentration of $c_{wall} \approx 0$ mol/m³ due to fast radical adsorption at the wall (sticking coefficient $S = 1$ for all radical species in the surface mechanism). Concentration

gradients are assumed to be constant across the transport path so that the transfer rate can be simplified to

$$r_{transport} = D_{i,j} \frac{\Delta c_i}{\Delta x} = D_{i,j} \frac{c_{max}}{r} \quad (6)$$

Since radical concentration is assumed to have a maximum at the channel center, c_i in the reaction rate term can be set to c_{max} .

The ratio of reaction to transport rate R thus is given by

$$R(r, T) = \frac{r_{reaction}}{r_{transport}} = \frac{k_\infty \exp(-\frac{E}{\Re T}) c_{max}}{D_{i,j} \frac{c_{max}}{r}} = \frac{k_\infty}{D_{i,j}} \exp(-\frac{E}{\Re T}) \cdot r. \quad (7)$$

The ratio of reaction to transport shows a functional dependence on temperature and radius. The frequency factor k_∞ is independent of radius r and temperature T and can therefore be treated as constant. The diffusion coefficient is independent of the radius and has a dependence on temperature of $D_{ij}(T) \sim T^{1.5}$ according to Chapman-Enskog theory [30] in gas diffusion processes. Since D_{ij} can at most vary by a factor of $(\frac{2400}{1700})^{1.5} \approx 1.7$ whereas the exponential reaction term varies by orders of magnitude in the investigated temperature range of $T = 1700-2400$ K, the diffusion coefficient is assumed to be constant. With these assumptions equation 7 can be transformed into

$$C = R(r, T) \frac{D_{i,j}}{k_\infty} = \exp(-\frac{E}{\Re T}) \cdot r \quad (8)$$

respectively

$$\ln r = \frac{E}{\Re} \cdot \frac{1}{T} + \ln C. \quad (9)$$

In figure 18, $\ln r$ is plotted as a function of $1/T$ to identify behavior of the ratio of reaction and transport rate. As depicted in figure 18, $\ln r$ shows linear dependence on $1/T$ and reveal that the y-coordinate for $1/T = 0$ as well as the gradient of the depicted line can be assumed as constant. In order to determine ratio R and activation energy E , a linear curve was fitted with $C = e^{-12.8}$ and $E/R = 1.09 \cdot 10^4$ 1/K as resulting values. An apparent activation energy of $E = 90.3$ kJ/mol is derived as well as the ratio $R = K(r, T) k_\infty / D_{ij} = 3 \cdot 10^6$ with an assumed frequency factor of $k_\infty = 6.6 \cdot 10^8$ 1/s (reaction III) and a binary Fickian diffusion coefficient of methane in air $D_{CH4,air} = 5.4 \cdot 10^{-4}$ m²/s for $T = 1700$ K by Chapman-Enskog theory. The activation energy is in the order of typical elementary-step reactions in the GRI mechanism and therefore represents the overall apparent activation energy of the gas-phase mechanism for these conditions. However, exact activation energies of contributing reactions cannot be predicted with this approach, since numerical deviations coming from fitting and approximation of the transition point by deviation calculations significantly influence the resulting values. In addition, a slight non-linear trend can be noticed which is due to the temperature dependence of diffusive transport. Also, no unique rate-determining step might exist, so that the apparent activation energy is a function of the activation

energies of individual reaction steps.

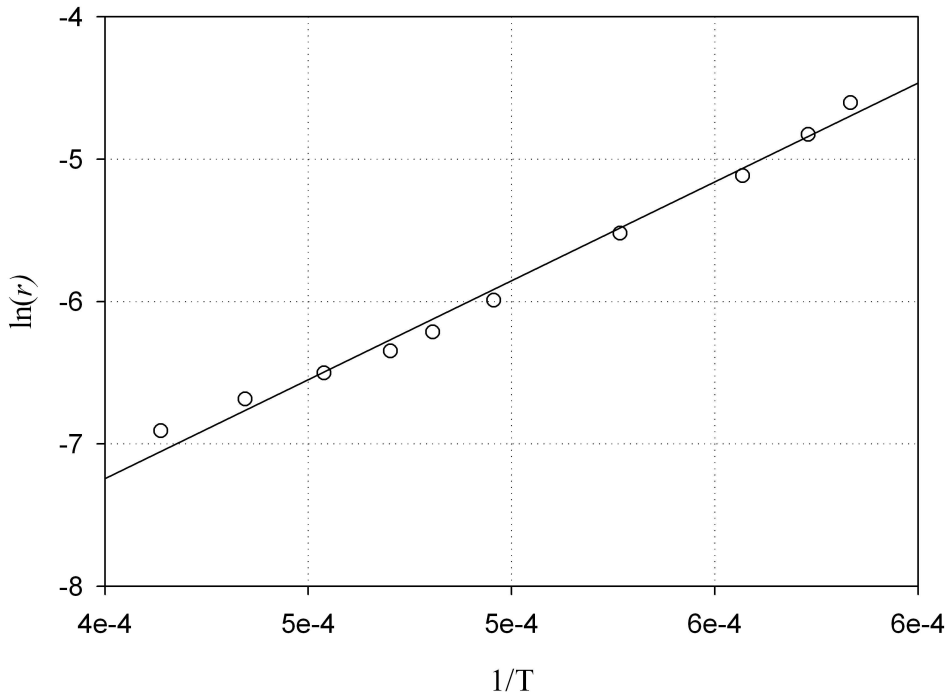


Figure 18: $\ln r$ as a function of $1/T$ for transition to wall independent behavior. The function gradient represents the apparent overall activation energy E/\mathfrak{R} , whereas the y-coordinate functions to determine the ratio of reaction to transport rate.

Nevertheless, the good fit to the linear behavior indicates that indeed the reaction rate exceeds the transport rate sufficiently to render the ignition behavior independent of the wall, i.e. independent of surface kinetics.

5.1.5 Homogeneous-Heterogeneous Interactions at High Temperatures

In section 5.1.3, quenching of homogeneous reactions in microscale reactors is explained and limits of quenching behavior have been revealed. As exemplified in figure 13, influence of homogeneous reactions cannot be neglected even for very small diameters of $d = 50 \mu\text{m}$. Simulation results in [34] showed that complete quenching of homogeneous reactions in the hydrogen/air system is possible for diameters smaller than $d = 285 \mu\text{m}$. Although a distinct qualitative change in the ignition behavior for small microscale channels is observable and heterogeneous reactions dominate the reaction behavior for very high temperatures above 2000 K, homogeneous reactions still yield significant contributions at high temperatures. In this section, heterogeneous-homogeneous interactions of is investigated for high temperatures above $T = 1700 \text{ K}$.

To exemplify characteristics of the homogeneous mechanism in catalytic channels, reaction rates of initiating and chain branching reactions (upper left and right) and concentrations of the most important molecular (lower left) and radical species (lower right) are pictured.

Figure 19 presents reaction rate and concentration profiles at the center line of a 2.0 mm channel reactor for $T = 1700 \text{ K}$ and $\Phi = 1.0$, i.e. conditions with predominantly homogeneous reaction behavior. As depicted in the upper left graph, reactions start off with initiating radical forming reactions (circles and diamonds). Reaction of H and O₂ to O and OH (filled circles) plays a crucial role in homogeneous ignition, as it is one of the main chain-branching reactions. The amount of H/O/OH radicals is strongly increased due to this reaction and thus a radical pool can be established. At the initial state, homogeneous reactions are distinctively slower than surface reactions compared to the initial surface adsorption and reaction step depicted in the upper right graph (triangles down). From a certain point at $z \approx 0.9 \text{ mm}$, the radical pool becomes large enough to rapidly accelerate chain-propagating reactions (squares and triangles up) to reaction rates larger than the surface reaction rate. As long as chain-propagating reactions are slow, methane is hardly consumed by the predominating initiating and chain-branching reactions as shown in the lower left picture. With increasing reaction rate of the chain-propagating reactions more and more methane is consumed and mainly transformed into methyl radicals (CH₃). At $z = 1.15 \text{ mm}$, chain-branching as well as chain-propagating reactions show a distinct spike of reaction rate which subsequently leads to a fast depletion of methane and fast production of product and radical species in combination with a temperature rise of about $\Delta T = 500 \text{ K}$ ($X_{ign} = 1.15 \text{ mm}$).

In conclusion, the diagrams in figure 19 prove that ignition delay is strongly dependent on initiating reactions in conjunction with chain-branching and -propagating reactions. Homogeneous ignition occurs if transport and conversion of initial radicals by the catalytic wall is not fast enough to control the accelerating build-up of a radical pool. Initiating reactions, like all chemical reactions, are strongly temperature dependent and need to be further investigated since they play a key role in ignition behavior at high temperatures.

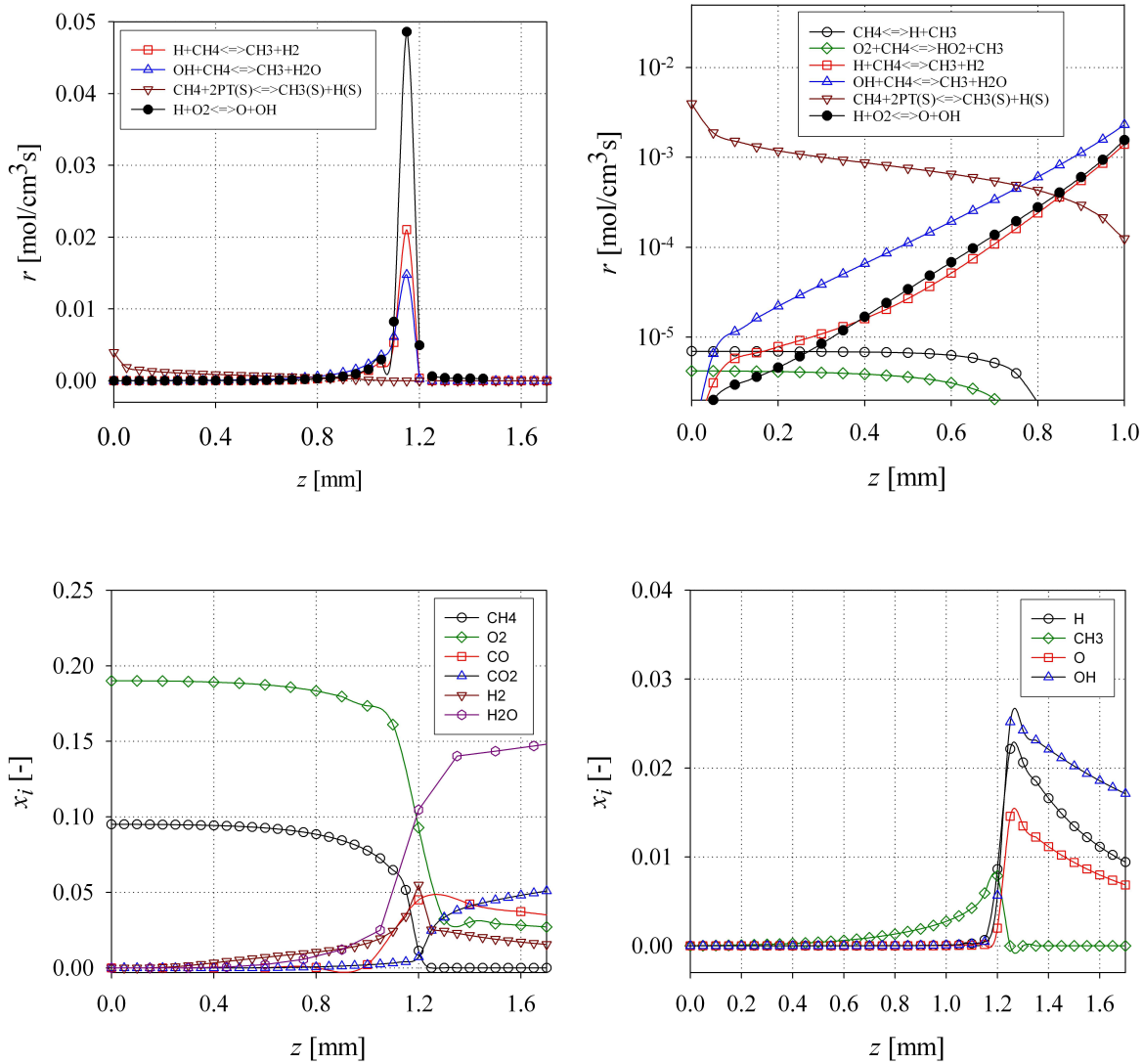


Figure 19: Concentration profiles and initiating, chain-branching and propagating reaction rates at the center line versus axial coordinate compared to surface reaction rates at $T = 1700$ K, $p = 1$ bar and stoichiometric ratio of CH_4 in air $\Phi = 1.0$. The upper left graph shows reactions rates from inlet to the homogenous ignition point. The upper right graph shows initial reaction behavior with logarithmic reaction rates. Lower graphs depict concentration profiles of molecular (left) and radical species (right).

Figure 20 displays reaction rates of initiating reactions at the center of the reactor entrance as a function of temperature. As demonstrated in figure 19, initiating reactions first proceed with a nearly constant reaction rate before chain-branching and propagating rates steeply increase and dominate the reaction behavior. Therefore, the initial reaction rates at the channel center represent the reaction rate of initiating steps with good proximity. Methane decomposition into methyl and hydrogen radicals (circles) and reaction of methane with oxygen to methyl and hydroxyl radicals (diamonds) constitute the main initial radical formation steps. These steps are displayed together

with dissociative CH_4 adsorption in order to compare surface reaction rates to the homogeneous initiating steps. Since surface reaction rates are given with respect to the surface area and homogeneous reaction rates refer to volume, surface reaction rates are transformed into volumetric reaction rates by

$$r^* = r_{\text{surface}} * A_v = \frac{4r_{\text{surface}}}{d}, \quad (10)$$

where A_v denotes the surface-to-volume ratio for the applied channel diameter of $d = 2.0$ mm.

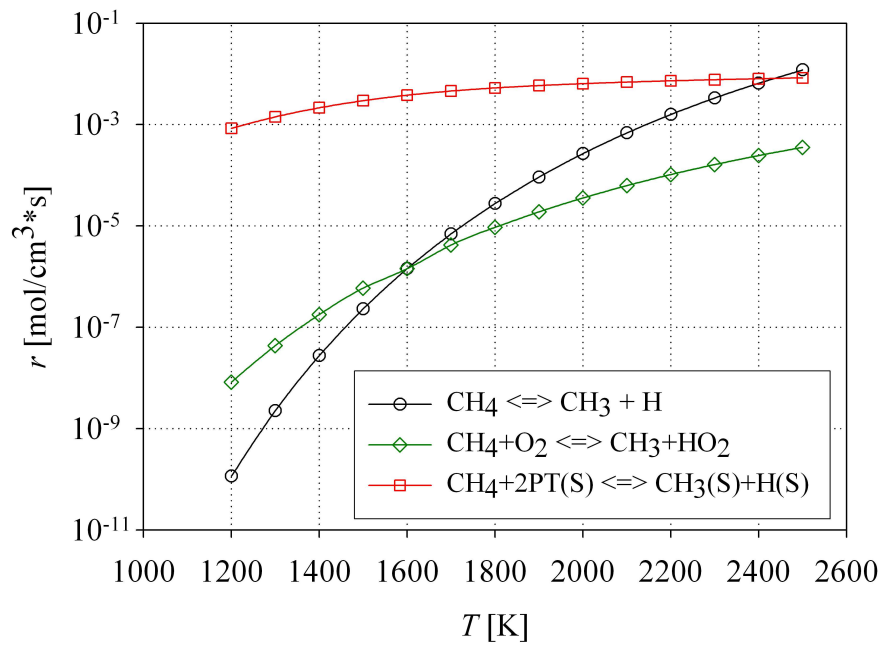


Figure 20: Rates of initiating homogeneous reactions at channel inlet center versus temperature compared to methane adsorption/reaction step, $d = 2.0$ mm, $p = 1$ bar and stoichiometric ratio of CH_4 in air $\Phi = 1.0$.

As expected, the methane decomposition reaction (circles) and the methane oxygen reactions (diamonds) exhibit significant increase with increasing temperature. Methane decomposition appears to be the dominating initiating reaction step for temperatures above 1600 K. In the temperature range above 2200 K, methane decomposition proceeds very fast and shows reaction rates in the order of the dissociative adsorption (squares) on the surface. In general, homogeneous reactions proceed faster for higher temperatures so that even relatively slow elementary steps become fast enough to significantly accelerate the oxidation process. Although radicals are rapidly produced by methane decomposition at high temperatures, surface reactions still play an important role in depleting radical concentrations.

A coupled carbon flux analysis was carried out to investigate behavior of catalytic reactions for

a temperature of $T = 2000$ K with fast methane decomposition and a surface-to-volume ratio of $A_v = 160.0 \text{ cm}^{-1}$, which corresponds to a $250 \mu\text{m}$ channel (figure 21).

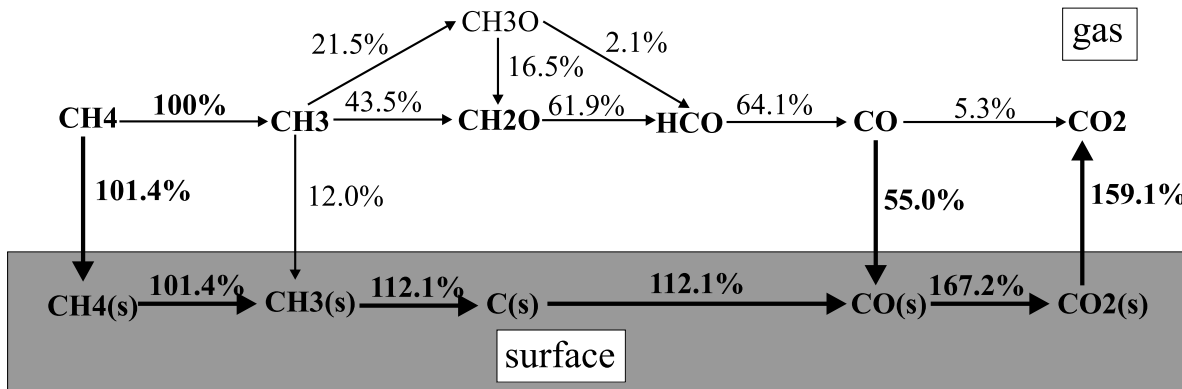


Figure 21: Reaction pathway analysis with an isothermal surface CSTR for $T = 2000$ K, residence time = 30 ms, $p = 1$ bar, $A_v = 160.0 \text{ cm}^{-1}$ and a stoichiometric ratio of CH_4 in air $\Phi = 1.0$, all fluxes are normalized with respect to $\text{CH}_4 \rightarrow \text{CH}_3$, fluxes smaller than 0.3 % are not shown.

As shown in the carbon flux analysis in figure 21, homogeneous oxidation proceeds through the same main pathway at $T = 2000$ K as already explained in chapter 3 for $T = 1400$ K. However, reaction steps show slower conversion with respect to the first reaction step $\text{CH}_4 \rightarrow \text{CH}_3$ that is enhanced by orders of magnitude from 1400 to 2000 K ($r_{\text{CH}_4, \text{CH}_3} = 5.2 \cdot 10^{-5}$). Main oxidation routes proceed via the catalytic surface, since surface reactions show the fastest reaction rates. Hence, homogeneous reaction are slowed down due to radical depletion in the gas phase. Although surface reactions constitute the main oxidation pathway and exhibit the fastest reaction rates, significant amounts of O/H/OH radicals as well as methyl radicals are formed mainly through the homogeneous methane decomposition reaction for elevated temperatures. Subsequently, homogeneously produced radicals are rapidly absorbed by the catalyst and converted into products. Even though radicals are absorbed and a radical pool cannot form, methane is depleted by the initiating methane decomposition reactions. This affects ignition distance and thus homogeneous influences are visible even though no explosion behavior can be observed. For high temperature and small diameters, the overall mechanism shows the strongest coupling effect, as both homogeneous and catalytic reactions proceed very rapidly and show an acceleration of the reaction progress. The coupling therefore leads to almost instantaneous ignition since both the homogeneous and the catalytic pathway proceed fast. Especially homogeneous reactions occur without ignition delay. Overall, catalytically dominated ignition for very small diameters is accelerated by homogeneous reactions but high radical concentrations can effectively be suppressed even up to very high temperatures.

5.1.6 Pressure Variation

Pressure is assumed to have a major effect on ignition, as for higher pressure production rates of homogeneous reactions are increased and transport between center line and wall is considerably slowed down. To determine the effect of pressure variation on the overall radical quenching behavior, temperatures for the transition from heterogeneous to the heterogeneous-homogeneous regimes were calculated as done in section 5.1.3 for four different pressures $p = 0.5, 1.0, 2.0$, and 5.0 bar. Results of transition temperatures for the low-temperature transition from catalytically dominated to homogeneously influenced behavior are depicted in figure 22.

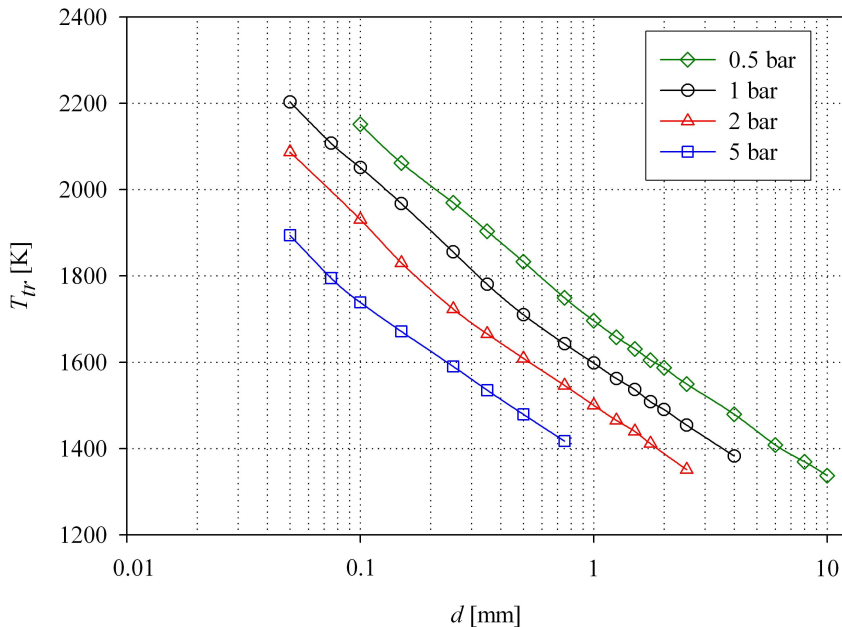


Figure 22: Transition temperatures versus diameter for transition from heterogeneously to homogeneously dominated behavior for $p = 0.5\text{--}5$ bar and stoichiometric ratio of CH_4 in air $\Phi = 1.0$.

Obviously, transition temperatures decrease with increasing pressure which proves distinctive impact of pressure on ignition behavior. Increasing pressure can strongly accelerate homogeneous ignition, as at high pressure, intermolecular collisions become more and more probable due to reduced mean free path of molecular and radical species. In addition, diffusive mass transfer is slowed down, as pressure increases the gas density, and thus adsorption and depletion of radical and reactant species by the surface is detrimentally affected.

To investigate functional dependences and limits of safe reactor operation for varied pressure conditions, a two-parameter exponential function was fitted to calculated transition temperature values dependent on pressure and diameter.

Since transition temperature shows an exponential dependence on diameter, following function was used to approximate previously determined data points:

$$d = a * \exp\left(-\frac{T_{tr}}{T_0}\right) \quad (11)$$

Following coefficients a and T_0 with corresponding correlation coefficients result from the fitting procedure as depicted in table 2.

Table 2: Table of parameters from fitting of the function $d = a * \exp\left(-\frac{T_{tr}}{T_0}\right)$ to calculated T_{tr} versus d .

pressure p [bar]	a [mm]	T_0 [K]	correlation coefficient R
0.5	23401	174.0	0.9996
1.0	9353	176.5	0.9996
2.0	4523	184.3	0.9997
5.0	2006	178.9	0.9997

To further determine pressure dependence in the functional behavior, parameter T_0 was averaged and the fitting procedure was repeated with an average value of T_0 (table 3).

Table 3: Table of parameters from re-fitting of the function $d = a * \exp\left(-\frac{T_{tr}}{T_0}\right)$ to calculated T_{tr} versus d with averaged parameter T_0 .

pressure p [bar]	a [mm]	T_0 [K]	correlation coefficient R
0.5	16950	178.3	0.9955
1.0	8730	178.3	0.9960
2.0	4742	178.3	0.9980
5.0	2025	178.3	0.9964

Pressure dependence of function 11 can be expressed by the following functional term for a :

$$d = a(p) * \exp\left(-\frac{T_{tr}}{T_0}\right) \quad (12)$$

with

$$a(p) = d_0 * \exp\left(\frac{p_0}{p + p_1}\right). \quad (13)$$

This leads to equation 14 for the transition temperature T_{tr} as a function of pressure p and diameter d

$$\frac{T_{tr}}{T_0} = \frac{p_0}{p + p_1} - \ln\left(\frac{d}{d_0}\right), \quad (14)$$

with T_{tr} in K, p in bar and d in mm. Parameters are derived as $T_0 = 178.3$, $p_0 = 4.67$, $p_1 = 1.17$, and $d_0 = 1026.9$ with a correlation coefficient of $R = 0.9996$ for the pressure fit. Functional behavior of T_{tr} versus diameter and pressure in equation 14 is depicted in figure 23.

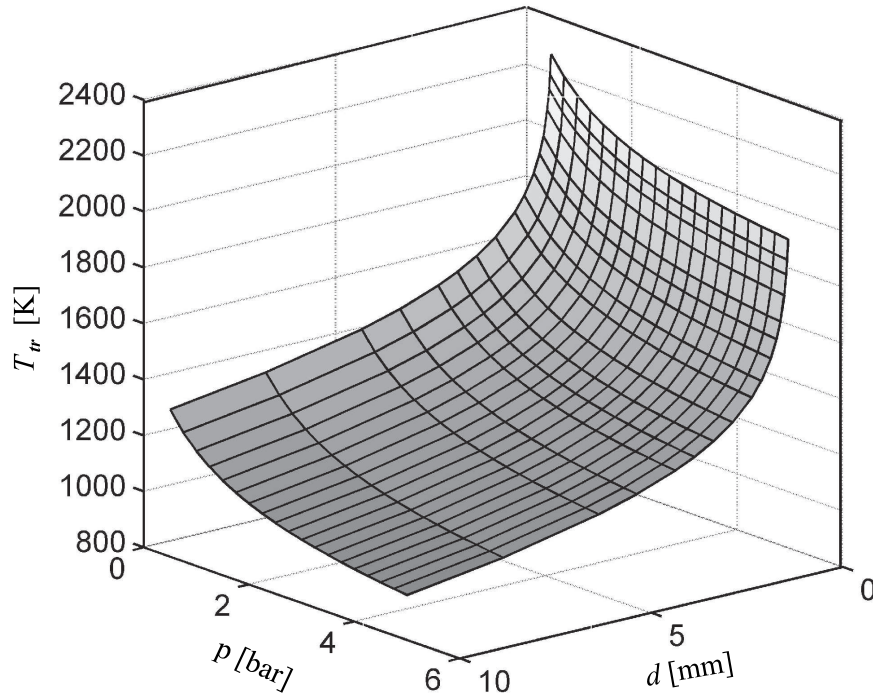


Figure 23: Fit of transition temperatures versus diameter and pressure for transition from heterogeneously to homogeneously dominated behavior for a stoichiometric ratio of CH_4 in air $\Phi = 1.0$.

The transition temperature area plot shows strong functional dependence on the diameter for all investigated pressures. Pressure appears to have a significant influence on transition temperatures, however, the typical quenching behavior of homogeneous reactions can be observed for all investigated pressure conditions as transition temperature increases considerably with decreasing diameters, even for high pressures up to 5 bar. Nevertheless, effective quenching is mainly achieved for low to ambient pressure conditions, since transition temperature drops with pressure and results in lower values for high pressure conditions as shown in table 4.

Table 4: Transition temperatures for a $250 \mu\text{m}$ channel at different pressure conditions.

pressure p [bar]	0.5	1.0	2.0	5.0
transition temperature T_{tr}	1970	1855	1723	1590

5.1.7 Variation of Inlet Composition

Quenching behavior can be observed for a wide range of different pressures, temperatures, and diameters and suppression of homogeneous reactions is particularly feasible for small channel dimensions with sub-millimeter diameters. Since inlet conditions can significantly change in real experimental setups, quenching behavior for different inlet conditions was investigated. This section deals with oxidation of methane by pure oxygen instead of air and additionally presents the effect of different methane concentrations in the inlet mixture. In fuel oxidation processes, fuel contents are usually given by the equivalence ratio Φ defined by the following equation:

$$\Phi = \frac{(n_{fuel}/n_{oxygen})}{(n_{fuel}/n_{oxygen})_{stoichiometric}} \quad (15)$$

The stoichiometric ratio for methane oxidation is given by the global total oxidation reaction



with a molar ratio for methane to oxygen of 1:2.

To investigate oxidation behavior for a stoichiometric ratio of methane and oxygen, temperatures for the low-temperature transition were calculated according to the method applied in section 5.1.3 and depicted in figure 24 as a function of diameter and in comparison to oxidation of methane in air.

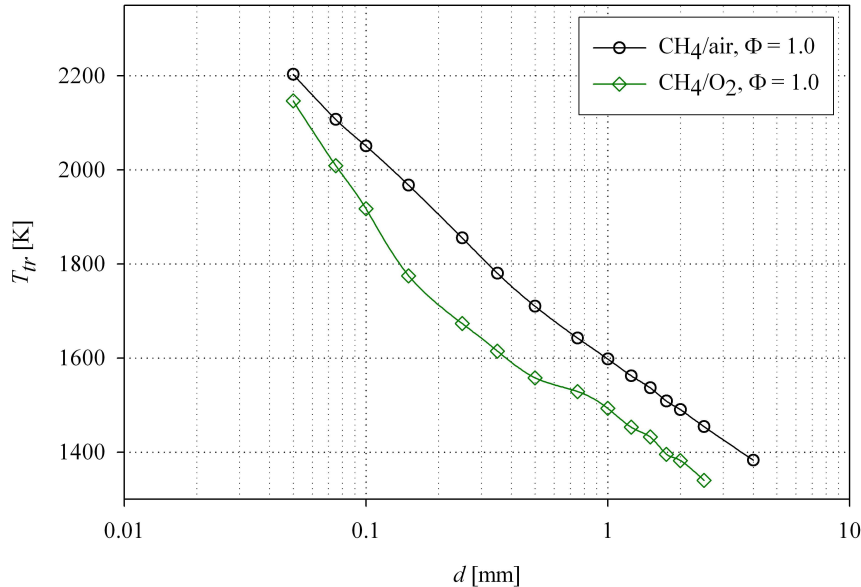


Figure 24: Transition temperatures versus diameter for transition from heterogeneously to homogeneously dominated behavior for $p = 1.0$ bar and stoichiometric ratio of CH_4 in air and pure oxygen $\Phi = 1.0$.

Transition temperatures of the pure oxygen system are in general lower than for the oxidation in air because the availability of oxygen has a strong influence on the homogeneous ignition behavior. In fact, partial pressures of both reactants are increased which increases collision probability between methane and oxygen molecules and therefore leads to faster homogeneous reactions. Nevertheless, quenching behavior can be observed, as transition temperatures show a strong increase for smaller diameters. In addition, interplay of homogeneous and heterogeneous reaction behavior is more distinct for the pure oxygen system. For large diameters $d > 1$ mm, the transition temperature curve for the pure oxygen case runs in parallel to the air system. At temperatures between 1500 K and 1600 K, the curve gradient is reduced which is assumed to be influenced by a strong acceleration of homogeneous reactions due to methane decomposition as described in section 5.1.5. Following the curve to smaller diameters, gradients become significantly steeper, since heterogeneous reactions increasingly control the transition temperature. The curve behavior at very high temperatures implies that the availability of oxygen enhances surface reaction rates and therefore the deviation between air and pure oxygen curve becomes smaller with increasing temperature. In general, oxidation reactions with pure oxygen were significantly faster and temperature rise and explosion behavior more distinct.

To further investigate influence of fuel and oxygen content in the system, transition temperatures for different equivalence ratios of methane in air were determined and displayed in figure 25. In general, determined transition curves show slight deviation for different equivalence ratios.

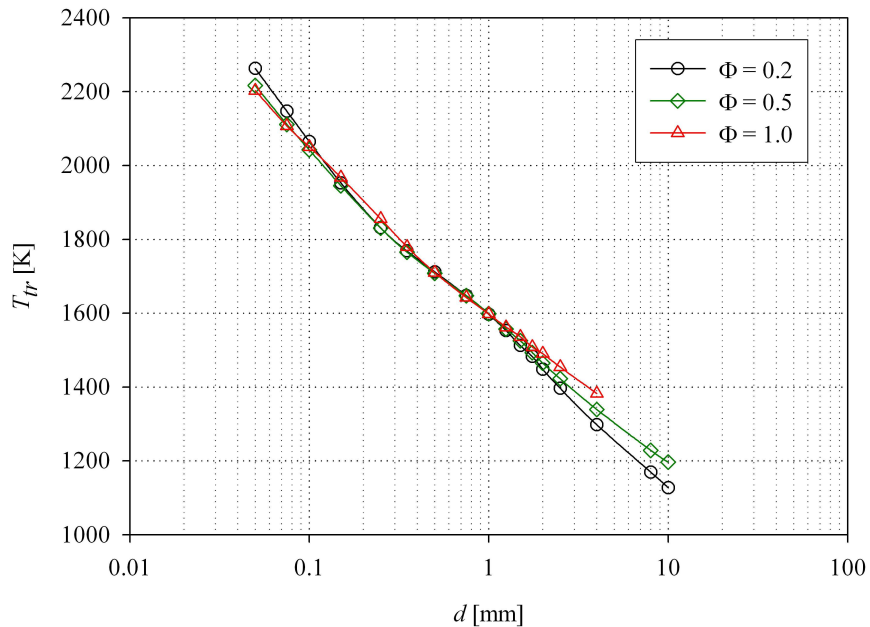


Figure 25: Transition temperatures versus diameter for transition from heterogeneously to homogeneously dominated behavior for $p = 1.0$ bar and $\Phi = 0.2-1.0$ of CH_4 in air .

However, for extreme conditions such as high temperatures and small diameters or large diameters in combination with lower temperatures, deviations can be observed. In fact, transition temperature curves show a slightly steeper gradient for fuel-lean conditions. This is most likely caused by surface poisoning with oxygen which slows down catalytic reactions at lower temperatures. For high temperature conditions, oxygen surface coverage is assumed to be smaller, as oxygen desorbs faster from the catalyst surface.

In conclusion, variation of methane concentration does hardly reveal effects in ignition behavior compared to temperature and pressure, although transition temperature shows slight deviations dependent on temperature which is most probably caused by temperature dependence of oxygen surface coverages.

5.1.8 Adiabatic Wall

Isothermal wall behavior constituted a main assumption in the investigation of quenching behavior in the previous sections. The assumption of an isothermal wall can possibly lead to explosion quenching effects due to fast withdrawal of thermal energy. This assumption may not image realistic system behavior if temperatures of catalytic walls cannot be kept constant due to fast heat production by oxidation reactions. Adiabatic behavior in fact constitutes an extreme case for which thermal energy is not withdrawn from the reactor and thus both catalytic and homogeneous are assumed to be significantly accelerated due to a higher temperature rise caused by the exothermic oxidation steps. To investigate effects of wall conditions on quenching behavior in micro-channels both isothermal and adiabatic simulations were carried out for different temperatures and channel diameters. Transition temperatures for both cases are depicted in figure 26 for a lean mixture of methane in air, ambient pressure, and channel diameters of $d = 50 \mu\text{m} - 8 \text{ mm}$. Transition temperatures for the adiabatic case are lower than for the isothermal case for the entire diameter range, but likewise confirm typical quenching effects visible by increasing transition temperatures with decreasing diameters. Since homogeneous radical forming reactions are very sensitive to temperature changes, heat production due to exothermic gas-phase reactions lead to acceleration of homogeneous reactions. Although surface reactions are likewise accelerated, heat and diffusive mass transport limit the adsorption of radical species by the surface. Hence, the higher temperature rise in an adiabatic compared to an isothermal channel accelerates gas phase reactions significantly more than transport and thus leads to lower transition temperatures for the adiabatic case. In general, large and small diameter branches show a transition point with a more distinct gradient change as observed in isothermal transition temperature curves. Surface reactions are in particular enhanced by higher wall temperatures so that the adiabatic and the isothermal curve more and more merge for smaller diameters.

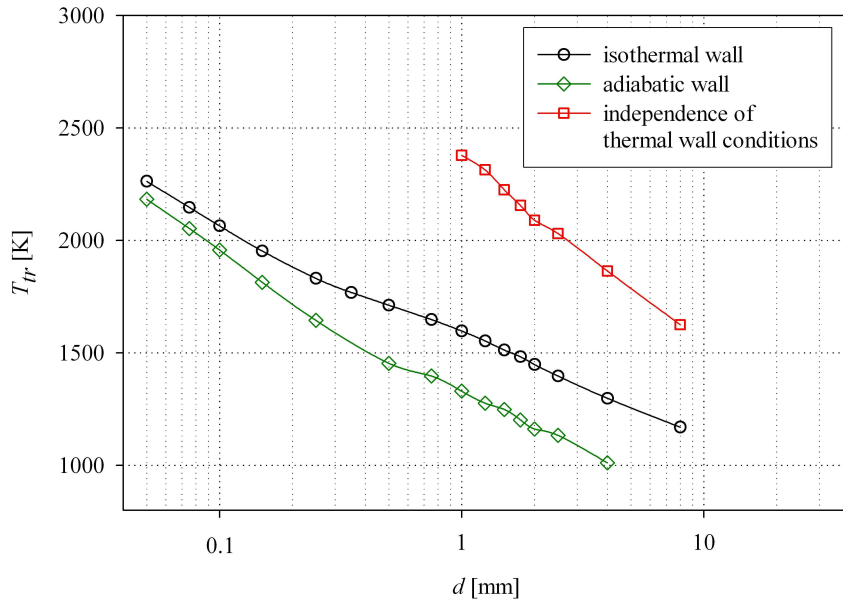


Figure 26: Transition temperatures versus diameter for transition from heterogeneously to homogeneously dominated behavior in channels with adiabatic compared to isothermal wall for $p = 1.0$ bar and $\Phi = 0.2$ of CH_4 in air.

For large diameters and high temperatures, homogeneous reaction behavior becomes independent of thermal wall conditions and shows similarities to the effect observed and exemplified in section 5.1.4. Reaction behavior is no more influenced by surface reactions for high temperatures and large diameters due to limitations of diffusive and heat transport. Comparison of isothermal and adiabatic ignition distances reveal independence of thermal wall conditions for larger diameters $d \geq 1$ mm as depicted in figure 26. Apparently, heat withdrawal through the boundary-layer and wall is not fast enough to significantly influence fast homogeneous reactions at the center line. In summary, adiabatic wall channels show similar quenching behavior as observed for isothermal channels, although homogeneous ignition already takes place at significantly lower temperatures. For high temperatures, homogeneous reactions become fast enough to suppress an influence of thermal wall conditions, since heat withdrawal by the wall no more affects reaction behavior at the channel core.

5.1.9 Comparison of Surface Mechanisms

In this work, the surface mechanism by Aghalayam et al. [27] has been primarily used to carry out simulations and investigate quenching behavior. Other elementary-step reaction sets were tested such as the mechanism by Veser et al. [13] and Deutschmann et al. [25]. These mechanisms were mainly developed for partial oxidation of methane to carbon monoxide and hydrogen and therefore fuel-rich conditions. In this work, investigations are focused on total oxidation of methane

for fuel-lean to stoichiometric conditions. The mechanisms by Veser et. al. and Deutschmann et. al. showed convergence limitations in particular for fuel-lean conditions and extreme values of temperature and diameter. To validate observed quenching effects for different surface mechanisms, simulation results with the mechanism by Aghalayam et al. are compared to results of the Deutschmann mechanism. To explain the differences in the interplay of heterogeneous and homogeneous reactions, transition temperatures for the Deutschmann mechanism were calculated and compared to results from simulations with the Aghalayam mechanism for a stoichiometric fuel oxygen ratio and ambient pressure, see figure 27.

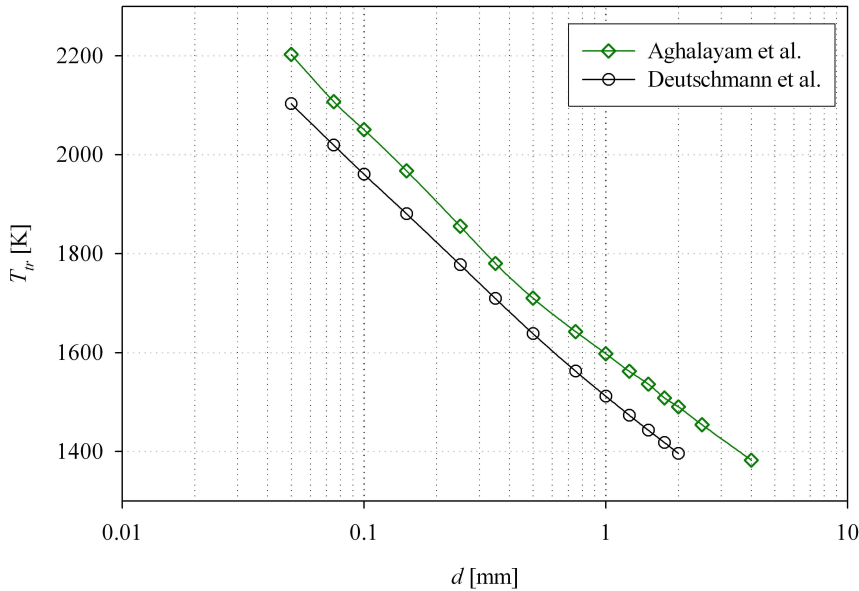


Figure 27: Comparison of transition temperatures versus diameter for transition from heterogeneously to homogeneously dominated behavior of different mechanisms by Deutschmann et. al. [25] and Aghalayam et. al. [27] at $p = 1.0$ bar and stoichiometric ratio of CH_4 in air $\Phi = 1.0$.

Quenching behavior is also observed for the Deutschmann mechanism, although transition temperatures are significantly lower by $\Delta T_{tr} \approx 100$ K. Apparently, quenching of radical species with the Deutschmann mechanism is much less effective than with the Aghalayam mechanism. This can be explained by the set of reactions that was used in either mechanism. The Deutschmann mechanism in contrary to the Aghalayam mechanism does not consider adsorption/desorption of carbon containing radical species on the platinum surface. Therefore, radical species like CH_3 , CH_2 and CH that are formed in the gas phase by homogeneous reactions do not interact with the catalytic surface. Aghalayam et al. account for surface adsorption and desorption behavior for the most important radical species which obviously has an important influence on ignition behavior. Nevertheless, the Deutschmann mechanism considers adsorption of hydrogen and oxygen radical species and thus quenching behavior due to reduction of channel size can be observed.

5.2 NO_x Formation

NO_x formation plays a crucial role in high temperature fuel/air oxidation systems. Catalytic oxidation processes offer the possibility to effectively suppress formation of nitric oxides that can have relevant impact on the environment. As already mentioned in chapter 3, thermal and prompt NO formation represent the dominant NO_x mechanisms in high temperature methane oxidation processes at ambient pressures. Catalytic combustion facilitates effective suppression of NO_x formation through the mentioned mechanisms, since it can be carried out at low temperatures and only produces negligible amounts of radicals. In contrary to homogeneous combustion, catalytic oxidation of methane neither causes high temperatures that are a prerequisite for considerably fast thermal NO formation nor CH_i radicals are produced that initiate prompt NO_x formation. In the present work, NO formation in small scale catalytic channels was observed to investigate possible NO quenching effects, in particular since prompt NO_x formation is initiated by carbon containing radicals.

In figure 28, NO concentrations at the center line are pictured for three different diameters $d = 2.5$ mm (top left), $750 \mu\text{m}$ (top right), and $250 \mu\text{m}$ (bottom). In each graph NO concentration x_{NO} versus axial distance z is depicted for four different temperatures. Temperatures are chosen so that NO_x concentration is visible on the ppm scale for the smallest displayed temperature and maximum temperature does not lead to wall independent behavior at the reactor center. Axial distance is chosen to be long enough to display equilibrium conditions in the post combustion zone.

The top left graph for a 2.5 mm diameter channel shows first detectable NO concentrations at about $T = 1550$ K, whereas NO_x concentrations are small $x_{NO} < 1$ ppm for lower temperatures and non detectable for temperatures below $T_{tr} = 1450$ K. For increasing temperatures, significant amounts of NO are formed and NO concentration curves show a distinct maximum. NO_x concentrations show a strong increase that lead to a concentration maximum and afterwards flattens out into equilibrium concentration with increasing axial distance. The observed maxima agree with calculated ignition distances of methane oxidation and reveal that NO_x formation is connected with homogeneous ignition, since in this temperature regime homogeneous reactions already show strong influence on overall reactions.

A similar behavior can be observed for a diameter of $d = 750 \mu\text{m}$. However, first detectable NO_x of $x_{NO} > 1$ ppm is seen at about $T = 1800$ K with a transition temperature of $T_{tr} = 1650$ K and maxima of concentration curves are not as prominent as for $d = 2.5$ mm. In general, NO concentrations stay relatively small even for temperatures up to 2200 K.

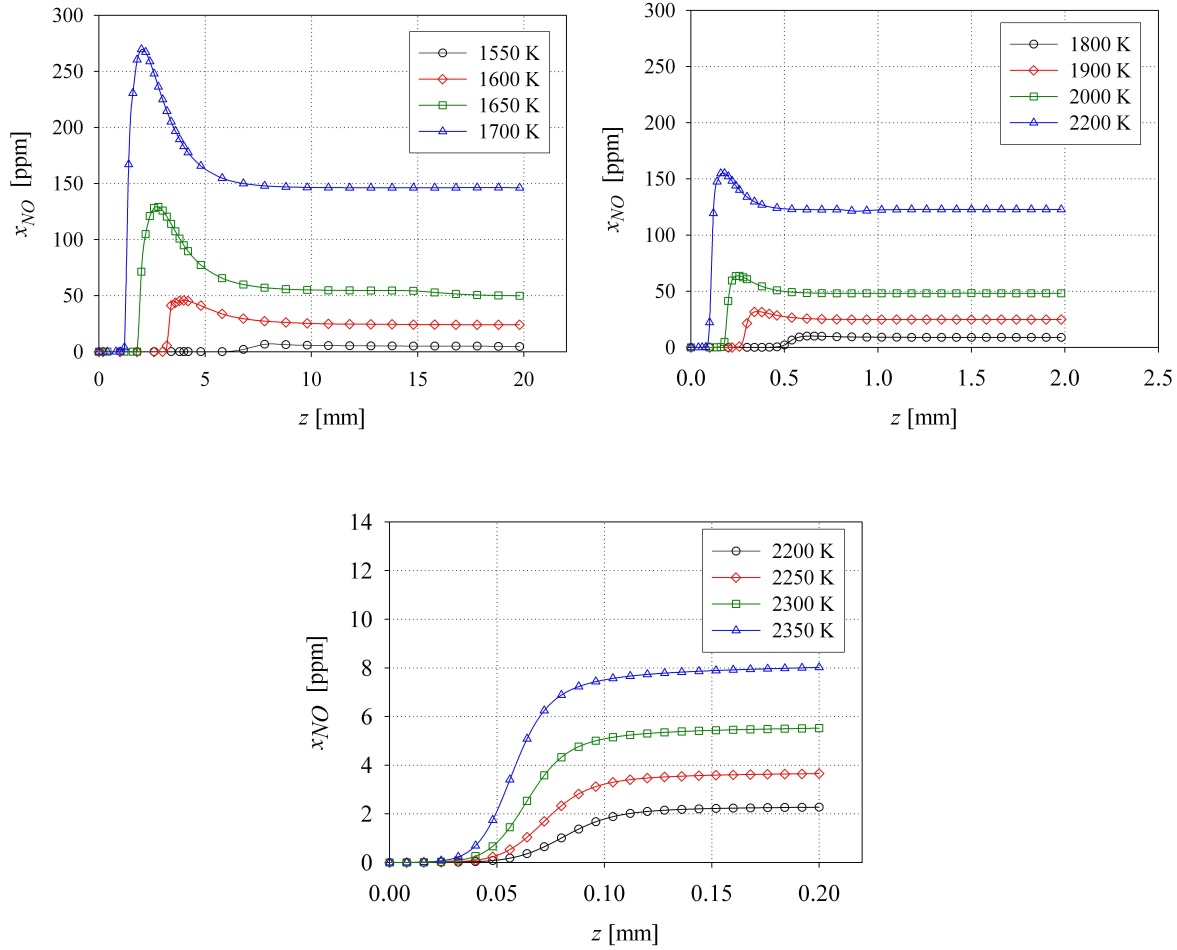


Figure 28: NO concentration versus axial distance for channel diameter of $d = 2.5$ mm (left), $d = 750 \mu\text{m}$ (middle) and $d = 250 \mu\text{m}$ (right) at $p = 1.0$ bar for a stoichiometric ratio of methane in air $\Phi = 1.0$.

The $250 \mu\text{m}$ channel concentration profiles depict a clearly visible change in the qualitative behavior of NO formation along the reactor center, since maxima of NO concentration curves are no longer existent. Furthermore, ignition distances for temperatures above $T = 2200$ K are extremely small ($X_{ign} < 20 \mu\text{m}$) so that conversion of methane is completed before significant NO concentrations can build up in the channel at $z = 50 - 100 \mu\text{m}$. Although homogeneous reactions already begin to influence reaction behavior for $T_{tr} = 1900$ K, NO concentrations are smaller than 1 ppm for $T < 2150$ K and do not exceed 10 ppm even for temperatures up to 2350 K. In conclusion, down-sizing of catalytic channels likewise effects NO formation mechanisms and leads to effective suppression of NO_x even for high temperatures. The observations concerning NO formation agree well with quenching of radicals of the CH_4 oxidation in section 5.1.2. For very small diameters in the micrometer range, ignition was strongly influenced by catalytic reactions, even up to the maximum temperatures studied in this work, which indicates that formation of radicals

was strongly weakened. Therefore, NO profiles indicate, the complete absence of Prompt- NO_x and only small amounts of Thermal- NO_x . To further quantify NO formation as a function of the channel diameter, maximum NO concentrations for diameters of $d = 50 \mu\text{m} - 2.5 \text{ mm}$ and temperatures between 1500 K and 2200 K were calculated along on channel center line, see figure 29. The gray area in figure 29 marks NO concentration values smaller than $x_{\text{NO}} = 1 \text{ ppm}$. At $d \approx 150 \mu\text{m}$ NO_x concentration are below 1 ppm for the entire temperature range.

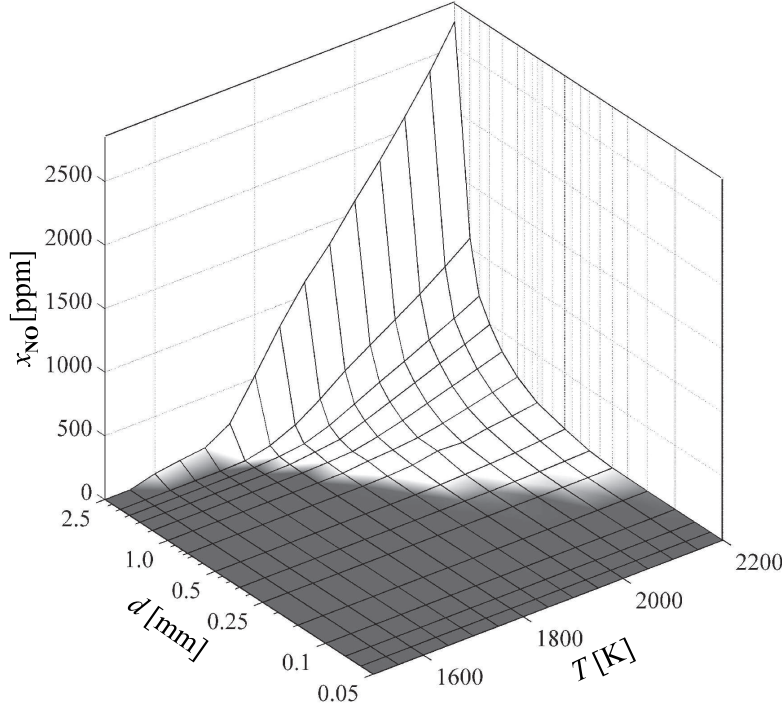


Figure 29: Maximum NO concentration in ppm vs. channel diameter and temperature. The dark area depicts NO concentration less than 1 ppm.

In conclusion, NO formation can be effectively suppressed by down-sizing channels to microscale dimensions even up to very high temperatures. However, the contribution of different NO formation mechanisms remains an open question and has to be further explained. Since thermal NO formation is comparatively slow, it is expected to occur at high temperatures where kinetics become fast enough. Prompt NO formation is strongly dependent on the amount of radicals in the system and mostly occurs at relatively low temperatures. Strong increase of NO in 2.5 mm channel and the observation of maxima at the methane ignition distance demonstrates NO formation characteristics of the prompt NO mechanism which was investigated by nitrogen species flux analysis and variation of equivalence ratio in the following graphs.

Figure 30 shows NO concentration versus axial distance for different equivalence ratios, i.e. different inlet reactant concentrations of methane between fuel-lean ($\Phi = 0.2$) and fuel-rich ($\Phi = 1.5$) conditions. According to figure 25, temperature and diameter were chosen so that transition from

heterogeneously dominated to homogeneously influenced regime occurs at exactly the same conditions and ignition distances. Therefore, it is ensured that NO formation is only dependent on NO formation mechanisms, whereas effects of temperature and different ignition states can be excluded. In this graph, the importance of the fuel content on NO concentrations can clearly be observed with changing methane concentrations. Not only NO concentrations increase significantly with increasing methane content but also the maximum at $z = 0.8$ mm becomes more and more prominent. The observed behavior proves that formation of NO through the active mechanism at these conditions is strongly dependent on initiating CH_i radicals and therefore clarifies that prompt NO formation is the dominant mechanism for applied conditions.

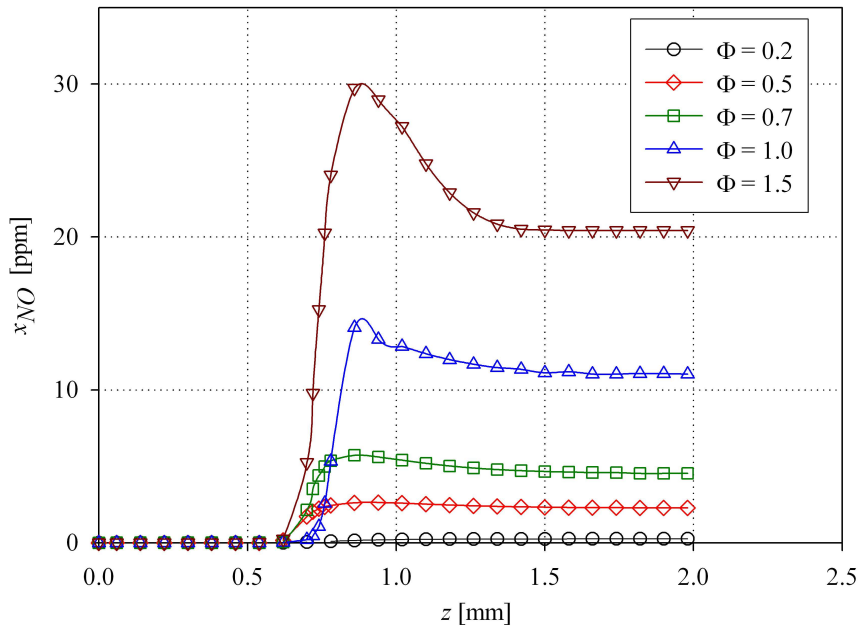
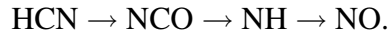


Figure 30: NO concentration versus axial distance for channel diameter of $d = 750 \mu\text{m}$ and different equivalent ratios at $p = 1.0$ bar and $T = 1650$ K.

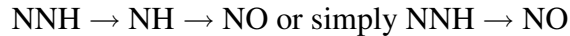
To further identify contributions of different NO mechanisms at temperatures of $T \approx 1700$ K for stoichiometric ratio of methane in air, an isothermal nitrogen flux analysis has been carried out according to the carbon flux analysis of figures 2 and 21. Nitric oxide formation pathways are depicted in figure 31. The dominating source of nitric oxide is as expected the prompt NO formation pathway mainly through



In addition, NO can alternatively form through the Prompt-NO route



Reaction fluxes of prompt NO pathways are initiated by CH_i radicals, that are significantly formed due to kinetic explosion caused by homogeneous methane oxidation mechanisms. Furthermore, a large amount of H/OH radicals are created by homogeneous ignition of methane and therefore NO formation route through diazenyl via



contributes considerably to the overall NO reaction behavior.

Typical thermal NO formation reactions like reaction IX were identified to proceed backwards and convert NO to molecular N_2 and thus contribute to the decrease of NO concentration to equilibrium concentrations in figures 28 and 25 in combination with surface NO reduction on platinum. Since the post combustion zone is characterized by elevated temperatures, thermal NO reaction kinetics become sufficiently fast to act as NO reducing mechanisms and lead to equilibrium conditions further downstream in the channel.

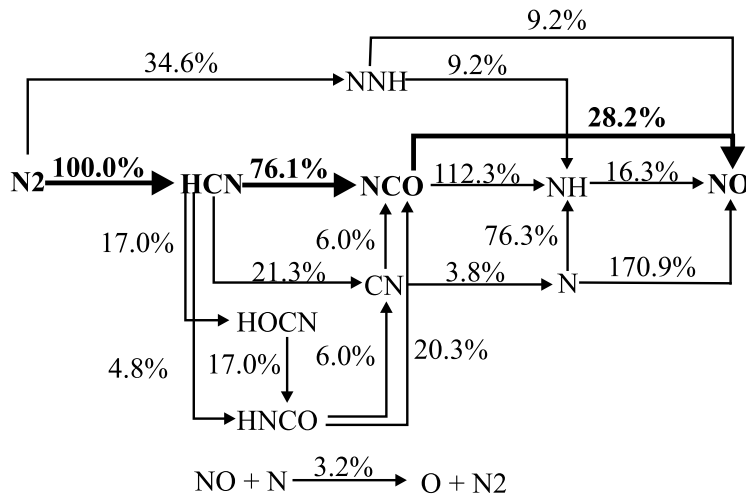


Figure 31: NO formation pathway analysis with an isothermal CSTR at $T = 1700$ K, residence time = 30 ms, $p = 1$ bar, stoichiometric ratio of CH_4 in air $\Phi = 1.0$, all fluxes are normalized with respect to overall N_2 conversion rate, fluxes smaller than 1.0 % are not shown.

To prove dominating influence of thermal NO reaction mechanism, reaction rates of the fastest NO formation reactions as a function of axial distance at the center line of a $250 \mu\text{m}$ channel are depicted in figure 32. The typical thermal NO formation reactions IX, X, and XI show the fastest reaction rates and a maximum at $z \approx 50 \mu\text{m}$, whereas reactions of other NO formation mechanisms are smaller by at least two orders of magnitude. In particular, formation of NO via the Prompt-NO mechanism is not active for these conditions. In fact, at small channel diameters, where concentrations of carbon and hydrogen radicals are effectively suppressed or reduced by surface reactions, thermal NO formation becomes the dominating source of nitrous oxides species and only the diazenyl pathway which is dependent on H radicals shows non-negligible reaction rates.

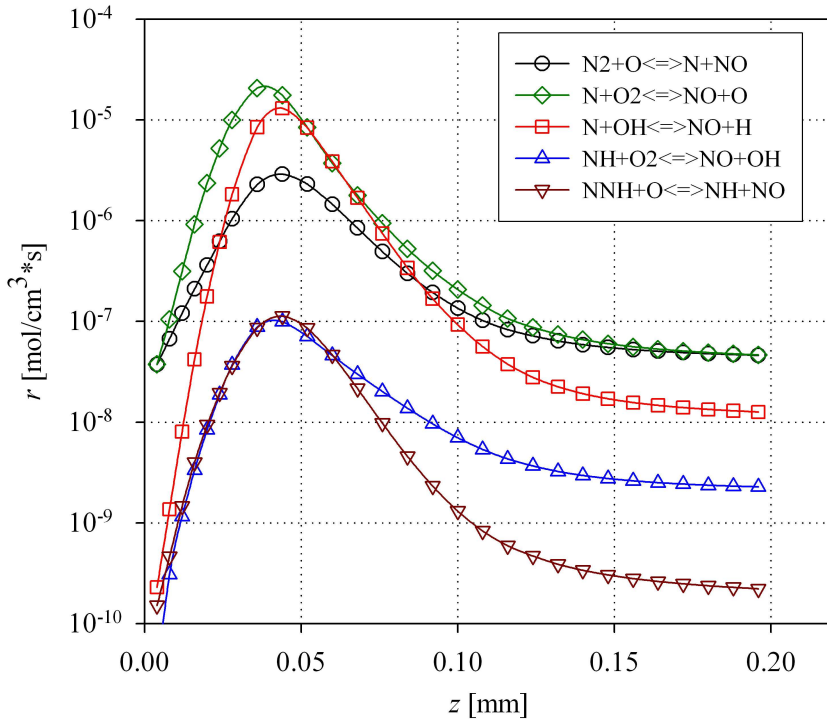


Figure 32: Homogeneous NO forming reaction rates versus axial distance at $T = 2500$ K, $p = 1$ bar and stoichiometric ratio of CH_4 in air $\Phi = 1.0$ in a $250\ \mu m$ channel.

In conclusion, Prompt-NO formation routes, which constitute the major source of nitrous oxides at temperatures below 2000 K, can effectively be quenched for diameters smaller than $d \approx 150 - 200\ \mu m$. At elevated temperatures above 2000 K, the thermal NO formation mechanism gains significant influence and hence constitutes the main source of NO_x species under these conditions. However, the overall observed reaction behavior shows a significant reduction of NO formation in sub-millimeter channels and prove micro-channel reactors to be an effective way to avoid environmentally harmful nitric oxides in combustion processes.

6 Summary and Outlook

6.1 Summary

In this work, the ignition behavior of methane oxidation with air was studied in a micro-channel reactor via numerical simulations with a two-dimensional boundary-layer model coupled with detailed reaction kinetics. Elementary-step kinetics both for surface as well as homogeneous gas phase reactions were used in the simulations. Parameters such as temperature, pressure and equivalence ratio were varied for experimentally relevant conditions. The influence of catalytic reactions was investigated for methane oxidation on platinum as a well-studied, typical noble-metal catalyst. Two theoretical cases of an inert wall reactor with only homogeneous reactions and pure the case with catalytic reactions served as reference to identify contributions of either homogeneous or heterogeneous reactions.

Strong wall effects were observed for reactor dimensions in the micrometer range. Due to the large surface-to-volume ratio and short transport paths in micro-reactors, homogeneous reactions are effectively suppressed up to very high temperatures. Radical concentration in micro-reactors is significantly reduced, as the catalytic surface adsorbs and converts radicals into products or reactants. In fact, complete radical quenching could be observed up to temperatures of $T = 2000$ K for reactor diameters smaller than $d = 200 \mu\text{m}$. Hence, in an experimental setup, suppression of homogeneous reactions is possible for the complete technically relevant temperature range.

Simulation results have additionally shown that in typical millimeter scale reactors transport of radicals inside the channel and thus influence of the catalytic wall on homogeneous reactions is limited. In fact, if a certain ratio of reaction to transport rate is exceeded, homogeneous reactions become independent of the catalytic wall. The fast acceleration of homogeneous reactions is due to increasing influence of methane decomposition for high temperatures. Although methane decomposition reactions rapidly produce radicals, these radicals can be adsorbed in small micro-reactors and acceleration of homogeneous reactions via chain-branching steps is inhibited.

In order to investigate suppression of homogeneous reactions in micro-reactors for different conditions, pressure and reactant composition were varied. The obtained results confirmed quenching behavior for different conditions and showed influence of pressure and composition. Pressure variation in particular showed a significant influence on quenching behavior and lead to stronger homogeneous influences with increasing pressure. Different reactant compositions hereby show only slight influences on transition from catalytically to homogeneously controlled behavior.

In typical combustion processes with air, oxidation of nitrogen can produce environmentally harmful nitric oxides which are mainly formed via the Thermal- or the Prompt- NO_x mechanism. The Prompt- NO_x mechanism in particular is dependent on the concentration of radical species in the system. Since dominance of catalytic reaction in micro-reactors leads to small radical concentrations, suppression of Prompt- NO_x formation could be observed up to high temperatures.

Overall, homogeneous reaction behavior in catalytic micro-reactors show a significant potential concerning suppression of homogeneous reactions and therefore enhanced safety. In addition, micro-reactor applications possibly facilitate an environmentally benign solution for decentralized and mobile combustion processes by avoiding formation of harmful nitric oxides.

6.2 Outlook

The study showed that micro-reactors have the potential to effectively suppress homogeneous reactions for the oxidation of methane in air. Since suppression effects were also observed for the hydrogen/air system in previous studies, it can be expected that reaction behavior of combustion and partial oxidation systems in general is beneficially influenced in micro-reactors and could therefore be applied to different oxidation reactions such as reactions with higher hydrocarbons or hydrogen production from methane via partial oxidation.

To validate the observed behavior, numerical and experimental methods are currently applied to investigate ignition behavior in our group. Simulations with a detailed three-dimensional Navier-Stokes model are carried out, in particular to investigate reactive flow under real mixing conditions and for different reactor geometries. Since fluid dynamics in microsystems is strongly influenced by laminar flow characteristics, mixing of incoming reactants is a crucial and intricate issue in these reactors. In detail, mixing studies with different reactor shapes including variation of inlet angles and nozzle sizes are currently carried out to determine an optimized reactor configuration. In the following, simulations of a full Navier-Stokes model including surface and homogeneous reactions will be conducted to prove and investigate quenching effects for a detailed reactor geometry.

In order to confirm theoretical investigations, an experimental configuration is currently being set up in our group. A simple micro-reactor configuration is constructed using wet- and dry etching methods to create a single reactor channel on a silicon wafer. In further steps, channel walls will be coated with platinum to obtain a catalyst surface inside the channel. This reactor setup will be employed in future investigations to confirm results from theoretical investigations for catalytic oxidation of hydrogen and methane in air. Furthermore, if suppression of homogeneous reactions can be obtained in experiments, detailed studies of surface kinetics can be carried out for elevated temperature conditions.

References

- [1] A.A. KONNOV, J.N. ZHU, J.H. BROMLY, D.-K. ZHANG: *Noncatalytic Partial Oxidation of Methane into Syngas over a wide Temperature Range*. Combustion Sci. and Tech., 176:1093–1116, 2004.
- [2] C.P. FENIMORE: *Studies of Fuel-Nitrogen in Rich Flame Gases*. Proc. Combust. Inst., 17:661, 1979.
- [3] D.A. HICKMAN, L.D. SCHMIDT: *Elementary Steps in Methane Oxidation on Pt and Rh: Reactor Modeling at High Temperature*. AIChE J., 39:1164–1177, 1993.
- [4] D. CHATTERJEE, O. DEUTSCHMANN, J. WARNATZ: *Detailed Surface Reaction Mechanism in a Three-way Catalyst*. Faraday Discussions, 119:371–384, 2001.
- [5] D.K. ZERKLE, M.D. ALLENDORF, M. WOLF, O. DEUTSCHMANN: *Homogeneous and Heterogeneous Contributions to the Partial Oxidation of Ethane: Pressure, Flow Rate, and Pore Size Effects*. J. Catal., 196:18–39, 2000.
- [6] E. CAO, K.K. YEONG, A. GAVRILIDIS, Z. CUI, D.W.K. JENKINS: *Microchemical Reactor for Oxidative Dehydrogenation of Methanol*. Microreaction Technology – IMRET 6, Springer-Verlag, Berlin, 2002.
- [7] F.K. MOORE: *Theory of Laminar Flows, Volume IV of the High Speed Aerodynamics and Jet Propulsion Series*. Princeton University Press, 1964.
- [8] G. DIXON-LEWIS: *Flame Structure and Flame Reaction Kinetics*. Proc. of the Royal Soc., 130:111–135, 1968.
- [9] G. EIGENBERGER: *Chemische Reaktionstechnik II*. Lecture Chemical Engineering at Universität Stuttgart, WS 2004.
- [10] G.P. SMITH, D.M. GOLDEN, M. FRENKLACH, N.W. MORIARTY, B. EITENEER, M. GOLDENBERG, C.T. BOWMAN, R.K. HANSON, S. SONG, W.C. GARDINER, V.V. LISIANSKI, Z. QIN: *GRI Mechanism 3.0 - An Optimized Detailed Chemical Reaction Mechanism for Methane Combustion*. Technical Report http://www.me.berkeley.edu/gri_mech, Gas Research Institute, 1999.
- [11] G. VESER: *Experimental and Theoretical Investigation of H₂-Oxidation in a High-Temperature Catalytic Microreactor*. Chem. Eng. Sci., 56:1265–1273, 2001.
- [12] G. VESER, G. FRIEDRICH, M. FREYGANG, R. ZENGERLE: *A Simple and Flexible Microreactor for Investigations of Heterogeneous Catalytic Gas Phase Reaction*. Reaction

- Kinetics and the Development of Catalytic Processes, G.F. Froment and K.C. Waugh (eds), Studies in Surf. Science and Cat., 122:237–246, 1999.
- [13] G. VESER, J. FRAUHAMMER: *Modeling Steady State and Ignition of Catalytic Methane Oxidation in a Monolith Reactor*. Chem. Eng. Sci., 55:2271–2286, 2000.
- [14] H. KESTENBAUM, A. LANGE DE OLIVEIRA, W. SCHMIDT, H. SCHÜTH, W. EHRFELD, K. GEBAUER, H. LÖWE, T. RICHTER: *Synthesis of Ethylene Oxide in a catalytic microreactor system*. Stud. Surf. Sci. Catal., 130, 2000.
- [15] H.K. MOFFAT, R.J. KEE, J.F. GRCAR, J.A. MILLER: *Surface PSR: a Fortran Program for Modeling Well-Stirred Reactors with Gas and Surface Reactions*, Sandia Laboratories Rep. SAND91-8001, Albuquerque, NM, 1993.
- [16] J. MAYER, M. FICHTNER, D. WOLF, K. SCHUBERT: *A Microstructured Reactor for the Catalytic Partial Oxidation of Methane to Syngas*. Microreaction Technology – IMRET 3, Springer-Verlag, Berlin, 2000.
- [17] J. WARNATZ, R.W. DIBBLE, U. MAAS: *Combustion, Physical and Chemical Fundamentals, Modeling and Simulation*. Springer-Verlag, New York, 1996.
- [18] J.W. BOZZELLI, A.M. DEAN: *O + NNH - A Possible New Route for NO_x Formation in Flames*. Int. J. Chem. Kinet., 27:1097–1109, 1995.
- [19] K.J. HUGHES, T. TURANYI, A. CLAGUE, M.J. PILLING: *Development and Testing of a Comprehensive Chemical Mechanism for the Oxidation of Methane*. Int. J. Chem. Kinet., 33:513–538, 2001.
- [20] K. SCHUBERT, J. BRANDNER, M. FICHTNER, G. LINDER, U. SCHYGULLA, A. WENKA: *Microstructure Devices for Applications in Thermal and Chemical Process Engineering*. Microscale Therm., 5:17–39, 2001.
- [21] K. SUNDMACHER, A. KIENLE: *Reactive Distillation - Status and Future Directions*. Wiley-VCH, 2003.
- [22] L.L. RAJA, R.J. KEE, O. DEUTSCHMANN, J. WARNATZ, L.D. SCHMIDT: *A Critical Evaluation of Navier-Stokes, Boundary-Layer, and Plug-Flow Models of the Flow and Chemistry in a Catalytic-Combustion Monolith*. Cat. Today, 59:47–60, 2000.
- [23] M.E. COLTRIN, H.K. MOFFAT, R.J. KEE, F.M. RUPLEY: *CRESLAF (Version 4.0): A Fortran Program for Modeling Laminar, Chemically Reacting, Boundary-Layer Flow in Cylindrical or Planar Channels*, Sandia Laboratories Rep. SAND93-0478, Albuquerque, NM, 1993.

- [24] M. REINKE, J. MANTZARAS, R. BOHMBACH, S. SCHENKER, A. INAUEN: *Gas Phase Chemistry in Catalytic Combustion of Methane/Air Mixtures over Platinum at Pressures of 1 to 16 bar.* Combust. Flame, 141:448–468, 2005.
- [25] O. DEUTSCHMANN, R. SCHMIDT, F. BEHRENDT, J. WARNATZ: *Numerical Modeling of Catalytic Ignition.* Twenty Sixth Symposium (International) on Combustion, The Combustion Institute, Pittsburgh, 1996.
- [26] P.-A. BUI, D.G. VLACHOS, P.R. WESTMORELAND: *Catalytic Ignition of Methane/Oxygen Mixtures over Platinum Surfaces: Comparison of Detailed Simulations and Experiments.* Surf. Science, 385(2):1029–1034, 1997.
- [27] P. AGHALAYAM, Y.K. PARK, N. FERNANDES, V. PAPAVASSILOU, A.B. MHADESHWAR, D.G. VLACHOS: *A CI Mechanism for Methane Oxidation on Platinum.* J. Catal., 213:23–28, 2003.
- [28] P. GLARBORG, R.J. KEE, J.F. GRCAR, J.A. MILLER: *PSR: a Fortran Program for Modeling Well-Stirred Reactors,* Sandia Laboratories Rep. SAND86-8209, Albuquerque, NM, 1996.
- [29] P. MARKATOU, L. PFEFFERLE, M. D. SMOOKE: *A Computational Study of Methane-Air Combustion over Heater Catalytic and Non-Catalytic Surfaces.* Combust. Flame, 93:185–201, 1993.
- [30] R.B. BIRD, W.R. STEWART, E.N. LIGHTFOOT: *Transport Phenomena.* Wiley-VCH, New York, 2002.
- [31] R.J. KEE, F.M. RUPLEY, J.A. MILLER, M.E. COLTRIN, J.F. GRCAR, E. MEEKS, H.K. MOFFAT, A.E. LUTZ, G. DIXON-LEWIS, M.D. SMOOKE, J. WARNATZ, G.H. EVANS, R.S. LARSON, R.E. MITCHELL, L.R. PETZOLD, W.C. REYNOLDS, M. CARACOTSIOS, P. STEWART, P. GLARBORG, C. WANG, C.L. MCLELLAN, O. ADIGUN, W.G. HOUF, C.P. CHOU, S.F. MILLER, P. HO, P.D. YOUNG, D.J. YOUNG: *Chemkin Release 4.0.2, Reaction Design,* San Diego, CA, 2005.
- [32] R.J. KEE, M.E. COLTRIN, P. GLARBORG: *Chemically Reacting Flow.* Wiley-Interscience, 2003.
- [33] R.S. BESSER, X. OUYANG, H. SURANGALIKAR: *Hydrocarbon Hydrogenation and Dehydrogenation Reactions in Microfabricated Catalytic Reactors.* Chem. Eng. Sci., 58:19–26, 2003.
- [34] S. CHATTOPADHYAY: *Navigating Reactor Safety in Catalytic Microchannel Reactors.* University of Pittsburgh, 2004.

- [35] S. CHATTOPADHYAY, G. VESER: *Detailed Simulations of Catalytic and Non-Catalytic Ignition during H₂-Oxidation in a Microchannel Reactor*. Proc. ChemCon2001, IIChE, Madras, India, 2001.
- [36] S.K. AJMERA, C. DELAITRE, K.F. JENSEN, M.A. SCHMIDT: *Microfabricated Packed-Bed Reactor for Phosgene Synthesis*. Chem. Eng. Sci., 58:19–26, 2003.
- [37] S. WALTER, E. JOANNET, M. SCHIEL, I. BOULLET, R. PHILLIPS, M.A. LIAUW: *Microchannel Reactor for the Partial Oxidation of Isoprene*. Microreaction Technology – IMRET 5, Springer-Verlag, Berlin, 2001.
- [38] W.C. GARDINER: *Gas Phase Combustion Chemistry*. Springer-Verlag, New York, 2000.
- [39] W. EHRFELD, V. HESSEL, H. LÖWE: *Microreactors*. Wiley-VCH, Weinheim, 2004.
- [40] X. SONG, W.R. WILLIAMS, L.D. SCHMIDT, R. ARIS: *Bifurcation Behavior in Homogeneous-Heterogeneous Combustion: II. Computations in Stagnation Point Flow*. Combust. Flame, 84:277–292, 1991.
- [41] Y.B. ZELDOVICH: *The Oxidation of Nitrogen in Combustion and Explosions*. Acta Physicochim., 21:577, 1946.

A Model Description

The CHEMKIN model CRESLAF for reactive channel flow employs boundary-layer approximation for the fluid-flow equations, coupled to gas phase and surface species continuity equations. Boundary-layer approximations, originally conceive by Ludwig Prandtl, are very well-known in fluid mechanics and have widely been used since the early twentieth century. Boundary-layer behavior can be anticipated if there is a dominant flow direction. It is thus capable of describing coupled fluid dynamics, gas-phase chemistry and surface chemistry in laminar flow channel configurations. The boundary-layer equations represent a coupled, nonlinear system of parabolic partial differential equations. It is restricted to a two-dimensional geometry, using either planar or radial coordinates. The simplification of this approximation leads to an efficient computational algorithm. After finite difference discretization, the resulting problem can be solved numerically by the method of lines as a differential-algebraic system of equations. The applicability of these equations relies on the existence of a principal flow direction in which flow-wise diffusive transport is negligible compared to convective transport. Mathematically this reduction causes the boundary-layer equations to essentially have parabolic characteristics instead of dealing with elliptic Navier-Stokes equations.

The following set of equations describe the applied boundary-layer model:

Momentum equation:

$$\rho v \frac{\partial v}{\partial z} - \frac{\rho v}{\dot{m}} \left(\xi \frac{d\dot{m}}{dz} - \frac{d\dot{m}_l}{dz} \right) \frac{\partial v}{\partial \xi} + \frac{dp}{dz} = \frac{\rho v}{\dot{m}^2} \frac{\partial}{\partial \xi} \left(\rho v \nu r^2 \frac{\partial v}{\partial \xi} \right) \quad (17)$$

Species equation:

$$\rho v \frac{\partial w_i}{\partial z} - \frac{\rho v}{\dot{m}} \left(\xi \frac{d\dot{m}}{dz} - \frac{d\dot{m}_l}{dz} \right) \frac{\partial w_i}{\partial \xi} = r_{reaction} MW_i - \frac{\rho v}{\dot{m}} \frac{\partial}{\partial \xi} \left(r \rho w_i v_i^D \right) \quad (18)$$

Energy equation:

$$\begin{aligned} \rho v c_p \frac{\partial T}{\partial z} - \frac{\rho v c_p}{\dot{m}} \left(\xi \frac{d\dot{m}}{dz} - \frac{d\dot{m}_l}{dz} \right) \frac{\partial T}{\partial \xi} &= \\ = \frac{\rho v}{\dot{m}^2} \frac{\partial}{\partial \xi} \left(\rho v \lambda r^2 \frac{\partial T}{\partial \xi} \right) - \sum_{i=1}^{N_g} r_{reaction} MW_i h_i &- \frac{\rho^2 v r}{\dot{m}} \sum_{i=1}^{N_g} w_i v_i^D c_{p,i} \frac{\partial T}{\partial \xi} \end{aligned} \quad (19)$$

Equation of State (Ideal Gas Law):

$$p = \frac{\rho \Re T}{\widetilde{MW}}$$

Diffusion velocity (Stephan-Maxwell equation):

$$v_i^D = \frac{\rho \nu r}{x_i \widetilde{MW} \dot{m}} \sum_{j \neq i}^{N_g} MW_j D_{i,j} \frac{\partial x_i}{\partial \xi} \quad (20)$$

For further simplification of the numerical procedure, the equations are recasted by using the Von Mises Transformation in which the cross-stream coordinate is replaced by the stream function as an independent variable. The independent variables z and ξ represent the axial coordinate and the normalized stream function respectively

The stream function is defined as:

$$\Psi = \frac{1}{2} \int_0^r \rho v dr^2 \quad (21)$$

The stream function is defined such that there is an equal mass flow rate between two lines of constant stream function value. Hereby, the reactor walls themselves are stream lines, i.e. lines of constant stream function. The numerical method uses a mesh in which each mesh point has a specified value of stream function. The relationships between the physical coordinates (r and z) and the transformed coordinates (ξ , Ψ and z) are stated in the following equations that define the Von Mises Transformation.

$$\left(\frac{\partial}{\partial z} \right)_r = \left(\frac{\partial}{\partial z} \right)_\Psi - \rho \nu r \left(\frac{\partial}{\partial \Psi} \right)_z \quad (22)$$

$$\left(\frac{\partial}{\partial z} \right)_r = \left(\frac{\partial}{\partial z} \right)_\xi - \frac{\xi}{\dot{m}} \frac{dm}{dz} \left(\frac{\partial}{\partial \xi} \right)_z - \rho \nu r \frac{1}{\dot{m}} \left(\frac{\partial}{\partial \xi} \right)_z \quad (23)$$

$$\left(\frac{\partial}{\partial r} \right)_z = \rho \nu r \frac{1}{\dot{m}} \left(\frac{\partial}{\partial \xi} \right)_z \quad (24)$$

The initial mass flux entering the channel is defined by

$$\dot{m}_0 = \left(\int_0^{r_{max}} \rho v r dr \right)_0 \quad (25)$$

The system of equations is completed by an equation that relates the cross-stream coordinate r to the normalized stream function

$$\frac{1}{\dot{m}} \frac{\partial r}{\partial \xi} = \frac{2}{\rho v} \quad (26)$$

which is derived by differentiating the definition of the stream function, equation 21.

The equations are subject to a set of algebraic constraints, which result from the equations for surface site fractions. The equation system is solved using the method of lines and is treated as a set of differential-algebraic equations. At the entrance of the reactor, the initial profiles of v , T , and w_i , the pressure and the surface site fractions z_i must be specified. The initial gas-phase species mass fractions w_i are taken to be uniform across the channel, with the exception of the mass fractions at reactive walls. As equations for surface reactions constitute algebraic equations, initial surface fractions have to be specified to form a self-consistent set of initial conditions at the reactor inlet. A common ODE solver facilitates the search for initial guesses for the surface fractions. From the initial profiles, the local mass flux \dot{m} and the physical locations of all the mesh points, i.e. a profile for r are calculated.

A Surface Mechanisms

The reactor model is coupled with detailed elementary-step reaction kinetics, which considers catalytic reactions and intermediate products of oxidation of methane on a platinum surface. The CHEMKIN software is used for the formulation of the surface mechanism. To describe the influence of the catalytic wall in micro-reactors, two different platinum surface mechanisms were employed. The kinetic equations and rate parameters on platinum for these mechanisms were used from Aghalayam et al. [27] and Deutschmann et al. [25]. To include reduction of NO on the Platinum surface, a subset of the mechanism by Chatterjee et al. [4] was used.

Table 5: Surface reaction mechanism for methane oxidation by Deutschmann et al.[25].

Reaction	A^a	β^a	E^a
1 $H_2 + 2Pt(s) \rightarrow 2H(s)$	4.46×10^{10}	0.5	
The reaction rate is first-order in Pt(s) equivalent sticking coefficient of 0.046			
2 $2H(s) \rightarrow H_2 + 2Pt(s)$	3.7×10^{10}		67.4
modified by an activated H(s) coverage, ^b i.e., $k = AT^\beta \exp(-E/RT) \times \exp(-\epsilon [H(s)] / RT)$		with $\epsilon = -6$ kJ/mol	
3 $H + Pt(s) \rightarrow H(s)$	1.00^c		
4 $O_2 + 2Pt(s) \rightarrow 2O(s)$	1.8×10^{21}		-0.5
5 $O_2 + 2Pt(s) \rightarrow 2O(s)$	0.023 ^c		
Reactions 4 and 5 represent alternative competing pathways			
6 $2O(s) \rightarrow O_2 + 2Pt(s)$	1.8×10^{21}		213.2
Reaction rate modified by activated O(s) coverage activation parameter $\epsilon = -60$ kJ/mol			
7 $O + Pt(s) \rightarrow O(s)$	1.0^c		
8 $H_2O + Pt(s) \rightarrow H_2O(s)$	1.0^c		
9 $H_2O(s) \rightarrow H_2O + Pt(s)$	1.0×10^{13}		40.3
10 $OH + Pt(s) \rightarrow OH(s)$	1.0^c		
11 $OH(s) \rightarrow OH + Pt(s)$	1.0×10^{13}		192.8
12 $H(s) + O(s) \rightarrow OH(s) + Pt(s)$	3.7×10^{21}		11.5
13 $H(s) + OH(s) \rightarrow H_2O(s) + Pt(s)$	3.7×10^{21}		17.4
14 $OH(s) + OH(s) \rightarrow H_2O(s) + O(s)$	3.7×10^{21}		48.2
15 $CO + Pt(s) \rightarrow CO(s)$	1.618×10^{20}	0.5	
reaction rate second order in Pt(s)			
reaction equivalent to sticking coefficient of 0.84			
16 $CO(s) \rightarrow CO + Pt(s)$	1.0×10^{13}		125.5
17 $CO_2 \rightarrow CO_2 + Pt(s)$	1.0×10^{13}		20.5
18 $CO(s) + O(s) \rightarrow CO_2 + Pt(s)$	3.7×10^{21}		105.0
19 $CH_4 + 2Pt(s) \rightarrow CH_3 + H(s)$	4.63×10^{20}	0.5	
reaction rate has 2.3 order dependence on Pt(s)			
reaction rate is equivalent to a sticking coefficient of 0.01			
20 $CH_3(s) + Pt(s) \rightarrow CH_2(s) + H(s)$	3.7×10^{21}		20.0
21 $CH_2(s) + Pt(s) \rightarrow CH(s) + H(s)$	3.7×10^{21}		20.0
22 $CH(s) + Pt(s) \rightarrow C(s) + H(s)$	3.7×10^{21}		20.0
23 $C(s) + O(s) \rightarrow CO(s) + Pt(s)$	3.7×10^{21}		62.8
24 $CO(s) + Pt(s) \rightarrow C(s) + O(s)$	1.0×10^{18}		184.0

^a Arrhenius parameter for the rate constants written in the form: $k = AT^\beta \exp(-E/RT)$. The units of A are given in terms of moles, cubic meters, and seconds. E is in kJ/mol.

^b The surface coverage (e.g., $[H(s)]$) is specified as a site fraction.

^c Sticking coefficient. Total available site density $s = 2.7 \times 10^{-9} \text{ mol/cm}^2$.

Table 6: Surface reaction mechanism for methane oxidation by Aghalayam et al.[27].

No.	Reaction	k_f	E_f	E_f	k_f	E_b	E_b
			$\theta_{Pt(s)} = 1$	$\theta_{O(s)} = 1$		$\theta_{Pt(s)} = 1$	$\theta_{O(s)} = 1$
1	$OH + Pt(s) \rightarrow H(s) + O(s)$	5.60×10^{11}	24.4	18.3	1.70×10^{10}	12.1	13.4
2	$H_2O + Pt(s) \rightarrow H(s) + OH(s)$	1.20×10^{10}	18.4	39.1	3.50×10^{11}	12.4	0.0
3	$H_2O + O(s) \rightarrow 2OH(s)$	1.00×10^{11}	12.6	34.1	1.00×10^{11}	18.9	0.0
4	$H_2 + 2Pt(s) \rightarrow 2H(s)$	0.09	0.0	0.0	3.33×10^{12}	20.0	20.0
5	$O_2 + 2Pt(s) \rightarrow 2O(s)$	0.03 ^a	0.0	0.0	1.00×10^{13}	51.0	19.0
6	$H_2O + Pt(s) \rightarrow H_2O(s)$	1.00	0.0	0.0	5.33×10^{12}	10.0	10.0
7	$OH + Pt(s) \rightarrow OH(s)$	1.00	0.0	0.0	1.00×10^{13}	63.0	30.0
8	$H + Pt(s) \rightarrow H(s)$	1.00	0.0	0.0	1.00×10^{13}	60.2	60.2
9	$O + Pt(s) \rightarrow O(s)$	1.00	0.0	0.0	1.00×10^{13}	92.6	67.0
10	$CH_4 + 2Pt(s) \rightarrow CH_3 + H(s)$	0.68	12.0	12.0	3.97×10^{10}	5.5	5.5
11	$CH_3 + Pt(s) \rightarrow CH_2(s) + H(s)$	1.32×10^{13}	25.8	25.8	4.04×10^{10}	6.1	6.1
12	$CH_2(s) + Pt(s) \rightarrow CH(s) + H(s)$	1.00×10^{11}	25.0	25.0	1.00×10^{11}	12.2	12.2
13	$CH(s) + Pt(s) \rightarrow C(s) + H(s)$	1.00×10^{11}	5.4	5.4	1.00×10^{11}	37.6	37.6
14	$CH_3 + O(s) \rightarrow CH_2(s) + OH(s)$	1.00×10^{11}	20.2	17.7	1.00×10^{11}	12.5	3.1
15	$CH(s) + OH(s) \rightarrow CH_2(s) + O(s)$	1.00×10^{11}	19.3	13.2	1.00×10^{11}	19.9	20.5
16	$C(s) + OH(s) \rightarrow CH(s) + O(s)$	1.00×10^{11}	45.9	38.2	1.00×10^{11}	1.5	1.5
17	$CH_2(s) + H_2O(s) \rightarrow CH_3(s) + OH(s)$	1.00×10^{11}	5.1	19.5	1.00×10^{11}	18.6	0.0
18	$CH(s) + H_2O(s) \rightarrow CH_2(s) + OH(s)$	1.00×10^{11}	13.2	26.7	1.00×10^{11}	19.5	0.0
19	$C(s) + H_2O(s) \rightarrow CH(s) + OH(s)$	1.00×10^{11}	38.1	70.9	1.00×10^{11}	0.1	0.0
20	$CO(s) + Pt(s) \rightarrow C(s) + O(s)$	1.00×10^{11}	53.0	74.2	1.00×10^{11}	4.3	0.0
21	$CO_2(s) + Pt(s) \rightarrow CO(s) + O(s)$	1.00×10^{11}	21.2	43.1	1.00×10^{11}	3.6	0.0
22	$CO + Pt(s) \rightarrow CO(s)$	0.71	0.0	0.0	1.21×10^{13}	34.0	34.0
23	$CO_2 + Pt(s) \rightarrow CO_2$	0.70	0.0	0.0	1.46×10^{12}	17.0	17.0
24	$CO_2 + H(s) \rightarrow CO(s) + OH(s)$	1.00×10^{11}	13.6	38.2	1.00×10^{11}	8.4	0.0
25	$CO + H(s) \rightarrow CH(s) + O(s)$	1.00×10^{11}	80.5	106.0	1.00×10^{11}	0.0	0.0
26	$CO + H(s) \rightarrow C(s) + OH(s)$	1.00×10^{11}	40.3	69.2	1.00×10^{11}	4.0	0.0
27	$CH_3 + Pt(s) \rightarrow CH_3(s)$	1.00	0.0	0.0	1.00×10^{13}	38.0	38.0
28	$CH_2 + Pt(s) \rightarrow CH_2(s)$	1.00	0.0	0.0	1.00×10^{13}	68.0	68.0
29	$CH + Pt(s) \rightarrow CH(s)$	1.00	0.0	0.0	1.00×10^{13}	97.0	97.0
30	$C + Pt(s) \rightarrow C(s)$	1.00	0.0	0.0	1.00×10^{13}	150.0	150.0
31	$2CO(s) \rightarrow C(s) + CO_2(s)$	2.40×10^{12}	31.0	31.0	4.17×10^{09}	0.0	0.0

Arrhenius parameter for the rate constants written in the form: $k = k_{f/b} \exp(-E_{f/b}/RT)$. The units of A are given in terms of moles, cubic meters, and seconds. E is in kcal/mol calculated at vacancy and oxygen dominated conditions.

Table 7: Surface reaction mechanism NO reduction by Chatterjee et al.[4].

No.	Reaction	A^a / S	β	E
1	$\text{NO} + \text{Pt(s)} \rightarrow \text{NO(s)}$	0.85	0.0	0.0
2	$\text{NO(s)} \rightarrow \text{NO} + \text{Pt(s)}$	1.00×10^{16}	0.0	140.0
3	$\text{N(s)} + \text{N(s)} \rightarrow \text{N}_2 + \text{Pt(s)} + \text{Pt(s)}$	3.70×10^{21}	0.0	113.9
	modified by an activated CO(s) coverage, with $\epsilon = -75 \text{ kJ/mol}$			
4	$\text{NO} + \text{Pt(s)} \rightarrow \text{N(s)} + \text{O(s)}$	5.00×10^{20}	0.0	107.8
	modified by an activated CO(s) coverage, with $\epsilon = -3 \text{ kJ/mol}$			
5	$\text{N(s)} + \text{O(s)} \rightarrow \text{NO(s)} + \text{Pt(s)}$	3.70×10^{21}	0.0	128.1
	modified by an activated CO(s) coverage, with $\epsilon = 45 \text{ kJ/mol}$			

Arrhenius parameter for the rate constants written in the form: $k = AT^\beta \exp(-E/RT)$. The units of A are given in terms of moles, cubic meters, and seconds. E is in kJ/mol.

B Model Validation

The boundary-layer model is based on several assumptions that have to be fulfilled in order to validate the simulations conducted in this work. Hence, the main model assumptions are verified in this section. Firstly, continuum assumptions of the underlying Navier-Stokes equations have to be proven valid for the investigated microscale systems. In addition, convection dominant behavior in the main flow direction, laminar flow and a negligible pressure drop are assumptions that have to be fulfilled for the conditions in these studies.

B.1 Continuum Assumption

The continuum assumption in the Navier-Stokes equations, which are used in a simplified form for the boundary-layer model, is valid provided the mean free path of the molecules is smaller than the characteristic dimension of the flow domain. In case, continuum assumptions are not valid, local thermodynamic equilibrium and fluid dynamics are affected by non-continuum effects. Continuum assumption can be verified with the Knudsen number of a molecular species in a characteristic channel dimension:

$$Kn = \frac{\lambda_i}{d} = \frac{kT}{\sqrt{2\pi\sigma^2 p}} \frac{1}{d} \quad (27)$$

As for $Kn \ll 1$, the continuum assumption is appropriate and the flow described by the boundary-layer model with conventional no-slip wall conditions. In this work temperatures ranged between $T = 800 \text{ K}$ and 2500 K and pressures from $p = 0.5 \text{ bar}$ to 5 bar . The minimum diameter was determined as $d = 50 \mu\text{m}$.

For these parameter combinations, Knudsen numbers Kn can be calculated in a range between

$Kn = 6.9 \cdot 10^{-4} - 2.2 \cdot 10^{-2}$ which proves the continuum assumptions to be valid.

B.2 Laminar Flow

Laminar flow is one of the main system characteristics when investigating reactive flow in micro-channels. These systems can be characterized by non-turbulent behavior and therefore a simple boundary-layer model can precisely describe flow characteristics in these reactors. Reynolds numbers were calculated for the relevant conditions to confirm laminar flow in the model assumptions. The Reynolds number is the ratio of inertial forces to viscous forces and hence, can be used to determine if laminar or turbulent flow occurs in a tubular channel:

$$Re = \frac{\rho v d}{\eta} \quad (28)$$

Reynolds numbers were calculated for reactor diameters $d = 50 \mu\text{m}-10 \text{ mm}$, $p = 1 \text{ bar}$, $T = 1000 \text{ K}-2000 \text{ K}$ and flow velocity was set to $v = 9 \text{ m/s}$. The calculated range of Reynolds numbers was determined as $Re = 1.2-728.7$, which confirms laminar flow behavior for the investigated parameter range, as $Re_{crit} = 2300$ for tubular flow characteristics.

B.3 Convection-Dominant Behavior in the Main Flow Direction

Flow in micro-chemical systems is normally convection dominant, as very high flow velocities can be realized in these reactors. Fast conversion due to short contact times are main advantages in micro-reactors and thus facilitate avoidance of back-mixing, axial heat transfer and high throughputs. In our simulations, the flow velocity was set to $v = 9 \text{ m/s}$, according to previous experiments [11]. Convection dominant behavior can be investigated by calculating the Peclet number Pe , which is the ratio of the forced convection of a system to its heat conduction:

$$Pe = \frac{d v c_p \rho}{\lambda} \quad (29)$$

The Peclet number was calculated as $Pe \geq 10$ for chosen parameters. This shows convection dominance for our simulations as Pe is larger than unity at least by one order of magnitude.

B.4 Pressure Drop

To calculate the pressure drop for different channel sizes we used the following Hagen-Poiseuille equation for laminar tubular flow. The Hagen-Poiseuille law correlates pressure drop and average linear velocity in a horizontal pipe [30].

$$\Delta p = \frac{8 \eta \tilde{v} l}{r^2} \quad (30)$$

The pressure drop was calculated for $d = 50 \mu\text{m}$ - $500 \mu\text{m}$ at ambient pressure and high temperature conditions. Results are shown in table 8.

Table 8: Pressure drop calculation for $p = 1 \text{ bar}$, $T = 1500 \text{ K}$ and $v = 9 \text{ m/s}$.

$d [\mu\text{m}]$	$\Delta p/l [\text{bar/mm}]$
50	$1.56 \cdot 10^{-2}$
100	$3.89 \cdot 10^{-3}$
250	$6.23 \cdot 10^{-4}$
500	$1.56 \cdot 10^{-4}$

The calculation shows that pressure drops can be limited to less than 10 % of the initial pressure if the reactor length is in the millimeter range. Pressure drop is determined to $\Delta p = 1.6 \cdot 10^{-2} \text{ bar}$ for a reactor of 25 mm length and a diameter of $d = 250 \mu\text{m}$. Hence, in a reactor with these measures, reactants are completely converted into products within the reactor length and the pressure drop is negligible compared to the absolute pressure.